RECK AND GPR124 ACTIVATE CANONICAL WNT SIGNALING TO CONTROL MAMMALIAN CENTRAL NERVOUS SYSTEM ANGIOGENESIS AND BLOOD-BRAIN BARRIER REGULATION

by

Chris Moonho Cho

A dissertation submitted to Johns Hopkins University in conformity with the requirements for the degree of Doctor of Philosophy

Baltimore, Maryland

July 2018

Abstract

Canonical Wnt signaling plays a pivotal role in promoting central nervous system (CNS) angiogenesis and blood-brain barrier (BBB) formation and maintenance. Specifically, Wnt7a and Wnt7b are required for vascular development in the forebrain and ventral spinal cord. Yet, how these two ligands – among the 19 mammalian Wnts – are selectively communicated to Frizzled receptors expressed on endothelial cells (ECs) remains largely unclear. In this thesis, we propose a novel paradigm for Wnt specificity. We have identified two EC surface proteins – orphan receptor Gpr124, and more recently, GPI-anchored Reck (reversion-inducing cysteine-rich protein with Kazal motifs) – as essential receptor co-factors that assemble into a multi-protein complex with Wnt7a/7b and Frizzled for the development of the mammalian neurovasculature.

Specifically, we show that EC-specific reduction in Reck impairs CNS angiogenesis and that EC-specific postnatal loss of Reck, combined with loss of Norrin, impairs BBB maintenance. We identify the critical domains of both Reck and Gpr124 that are required for Wnt activity, and demonstrate that these regions are important for

direct binding and complex formation. Importantly, weakening this interaction by targeted mutagenesis reduces Reck-Gpr124 stimulation of Wnt7a signaling in cell culture and impairs CNS angiogenesis. Finally, a soluble Gpr124 probe binds specifically to cells expressing Frizzled (Fz), Wnt7a or Wnt7b, and Reck; and a soluble Reck probe binds specifically to cells expressing Fz, Wnt7a or Wnt7b, and Gpr124.

In the 20 years since the discovery that Frizzleds constitute the principal receptors for Wnts, and the contemporaneous appreciation that the mammalian genome encodes for 10 Frizzleds and 19 Wnt ligands, the extent of Wnt-Frizzled specificity and the biological roles that such specificity might play have largely remained open questions. Here, we present a novel model for Wnt specificity with important biological function: Reck and Gpr124 are integral parts of the cell surface protein complex that transduces Wnt7a- and Wnt7b-specific signals in mammalian CNS ECs to promote angiogenesis and regulate the BBB. These findings signify the exciting possibility that receptor co-factors like Reck and Gpr124 exist for the other 17 Wnt ligands, and identifying these factors will be an important future direction for the field.

Primary Reader: Jeremy Nathans, M.D., Ph.D.

Secondary Reader: Alex Kolodkin, Ph.D.

Acknowledgments

First and foremost, I'd like to thank my thesis advisor, Dr. Jeremy Nathans. From the onset of my graduate training, he challenged me to think deeply and work rigorously. He taught me to carve out hypotheses and to learn how to "kill" them – that is, to do the one experiment that would prove your favorite hypothesis wrong. He encouraged me to be clever and curious. And, he showed all of this by example, every day, in his office or at his bench.

The second person I'd like to acknowledge is Philip Smallwood, a senior technician in the lab and a dear friend. In addition to all of his technical support over the years, which includes the molecular cloning of hundreds of plasmid constructs, he has reminded me that scientific work ultimately stems from people and to never forget the importance of that humanity.

I extend my gratitude to my thesis committee: Geraldine Seydoux, Ph.D., Shanthini Sockanathan, Ph.D., and Alex Kolodkin, Ph.D. Their guidance and feedback

were critical for the advancement of my thesis work.

I'd like to also thank the past and present members of the lab with whom I overlapped with, such as Yulian Zhou, Alisa Mo, Hao Chang, Mark Sabbagh, Jacob Heng, Xiaowu Gu, Francesco Emiliani, Tao-Hsin Chang, Xi Peng, and Amir Rattner, for thought-provoking discussions and cheerful times. Special thanks goes to Yanshu Wang for her assistance with retina and brain dissections and John Williams for additional support with molecular cloning.

Outside of the lab, I'd like to thank my graduate school friends – Karole d'Orazio, Joyce Lee, Michelle Levine, and Chirag Vasavda – for being my pillars of strength and arches of inspiration. Additionally, I'd like to thank Charm City Ballet, specifically Rebecca Friedman, Peter Commander, and Ellen Bast, for providing a creative space and community that have been instrumental in my growth as a scientist-artist.

Finally, I'd like to acknowledge my family. A huge thank you goes to my older brother Brian and sister-in-law Susie who serendipitously moved to Baltimore for work at the same time I began my training at Hopkins: thank you for being by my side throughout these past several years. And most importantly, I'd like to thank my parents for sacrificing so much of themselves so that we could dream the big dreams, and accomplish them.

Table of Contents

List of Tables

List of Figures

Chapter 1

Introduction

1.1 Overview

The proper development and function of the central nervous system (CNS) vasculature is required for neural tissue survival and homeostasis. Unlike the peripheral vascular network, the CNS vasculature consists of highly specialized cells and molecules that endow it with the unique property of a blood-brain barrier (BBB) (Blanchette and Daneman, 2015; Daneman and Prat, 2015; Zhao et al., 2015). The formation of this highly specialized vascular network and the regulation of the BBB is largely dependent on canonical Wnt signaling in CNS endothelial cells (ECs) (Xu et al., 2004; Liebner et al., 2008; Daneman et al., 2009; Stenman et al., 2008; Ye et al., 2009).

1.2 The Neurovascular Unit

The neurovascular unit (NVU) is defined by the cellular and molecular constituents that reside at the interface of blood and neural tissue and contribute to the formation of a functional blood-brain barrier (BBB) (Blanchette and Daneman, 2015; Daneman and Prat, 2015; Zhao et al., 2015). The NVU is comprised of an intimate group of different cell types that includes endothelial cells (ECs), pericytes, astrocytes, perivascular macrophages, neurons, and microglia (Blanchette and Daneman, 2015; Daneman and Prat, 2015; Zhao et al., 2015). The ECs establish the tubular architecture of the vessels for the flux of cells, molecules, and ions through the vessel lumen (Blanchette and Daneman, 2015; Daneman and Prat, 2015; Zhao et al., 2015). Pericytes are tightly associated with the ECs on their ablumenal surface, and together are embedded within the basement membrane (Blanchette and Daneman, 2015; Daneman and Prat, 2015; Zhao et al., 2015). Astrocytes extend and wrap their end foot processes to cover the near-entirety of the vascular network (Blanchette and Daneman, 2015; Daneman and Prat, 2015; Zhao et al., 2015). Additional cell types, such as neurons, microglia, and perivascular macrophages, signal and interact with the vascular network to complete the neurovascular unit (Blanchette and Daneman, 2015; Daneman and Prat, 2015; Zhao et al., 2015).

1.3 Mammalian CNS angiogenesis

In mammals, the development of the neurovascular network is a highly stereotyped process that relies on angiogenesis, the development of new blood vessels from pre-existing ones. In mice, CNS angiogenesis begins at embryonic day 9.5 (E9.5) after the formation of the perineural vascular plexus (PNVP), the immature vascular network that circumscribes the outermost neuroepithelium (Blanchette and Daneman, 2015). Capillaries migrate from the PNVP into the deeper avascular regions of the neural parenchyma, ultimately forming the intraneural vascular plexus (INVP) (Blanchette and Daneman, 2015). Extensive branching, pruning and remodeling of the vessels, in addition to recruitment of perivascular cells, result in a mature neurovascular network (Blanchette and Daneman, 2015). While VEGF signaling in ECs is required for angiogenesis throughout the body, including the CNS, a unique angiogenic program that depends on canonical Wnt signaling is also required in CNS ECs (Xu et al., 2004; Liebner et al., 2008; Daneman et al., 2009; Stenman et al., 2008; Ye et al., 2009).

1.4 Characteristics of the BBB

The BBB is a specialized property of CNS ECs that provides a unique layer of filtration and protection for the neural tissue. The characteristics of this property include: (1) presence of tight junctions (consisting of claudins, occludins, and zona occludens) that restrict paracellular transport of small molecules and ions; (2) absence of fenestrations;

(3) suppression of transcytosis, which is largely regulated by the lipid transporter Mfsd2a; (4) downregulation of leukocyte adhesion molecules to minimize immune surveillance; (5) upregulation of efflux pumps; and (6) upregulation of nutrient transporters, such as the glucose transporter Glut1 and amino acid transporter Lat1 (Blanchette and Daneman, 2015; Daneman and Prat, 2015; Zhao et al., 2015). Recent studies have shown that these barrier properties are completely established by E15 in the developing mouse (Ben-Zvi et al., 2014). Furthermore, extensive genetic experiments have revealed that canonical Wnt signaling is critically important for the formation and maintenance of the BBB (Liebner et al., 2008; Daneman et al., 2009; Stenman et al., 2008; Wang et al., 2012; Zhou et al., 2014).

1.5 Canonical Wnt Signaling in CNS Endothelial Cells

In both development and disease, canonical Wnt signaling plays an important role in promoting cell proliferation, differentiation, and migration. Wnt ligands constitute a family of secreted glycoproteins that are highly conserved across metazoans, and they harbor a key lipid modification that is important for their secretion and signaling function (MacDonald et al., 2009). Frizzleds are seven-pass transmembrane proteins and the principal receptors for Wnt ligands (Bhanot et al., 1996). In mammals, there are 19 Wnt

ligands and 10 Fz receptors. The extent of Wnt-Fz specificity and the biological roles that such specificity might play have largely remained open questions.

In the absence of Wnt ligand, the transcriptional co-activator β-catenin is actively degraded by a multi-protein 'destruction complex' that consists of Axin, adenomatous polyposis coli (APC), glycogen synthase kinase 3 (GSK3), casein kinase 1 (CK1), and the E3 ubiquitin ligase subunit, β-Trcp (MacDonald et al., 2009). Specifically, the lack of a Wnt stimulus results in GSK3 and CK1 phosphorylation of β-catenin, which targets it for ubiquitination and subsequent proteosomal degradation (MacDonald et al., 2009). Upon Wnt binding to a Fz receptor and LDL receptor-related protein 5 or 6 (LRP5 or LRP6) co-receptor, GSK3 and CK1 activity are inhibited and cytoplasmic β-catenin levels are stabilized, allowing for increased translocation of β-catenin into the nucleus and subsequent transcriptional activation of T cell factor/lymphoid enhancer factor (TCF/LEF) target genes (MacDonald et al., 2009).

Multiple groups have shown that canonical Wnt signaling is essential for CNS angiogenesis and the development and maintenance of the blood-brain barrier (Xu et al., 2004; Liebner et al., 2008; Daneman et al., 2009; Stenman et al., 2008; Ye et al., 2009). For example, mice with endothelial cell-specific depletion of β-catenin display severe hemorrhaging in the brain and spinal cord (Daneman et al., 2009; Stenman et al., 2008; Zhou et al., 2014). These mutant vessels fail to migrate and sprout into the deeper layers

of the neural parenchyma, which leads to severe hypoxia and ischemia of the neural tissue (Daneman et al., 2009; Stenman et al., 2008; Zhou et al., 2014). Notably, these endothelial defects are only evident in the developing CNS vasculature, and not in the peripheral vasculature (Daneman et al., 2009; Stenman et al., 2008; Zhou et al., 2014). Furthermore, these vessels display a loss of BBB status (i.e. down-regulation of Glut1 and up-regulation of the fenestral diaphragm protein, plasmalemma vesicle-associated protein or PLVAP) (Daneman et al., 2009; Stenman et al., 2008; Zhou et al., 2014). Finally, post-natal removal of β-catenin in endothelial cells can also result in the loss of barrier status, suggesting that canonical Wnt signaling, in addition to its role in BBB development, is required for BBB maintenance (Liebner et al., 2008; Daneman et al., 2009; Stenman et al., 2008; Zhou et al., 2014).

In mice, different Wnts are expressed in various regions of the developing CNS. By *in situ* hybridization analysis, Wnt1, Wnt3, Wnt3a, and Wnt4 are predominantly found in the dorsal neural tube and spinal cord, while Wnt7a and Wnt7b are expressed in the ventral region (Daneman et al., 2009). Remarkably, embryos with genetic knockout of both Wnt7a and Wnt7b exhibit severe neurovascular defects that mirror the phenotypes observed from endothelial cell depletion of β-catenin (Daneman et al., 2009; Stenman et al., 2008). While Wnt7a and Wnt7b appear to be the primary Wnts involved in CNS angiogenesis, the set of Fz receptors that is responsible for transducing the signal

remains unclear. Fz4 has been shown to be involved in retinal and cerebellar angiogenesis, as well as barrier formation and maintenance in those regions; however, genetic removal of Fz4 does not completely recapitulate the Wnt7a and Wnt7b double KO phenotype (Xu et al., 2004; Stenman et al., 2008; Ye et al., 2009; Wang et al., 2012). Given that there are multiple Frizzleds expressed in endothelial cells (i.e. Fz1, Fz4, Fz6, and Fz8), these receptors may function redundantly in activating Wnt signaling for the proper development of the neurovasculature (Zhang et al., 2014).

1.6 Norrin-Fz4 Signaling in Retinal Angiogenesis and Blood-Retinal Barrier (BRB) Regulation

Canonical Wnt signaling also controls angiogenesis in the retina. Unlike the developing brain vasculature, which relies predominantly on Wnt7a and Wnt7b, the primary ligand responsible for retinal angiogenesis is Norrin (Figure 1A; Xu et al., 2004; Ye et al., 2009). A member of the TGFβ family, Norrin shares no homology with Wnt proteins and binds uniquely to Fz4 (Xu et al., 2004). Genetic deletion of Norrin results in glomeruloid vascular malformations and the failure of vessels to invade the retina (Ye et al., 2009). These phenotypes are completely phenocopied in the Fz4 knockout animals, supporting the model that Norrin functions through Fz4 in controlling retinal angiogenesis (Xu et al., 2004; Ye et al., 2009).

In the brain, Fz4 knockout mice exhibit a more severe vascular defect compared to Norrin knockout mice (Wang et al., 2012; Zhou et al., 2014). For example, genetic deletion of Fz4 results in a BBB breakdown in the cerebellum (demonstrated by up-regulation of PLVAP, and leakage of a molecular tracer into the neural parenchyma) (Wang et al., 2012; Zhou et al., 2014), whereas, Norrin knockout animals exhibit a milder BBB defect in this region (Wang et al., 2012; Zhou et al., 2014). The more severe phenotype in Fz4 knockout animals may be attributed to other ligands, such as Wnt7a and Wnt7b, which are signaling through Fz4.

In an attempt to identify novel transmembrane and secreted proteins involved in regulating the retinal vasculature, Junge et al. conducted a reverse genetic screen in mice targeting 475 genes (Junge et al., 2009). From this screen, Tetraspan12 (Tspan12) was identified to be involved in retinal angiogenesis (Figure 1A; Junge et al., 2009). Remarkably, knockout of Tspan12 exhibited phenotypes that were reminiscent of the Norrin and Fz4 knockout mice, albeit the vascular defects in the Tspan12 KO mice were slightly milder (Junge et al., 2009). Furthermore, Tspan12 KO animals exhibit no BBB defects in the brain (unpublished). While the mechanism of action for Tspan12 remains unclear, it appears to boost Norrin-Fz4 signaling specifically, as assessed by an *in vitro* reporter assay for canonical Wnt signaling (Junge et al., 2009; Lai et al., 2017).

1.7 Gpr124 is a Specific Co-activator for Wnt7a and Wnt7b

To identify novel genes involved in tumor angiogenesis, St. Croix et al. compared gene expression data from human endothelial cells derived from tumors or from normal tissue (St. Croix et al., 2000). From this analysis, they identified nine novel cell surface receptors that appeared to be highly upregulated in tumor endothelium (St. Croix et al., 2000). Among the nine was tumor endothelial marker 5 (TEM5), also known as G-protein-coupled receptor 124 (Gpr124) (St. Croix et al., 2000).

An orphan receptor classified under the adhesion GPCR family, Gpr124 is predominantly and abundantly expressed in endothelial cells (Kuhnert et al., 2010; Anderson et al., 2011; Cullen et al., 2011). Surprisingly, genetic knockout of Gpr124 in mice displayed a severe CNS-specific vascular defect: hemorrhaging in the forebrain and spinal cord with vessels that failed to properly vascularize the neural tissue in these regions (Kuhnert et al., 2010; Anderson et al., 2011; Cullen et al., 2011). Given the similarity between Gpr124 knockout and the Wnt7a and Wnt7b double knockout phenotypes, our lab explored whether Gpr124 was activating the canonical Wnt signaling pathway to promote CNS angiogenesis (Zhou and Nathans, 2014). Through extensive *in vitro* Wnt reporter assays and *in vivo* genetic experiments, our lab discovered that Gpr124 is a ligand-specific co-activator for Wnt7a and Wnt7b (Figure 1B; Zhou and Nathans, 2014). What remained unclear, however, was how mechanistically Gpr124 functions with

Wnt7a and Wnt7b to activate the canonical pathway. Furthermore, while Gpr124 could stimulate Wnt7a-Fz4-Lrp5 signaling, it had essentially no effect on Wnt7a-Fz4-Lrp6 signaling (Figure 1B; Zhou and Nathans, 2014). Both Lrp5 and Lrp6 are highly homologous co-receptors for Wnt ligands, and are largely interchangeable and functionally redundant in neurovascular development (MacDonald et al., 2009; Zhou et al., 2014). Given the inability of Gpr124 to stimulate Wnt7a-Fz4-Lrp6 signaling *in vitro*, our lab proposed that perhaps a missing component (Protein X) is required in conjunction with Gpr124 to activate this pathway (Figure 1B; Zhou and Nathans, 2014).

Figure 1. Canonical Wnt Signaling in CNS angiogenesis and the regulation of the BRB/BBB.

(A) Norrin/Fz4/Lrp5/Tspan12 signaling promotes angiogenesis in the retina and regulates the BRB. (B) Wnt7/Fz/Lrp5/Gpr124 signaling controls angiogenesis in the forebrain and regulates the BBB. An unidentified 'Protein X' may be a part of the Wnt7/Fz/Lrp5/Gpr124 signaling cassette. Modified from Zhou and Nathans, 2014.

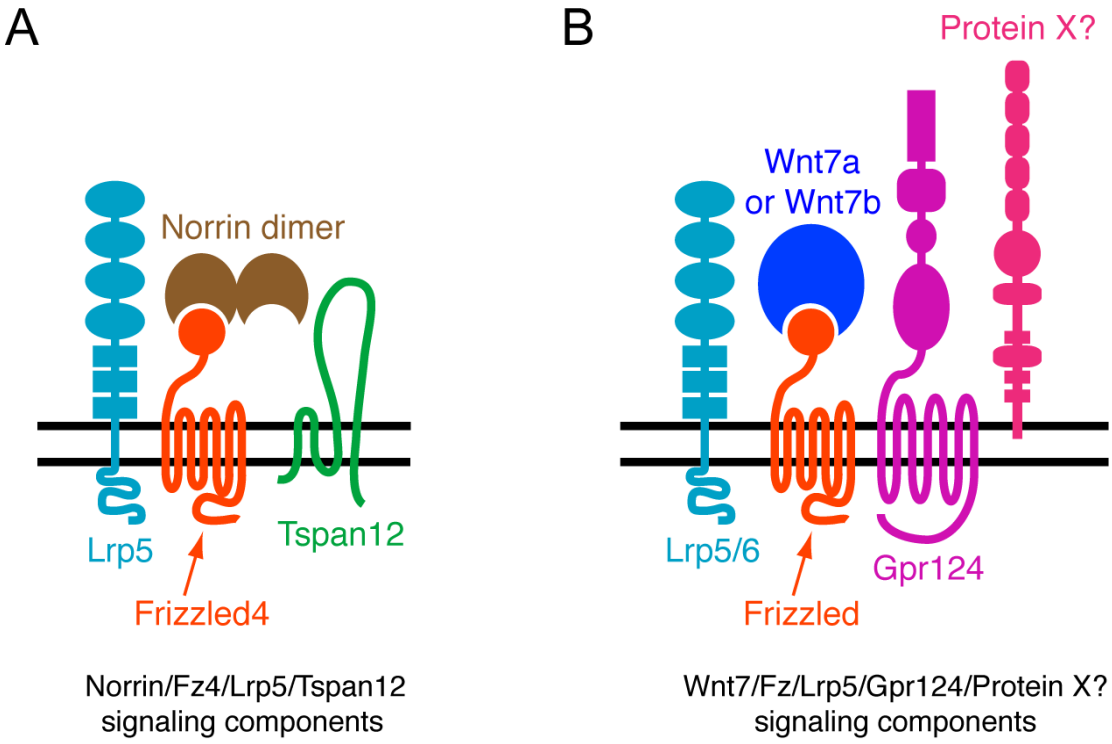

Chapter 2

Reck is a novel activator of Wnt7a/Wnt7b signaling

Modified from: Vanhollebeke, B., Stone, O.A., Bostaille, N., Cho, C., Zhou, Y., Maquet, E., Gauquier, A., Cabochette, P., Fukuhara, S., Mochizuki, N., Nathans, J., Stainier, D.Y. (2015). Tip cell-specific requirement for an atypical Gpr124- and Reck-dependent Wnt/β-catenin pathway during brain angiogenesis. *eLife*. 4:e06489.

Data generated by Chris Cho: Section 2.2

2.1 Reck is required for brain vascular development in zebrafish

In zebrafish, *gpr124* mutants display brain-specific vascular defects as well as missing dorsal root ganglia (DRG). In order to identify the components of the molecular pathway through which Gpr124 operates, we tested whether previously described regulators of

DRG formation (Budi et al., 2008; Honjo et al., 2008; Prendergast et al., 2012; Malmquist et al., 2013) could, like Gpr124, additionally control CNS angiogenesis. Using a morpholino knock-down approach, we identified Reck, a GPI-anchored MMP inhibitor and angiogenic modulator (Oh et al., 2001) as a novel essential regulator of brain vascularization (Figure 2A). Reck and Gpr124 knockdown embryos exhibit identical CNS-specific vascular defects without detectable intersegmental vessels (ISV) or gross morphological phenotypes (Figure 2B and 2E). Other DRG regulators like Sorbs3 (Malmquist et al., 2013) and Erbb3b (Honjo et al., 2008) do not appear to modulate CNS angiogenesis specifically (Figure 2A). Reck knock-down dose-dependently blocked brain vascularization (Figure 2B), and at doses of morpholino above 1 ng, brains remained avascular. As previously reported, *reck* morphants completely lack DRGs at 72 hpf (Prendergast et al., 2012) despite normal initial specification of *sox10*:mRFP^{+} neuroglial cells, much like *gpr124* mutants.

The remarkable phenotypic similarities observed after *gpr124* and *reck* knock-downs in two settings of distinct embryological origin led us to probe their functional relationship. In both the CNS vascular and peripheral neurogenic settings, ectopic expression of Gpr124 or Reck could compensate for their respective loss-of-function but no functional epistatic relationship could be detected, that is, the absence of one protein could not be rescued by overexpression of the other (Figure 2C and 2D). This result is

compatible with one of the following two scenarios: Gpr124 and Reck act in independent parallel pathways, or they act in concert to control a common signaling pathway during both CNS angiogenesis and DRG neurogenesis.

2.2 Reck and Gpr124 synergize to co-activate Wnt7a/Wnt7b signaling in reporter cells

In a previous study, we found that mouse Gpr124 co-activates Wnt/β-catenin signaling via Wnt7a/Wnt7b in a reporter cell line (Super Top Flash; STF [Xu et al., 2004]) and that signaling was further enhanced by co-transfection with Fz4 and Lrp5 (Zhou and Nathans, 2014). (We note that RNAseq analysis of STF cells showed low level expression of many Wnt signaling components, including Frizzled receptors, Lrp co-receptors, Gpr124, and Reck [Zhou and Nathans, 2014], which likely accounts for the signals observed when individual components are omitted from the transfection.) To determine whether Reck influences the Gpr124 dependence of Wnt7a- and Wnt7b-induced signaling, we co-transfected various combinations of Wnt7a or Wnt7b, Fz4, Lrp5 or Lrp6, Gpr124, and Reck into STF cells (Figure 3A). These experiments showed that Reck dramatically synergizes with Gpr124 in activating Wnt/β-catenin signaling in response to Wnt7a and Wnt7b, and that signaling is further increased by co-transfection with Fz4 together with Lrp5 or Lrp6. Both Gpr124 and Reck show well behaved dose–response curves, with

synergistic activity over a wide range of DNA concentrations (Figure 3B).

To test whether the combination of Reck and Gpr124 can co-activate signaling by Wnts other than Wnt7a and Wnt7b, we screened all 19 Wnts and Norrin for co-activation by Gpr124 alone, Reck alone, or Gpr124 plus Reck (Figure 3D). This experiment shows that the highest co-activation with Gpr124 plus Reck occurs with Wnt7a and Wnt7b, with other Wnts and Norrin showing little or no response. An analogous comparison among the ten Frizzled receptors showed that Gpr124/Reck stimulates Wnt7a- and Wnt7b-mediated signaling by multiple Frizzleds (Figure 3C). These data predict that cells expressing Gpr124, Reck, Lrp5 and/or Lrp6, and any of multiple Frizzleds will be responsive to Wnt7a or Wnt7b.

In earlier experiments, we observed that Gpr124 co-activation of Wnt7a- and Wnt7b-dependent signaling in STF cells could be stimulated by Lrp5 but not by Lrp6, and we postulated that one or more additional proteins might be required to enhance signaling in the presence of Lrp6 (Zhou and Nathans, 2014). The present experiments identify Reck as the missing protein since signaling in the presence of Reck can be stimulated by both Lrp5 and Lrp6 (Figure 3A), and they provide functional evidence that Gpr124 and Reck are major determinants of both the amplitude and ligand specificity of Wnt/β-catenin signaling.

Figure 2. Reck regulates CNS angiogenesis in zebrafish.

(A) Lateral views (anterior to the left) of *Tg(kdrl:GFP)* control and morphant embryos at 36 hpf (hindbrain region, upper panels) and 24 hpf (trunk region, bottom panels). Arrows point to the forming intracerebral central arteries (CtAs, upper panels) and intersegmental vessels (ISVs, lower panels). Scale bar, 50 μm. (B) Maximal intensity projection of a confocal *z*-stack of *Tg(kdrl:GFP)* wild-type and *reck* morphant cranial vasculature at 60 hpf in dorsal views (anterior to the left; scale bar, 100 μm) and quantification of hindbrain CtAs after Reck downregulation by anti-sense morpholino injections at various doses. (C) Quantification of hindbrain CtAs in control and *gpr124* or *reck* morphants at 60 hpf after injection at the one-cell stage of 100 pg RNA encoding Gpr124 or Reck. The insert shows a typical rescue. (D) Quantification of *ngn1*:GFP$^+$ DRGs in control and *gpr124* or *reck* morphants at 72 hpf after injection at the one-cell stage of 200 pg RNA encoding Gpr124 or Reck. *ngn1*:GFP$^+$ DRGs were counted on one side of the larvae. (E) Lateral view of wild-type and *reck* morphants at 5 dpf. In all panels, values represent means ± SD (*$p < 0.05$; **$p < 0.01$; Kruskal–Wallis test). Morpholino and RNA injections were performed as described in 'Materials and Methods'.

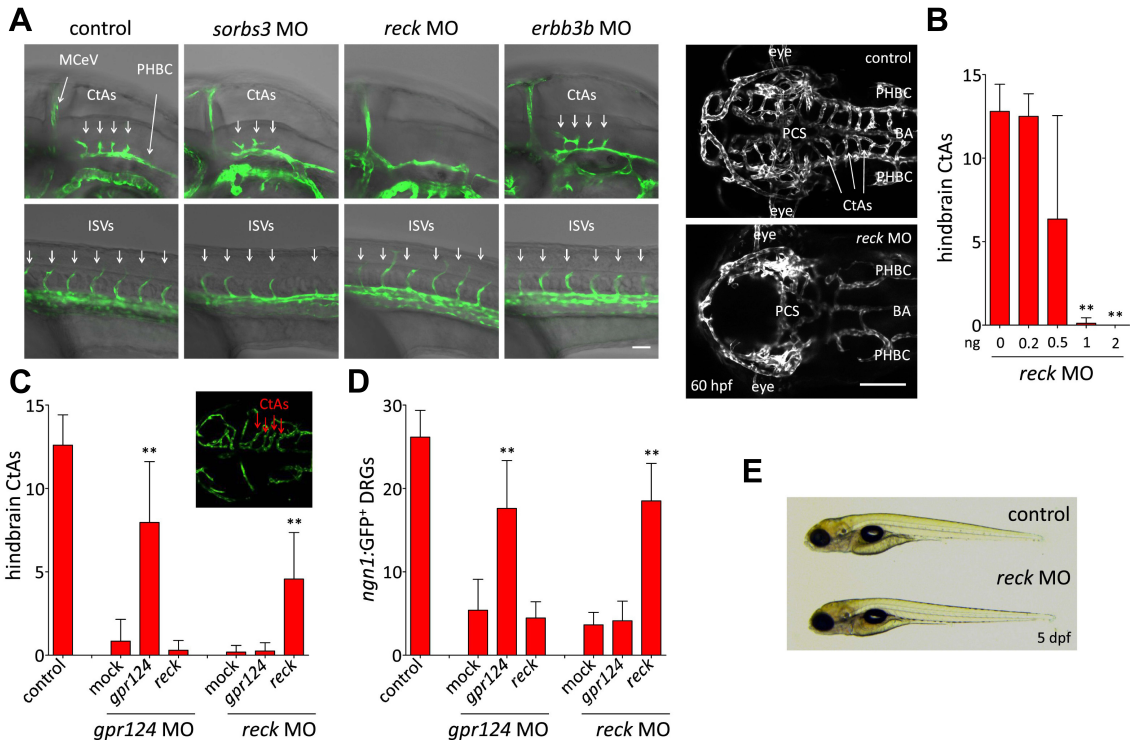
A
control
sorbs3 MO
reck MO
erbb3b MO
MCeV
PHBC
CtAs
ISVs
eye
control
PHBC
PCS
BA
reck MO
60 hpf
B
hindbrain CtAs
ng
0
0.2
0.5
1
2
reck MO
C
hindbrain CtAs
mock
gpr124
reck
gpr124 MO
reck MO
D
ngn1:GFP+ DRGs
E
control
reck MO
5 dpf

Figure 3. Synergy between Gpr124 and Reck in co-activating Wnt7a- and Wnt7b-dependent Wnt/β-catenin signaling in cell culture.

(A) Plasmids encoding Wnt7a (left) or Wnt7b (right), together with Lrp5 (top row), Lrp6 (center row), or no Lrp (bottom row) were transfected with Gpr124, Fz4, and/or Reck plasmids as indicated.(B) Titration of Gpr124 with or without Reck (left), and titration of Reck with or without Gpr124 (right). (C) Comparison of the ten mouse Frizzleds transfected with Lrp5 and Wnt7a, with or without Gpr124 and/or Reck. (D) Comparison of the nineteen mouse Wnts and Norrin, transfected with or without Gpr124 and/or Reck. Arrows point to Wnt7a and Wnt7b responses. Luciferase assays in transiently transfected STF cells were performed as described in 'Materials and Methods'. Values represent means ± SD.

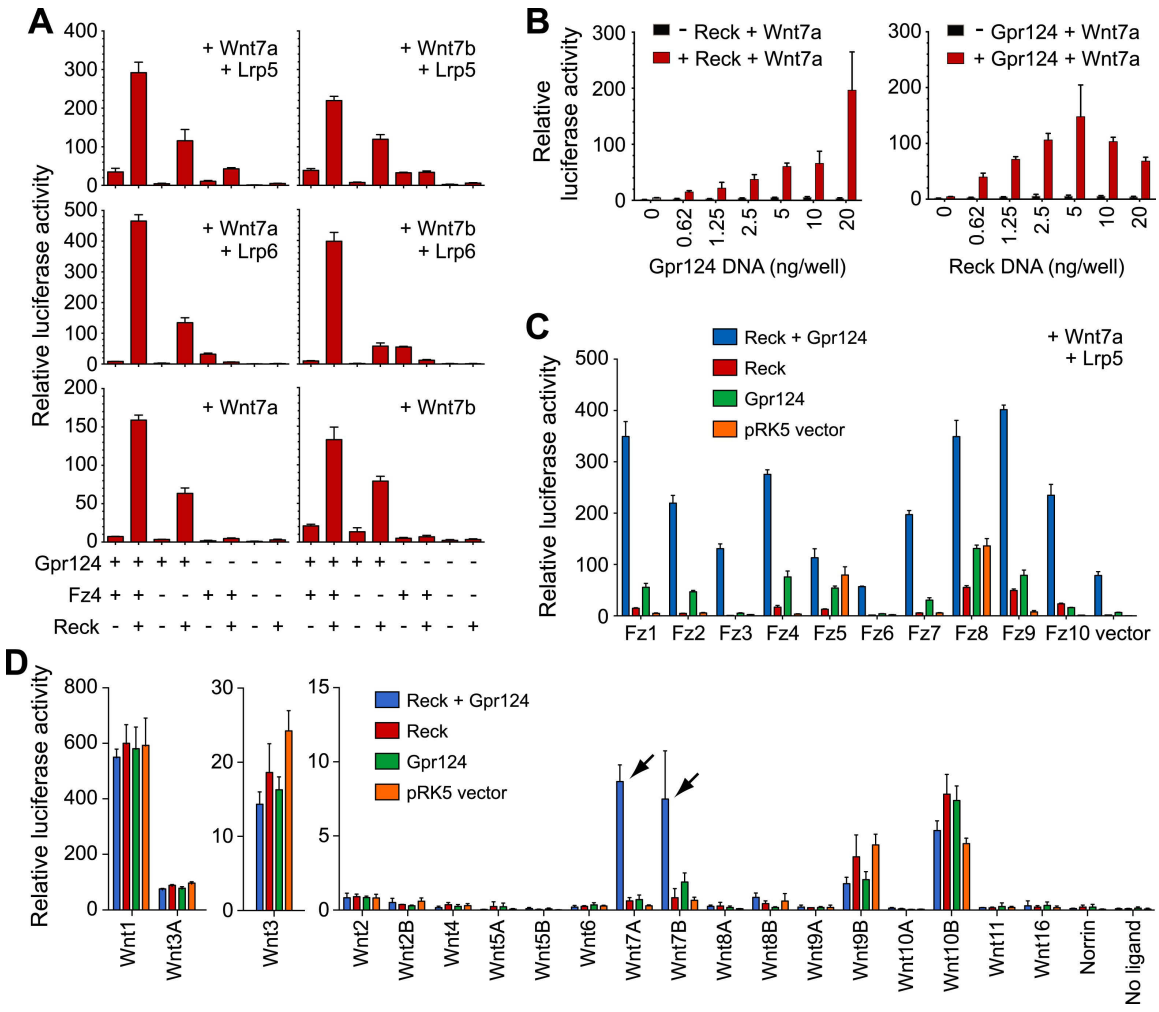
A
Relative luciferase activity
+ Wnt7a + Lrp5
+ Wnt7b + Lrp5
+ Wnt7a + Lrp6
+ Wnt7b + Lrp6
+ Wnt7a
+ Wnt7b
Gpr124
Fz4
Reck
B
Relative luciferase activity
- Reck + Wnt7a
+ Reck + Wnt7a
Gpr124 DNA (ng/well)
- Gpr124 + Wnt7a
+ Gpr124 + Wnt7a
Reck DNA (ng/well)
C
Relative luciferase activity
Reck + Gpr124
Reck
Gpr124
pRK5 vector
+ Wnt7a + Lrp5
Fz1 Fz2 Fz3 Fz4 Fz5 Fz6 Fz7 Fz8 Fz9 Fz10 vector
D
Relative luciferase activity
Reck + Gpr124
Reck
Gpr124
pRK5 vector
Wnt1 Wnt3A Wnt3 Wnt2 Wnt2B Wnt4 Wnt5A Wnt5B Wnt6 Wnt7A Wnt7B Wnt8A Wnt8B Wnt9A Wnt9B Wnt10A Wnt10B Wnt11 Wnt16 Norrin No ligand

Chapter 3

Reck and Gpr124 are essential receptor cofactors for Wnt7a/Wnt7b-specific signaling in mammalian CNS angiogenesis and BBB regulation

Modified from: Cho, C., Smallwood, P.M., Nathans, J. (2017). Reck and Gpr124 are essential receptor cofactors for Wnt7a/Wnt7b-specific signaling in mammalian CNS angiogenesis and blood-brain barrier regulation. *Neuron*. 95, 1056-1073.

Data generated by Chris Cho: All sections

3.1 Reck is required for canonical Wnt signaling in CNS ECs and for normal CNS angiogenesis

Reck has been extensively characterized as a matrix metalloproteinase (MMP) inhibitor; however, a connection to canonical Wnt signaling has not been previously described. To determine whether this novel Wnt function of Reck plays a role in mammalian neurovascular development, we studied *Reck* $^{\Delta ex2/\Delta ex2}$ and *Reck* $^{flex2/\Delta ex1}$*;Tie2-Cre* EC-specific knockout mouse embryos (Figure 4). *Reck* exon 2 deletion produces a hypomorphic allele (Chandana et al., 2010), whereas *Reck* exon 1 deletion produces a null allele (Oh et al., 2001). *Reck* ^{flex2} is a conditional allele in which exon 2 is flanked by *loxP* sites. The *Reck* $^{\Delta ex2/\Delta ex2}$ and *Reck* $^{flex2/\Delta ex1}$*;Tie2-Cre* genotypes circumvent the embryonic day (E)10.5 lethality seen with the *Reck* $^{\Delta ex1/\Delta ex1}$ genotype, which precludes an analysis of CNS vascularization (Oh et al., 2001; Chandana et al., 2010). In E13.5 embryos of both genotypes, hemorrhaging occurs in the forebrain and spinal cord (Figure 4B and 4C; Chandana et al., 2010; de Almeida et al., 2015), and ECs in the cortex, ganglionic eminences, and spinal cord form glomeruloid-like tufts instead of an interconnected vascular network (Figure 4A-C). Vascular density was significantly reduced in these regions (quantified in Figure 4E), and the hypovascular territories showed increased infiltration of non-endothelial GS Lectin$^+$ cells that predominantly co-stain for macrophage markers F4/80 or Cd11b (referred to hereafter as GS Lectin$^+$

macrophages; Figure 5). This phenotype closely matches the phenotype of *Gpr124* null embryos (Kuhnert et al., 2010; Anderson et al., 2011; Cullen et al., 2011; Zhou and Nathans, 2014). In these and all embryos described below, the growth of the embryo and the appearance of non-CNS vasculature were normal, implying that vascular defects were confined to the CNS. A complete list of all embryonic genotypes examined and the severities of their vascular phenotypes can be found in Table 1.

Given the emerging role of Reck as a specific co-activator of Wnt7a/Wnt7b signaling (Vanhollebeke et al., 2015), we investigated whether the CNS vascular defects in *Reck* mutant embryos are associated with a reduction in canonical Wnt signaling. Existing reporter lines for canonical Wnt signaling are based on transgenes expressing beta-galactosidase or GFP under the control of either the *Axin2* promoter or a juxtaposition of multimerized TCF/LEF sites and a minimal promoter (Jho et al., 2002; Maretto et al., 2003; Ferrer-Vaquer et al., 2010). The utility of these reporter lines is limited by (1) their capacity for expression in many cell types, which can make it difficult to visualize changes in canonical Wnt signaling in a minor cell type, and (2) random variegation in transgene expression. To resolve these problems, we generated a new Wnt reporter line by knocking into the ubiquitously expressed *Rosa26* locus the sequences coding for a histone H2B-GFP-6xmyc fusion protein under the control of 8xTCF/LEF binding sites and a minimal promoter, with the added feature that reporter expression also

requires removal of a *loxP-stop-loxP* (*LSL*) cassette by Cre-mediated recombination (Figure 6). This last feature represents a general strategy for cell-type-specific visualization of any reporter. Figure 6B-D shows that CNS ECs in phenotypically wild-type (WT) *Reck* $^{flex2/+}$*;Rosa26 Tcf/Lef-LSL-H2B-GFP;Tie2-Cre* embryos show strong and specific nuclear GFP that is absent in neighboring, non-ECs. In contrast, *Reck* $^{flex2/\Delta ex1}$*;Rosa26 Tcf/Lef-LSL-H2B-GFP;Tie2-Cre* embryos show significantly reduced nuclear GFP in the vascular tufts in the cortex, ganglionic eminences, and spinal cord compared to the phenotypically WT control, implying that Reck activity is required in CNS ECs for canonical Wnt signaling (Figure 6B-H).

If Reck is responsible for activating canonical Wnt signaling at a level upstream of beta-catenin stabilization, then artificially stabilizing beta-catenin should rescue the *Reck* mutant vascular phenotype. Exon 3 of the beta-catenin gene (*Ctnnb1*) harbors key phosphorylation sites for glycogen synthase kinase-3 (GSK-3) that target beta-catenin for degradation. We therefore combined EC-specific expression of CreER (from a *Pdgfb-CreER* transgene) and the *Ctnnb1*^{flex3} allele, which contains *loxP* sites flanking exon 3, to produce an in-frame deletion of this region and artificially stabilize beta-catenin specifically in ECs. Gestational day (GD)10.5 females were injected intraperitoneally (IP) with 1.5 mg of tamoxifen, and their embryos were harvested three days later for analysis. The resulting E13.5 *Reck* $^{\Delta ex2/\Delta ex2}$*;Ctnnb1*$^{flex3/+}$*;Pdgfb-CreER* embryos display

little to no hemorrhaging in the forebrain and spinal cord, and the vascular network in the cortex, ganglionic eminences, and spinal cord is substantially denser than in *Reck* $^{\Delta ex2/\Delta ex2}$ embryos (compare Figure 4C and 4D; quantification in Figure 4E). We ascribe the incomplete phenotypic rescue to the relatively brief (three day) time window during which rapid CNS growth may make it difficult for angiogenesis in *Reck* $^{\Delta ex2/\Delta ex2}$*;Ctnnb1*$^{flex3/+}$*;Pdgfb-CreER* embryos to catch up to their WT counterparts. Control experiments in which *Ctnnb1*$^{flex3/+}$*;Pdgfb-CreER* was used to stabilize beta-catenin in ECs on a phenotypically WT genetic background during the same E10.5-13.5 time window showed little or no effect on CNS angiogenesis (Zhou and Nathans, 2014). Despite the partial rescue of the CNS angiogenesis phenotype, *Reck* $^{\Delta ex2/\Delta ex2}$*;Ctnnb1*$^{flex3/+}$*;Pdgfb-CreER* embryos continue to show elevated numbers of GS Lectin^{+} macrophages in the CNS parenchyma (Figure 4D and 4F). Together, these data imply that Reck's role in CNS angiogenesis is via activation of canonical Wnt signaling in ECs.

3.2 Reck is required for the development of the BBB

The development of the BBB is tightly coupled to CNS angiogenesis, and decreased canonical Wnt signaling perturbs both of these processes (Wang et al., 2012; Zhou et al., 2014). We therefore studied *Reck* $^{flex2/\Delta ex1}$*;Tie2-Cre* mice to determine whether Reck activity in ECs also plays a role in BBB development. Since BBB development is largely

complete by E15.5 (Ben-Zvi et al., 2014) and *Reck* $^{flex2/\Delta ex1}$*;Tie2-Cre* embryos survive to birth, we assessed BBB integrity in neonatal pups by IP injection of a membrane impermeable sulfo-N-hydroxysuccinimide-long chain-biotin (sulfo-NHS-biotin) tracer. As expected from their appearance at E13.5, *Reck* $^{flex2/\Delta ex1}$*;Tie2-Cre* neonates exhibit impaired angiogenesis and severe hemorrhaging in the cortex (Figure 7). Interestingly, the hypothalamus and brainstem, where vascular density was close to normal and there was no hemorrhaging, showed extensive sulfo-NHS-biotin leakage, and lower level leakage was widely present in many subcortical regions. Consistent with a defect in BBB development, the fenestral diaphragm protein plasmalemma vesicle-associated protein (PLVAP), which serves as a marker for the differentiation state of ECs and correlates with a compromised BBB (Stan et al., 2004; Wang et al., 2012), was elevated throughout the *Reck* $^{flex2/\Delta ex1}$*;Tie2-Cre* CNS. These data point to a central role for endothelial Reck in BBB development.

3.3 Reck signaling is partially redundant with Norrin signaling in promoting CNS angiogenesis and BBB maintenance

Norrin signaling, in addition to being largely responsible for retinal angiogenesis and the development of the BRB, has been shown to function in parallel with Gpr124 to regulate angiogenesis and barrier integrity in the brain (Zhou et al., 2014; Zhou and Nathans, 2014). To examine the functional and anatomic relationship between Reck- and Norrin-mediated Wnt signaling in CNS angiogenesis, we analyzed embryos that carry various allelic combinations of *Reck* and *Ndp* (Norrin) mutant alleles (Figure 8). (Since *Ndp* is an X-linked gene, *Ndp* null male mutant mice are designated $Ndp^{\Delta/Y}$). Previous analyses of hindbrain vasculature of *Gpr124* and *Ndp* mutant embryos were performed at E11.5 (Zhou and Nathans, 2014). To facilitate comparisons between that study and this one, we analyzed embryos at this time point. Consistent with the phenotypes observed at E13.5, E11.5 $Reck^{flex2/\Delta ex2}$*;Tie2-Cre* embryos show hemorrhaging in the forebrain and spinal cord (data not shown) with no obvious vascular defects in subcortical tissue, including the hindbrain (Figure 8B and 8F). $Reck^{flex2/+}$*;*$Ndp^{\Delta/Y}$*;Tie2-Cre* embryos appear phenotypically normal and show no vascular abnormalities in the developing CNS, similar to $Reck^{flex2/+}$*;Tie2-Cre* embryos (Figure 8A, 8C, and 8F). However, a dramatic phenotype is observed in $Reck^{flex2/\Delta ex2}$*;*$Ndp^{\Delta/Y}$*; Tie2-Cre* mutants: in addition to more pronounced hemorrhaging in the forebrain and spinal cord (data not shown), vascular density is markedly reduced in the hindbrain, and these hypovascular areas are infiltrated with a large numbers of GS Lectin^{+} macrophages (Figure 8D and 8F). Interestingly, vascular

knockout of both *Reck* and *Gpr124* produces a very similar hindbrain vascular phenotype (Figure 8E and 8F), implying that the actions of Reck and Gpr124 in Wnt7a/Wnt7b signaling in vivo are synergistic, as observed in cell culture experiments (Vanhollebeke et al., 2015), and that the absence of either one reduces but does not abolish Wnt7a/Wnt7b signaling. The genetic interaction between *Reck* and *Ndp* closely mirrors that observed between *Gpr124* and *Ndp* (Zhou and Nathans, 2014), and together they support a model in which Reck/Gpr124- and Norrin-mediated signaling represent two parallel pathways that function redundantly in the hindbrain to promote angiogenesis.

Maintenance of the BBB depends on canonical Wnt signaling in mature ECs (Liebner et al., 2008; Wang et al., 2012; Zhou et al., 2014). We therefore investigated the functional relationship between Reck- and Norrin-mediated signaling on BBB maintenance postnatally. Mice carrying various combinations of *Reck* and *Ndp* alleles together with *Pdgfb-CreER* were injected IP with 50 μg of 4-hydroxytamoxifen (4-HT) at P3 and P4, followed by analysis of P7 brains for sulfo-NHS-biotin leakage. For all genotypes characterized, the vasculature was structurally intact and devoid of hemorrhaging. $Reck^{flex2/\Delta ex1}$*;Pdgfb-CreER* and $Reck^{flex2/+}$*;*$Ndp^{\Delta/Y}$*;Pdgfb-CreER* mice showed no evidence of vascular leakage in the brain parenchyma (Figure 8G and 8H). Consistent with the presence of an intact BBB, CNS ECs in these mice express the tight junction marker Claudin-5 with little or no expression of PLVAP (Claudin-5^{+};$PLVAP^{-}$)

(Figure 8G, 8H, and quantified in 8J). In contrast, postnatal loss of both Reck and Norrin (*Reck* $^{flex2/\Delta ex1}$*;Ndp*$^{\Delta/Y}$*;Pdgfb-CreER*) produced extensive leakage throughout the brain, most prominently in the cortex (Figure 8I). In these mice, CNS ECs showed reduced Claudin-5 expression and widespread PLVAP upregulation (Claudin-5^{-};PLVAP^{+}), consistent with the loss of BBB integrity (Figure 8I and quantified in 8J).

These changes closely resemble the BBB breakdown and Claudin-5^{-};PLVAP^{+} conversion produced in an analogous experiment featuring the combined postnatal loss of Gpr124 and Norrin (Zhou and Nathans, 2014). In both of these experiments, treatment with 4-HT in early postnatal life produced efficient *Pdgfb-CreER*-mediated recombination of the *Reck* or *Gpr124* conditional alleles, as judged by the near-complete conversion of CNS ECs from PLVAP- to PLVAP+ (Figure 8I; Zhou and Nathans, 2014). To the extent that some ECs do not undergo recombination, then these experiments would be under-estimating the severity of the loss-of-function phenotypes. We also quantified cortical vascular density and observed a ~35% reduction for both *Reck* $^{flex2/\Delta ex1}$*;Pdgfb-CreER* and *Reck* $^{flex2/\Delta ex1}$*;Ndp*$^{\Delta/Y}$*;Pdgfb-CreER* when compared to *Reck* $^{flex2/+}$*;Ndp*$^{\Delta/Y}$*;Pdgfb-CreER*, suggesting a role for Reck in post-natal vascular development and remodeling (p-value<0.01, data not shown). Together, these data imply functionally redundant roles for Reck/Gpr124 and Norrin signaling in maintaining BBB integrity.

3.4 *Reck* genetically interacts with *Gpr124* and *Wnt7a/Wnt7b*

The severe E11.5 hindbrain angiogenesis defect produced by the combined EC-specific loss of Reck and Gpr124 suggested that a systematic exploration of the effects of reduced *Reck* and *Gpr124* gene dosage would be of interest. Figure 9 shows such an analysis at a time point (E13.5) and in a format that are identical to those in Figure 4. *Reck* $^{flex2/+}$*;Gpr124* $^{fl/+}$*;Tie2-Cre* embryos appear phenotypically normal (Figure 9A), while *Reck* $^{flex2/\Delta ex2}$*;Gpr124* $^{fl/+}$*;Tie2-Cre* and *Gpr124* $^{fl/\Delta}$*;Tie2-Cre* embryos exhibit vascular defects that are comparable to those of *Reck* $^{flex2/\Delta ex1}$*;Tie2-Cre* embryos (compare Figures 4B and 9B-C). Specifically, these embryos show: (1) moderate hemorrhaging in the forebrain and distal spinal cord; (2) reduced vascular density in the cortex, MGE, and spinal cord; and (3) increased abundance of GS Lectin^{+} macrophages in the MGE and spinal cord (Figure 9B, 9C, 9F, and 9G). This phenotype is exacerbated in *Reck* $^{flex2/+}$*;Gpr124* $^{fl/\Delta}$*;Tie2-Cre* and *Reck* $^{flex2/\Delta ex2}$*;Gpr124* $^{fl/\Delta}$*;Tie2-Cre* mutants, the latter exhibiting the most severe phenotype with pronounced hemorrhaging in the forebrain and along the entire length of the spinal cord (Figure 9D and 9E). Additionally, the vascular density is further reduced in the cortex and MGE for both of these mutants, as well as in the spinal cord for *Reck* $^{flex2/\Delta ex2}$*;Gpr124* $^{fl/\Delta}$*;Tie2-Cre* mutants when compared to *Reck* $^{flex2/\Delta ex2}$*;Gpr124* $^{fl/+}$*;Tie2-Cre* and *Gpr124* $^{fl/\Delta}$*;Tie2-Cre* mutants (Figure 9B-F). The progressive increase in severity of the angiogenic phenotype that is elicited by EC-

specific decrements in *Reck* and/or *Gpr124* gene dosage imply that there is a correspondingly graded cell biological response of developing ECs to different levels of Reck/Gpr124-mediated signaling.

Although all of the CNS angiogenesis phenotypes described here are associated with accumulation of GS Lectin^{+} macrophages in the CNS parenchyma, the number of macrophages does not continue to increase with increasing severity of the angiogenic phenotype (i.e. reduced vascular density; Figure 9G). Instead, there is a drop in the number of macrophages in the cortex in *Reck* $^{flex2/+}$*;Gpr124* $^{fl/\Delta}$*;Tie2-Cre* and *Reck* $^{flex2/\Delta ex2}$*;Gpr124* $^{fl/\Delta}$*;Tie2-Cre* embryos compared to *Gpr124* $^{fl/\Delta}$*;Tie2-Cre* embryos, and there is a similar drop in the number of macrophages in the spinal cord in *Reck* $^{flex2/\Delta ex2}$*;Gpr124* $^{fl/\Delta}$*;Tie2-Cre* embryos when compared to *Reck* $^{flex2/+}$*;Gpr124* $^{fl/\Delta}$*;Tie2-Cre* embryos. These data suggest that a baseline vascular infrastructure is required for maximal macrophage infiltration into damaged CNS tissue.

Cell culture experiments show that Reck functions as a specific co-activator for Wnt7a/Wnt7b signaling (Vanhollebeke et al., 2015), but, as yet, there is no *in vivo* evidence for such an interaction. Previous work has shown that *Wnt7a* $^{\Delta/\Delta}$*;Wnt7b* $^{+/\Delta}$ mutant mice have a near-normal neurovascular phenotype (Stenman et al., 2008; Daneman et al., 2009; Posokhova et al., 2015). Consistent with that work, Figure 10 (A, B, E and F) shows that the vascular densities in the cortex, MGE, and spinal cord of

Wnt7a$^{\Delta/\Delta}$*;Wnt7b*$^{+/\Delta}$ and *Reck*$^{+/\Delta ex2}$*;Wnt7a*$^{+/\Delta}$*;Wnt7b*$^{+/\Delta}$ embryos at E13.5 are comparable to that of WT embryos, the only difference being modest elevations in macrophage counts in the cortex in *Reck*$^{+/\Delta ex2}$*;Wnt7a*$^{+/\Delta}$*;Wnt7b*$^{+/\Delta}$ embryos and in the cortex, MGE, and spinal cord in *Wnt7a*$^{\Delta/\Delta}$*;Wnt7b*$^{+/\Delta}$ embryos (Figure 10A, 10B, and 10F). We reasoned that if Reck and Wnt7a/Wnt7b function through the same signaling complex, then heterozygosity for *Reck*$^{\Delta ex2}$, which by itself confers a normal phenotype, on a genetically sensitized *Wnt7a*$^{\Delta/\Delta}$*; Wnt7b*$^{+/\Delta}$ background could bring out a vascular phenotype. In agreement with this idea, Figures 10C, 10E, and 10F show that *Reck*$^{+/\Delta ex2}$*;Wnt7a* $^{\Delta/\Delta}$*;Wnt7b*$^{+/\Delta}$ embryos have decreased CNS vascular density in the cortex and MGE together with increased numbers of GS Lectin^{+} macrophages in the MGE. Furthermore, homozygosity for *Reck*$^{\Delta ex2}$ on the *Wnt7a*$^{\Delta/\Delta}$*;Wnt7b*$^{+/\Delta}$ background produces a phenotype that is substantially more severe than that of *Reck*$^{\Delta ex2/\Delta ex2}$ embryos (Figure 10D-F). Specifically, the cortex and spinal cord of *Reck*$^{\Delta ex2/\Delta ex2}$*;Wnt7a*$^{\Delta/\Delta}$*;Wnt7b*$^{+/\Delta}$ mutants are almost completely avascular. We also observe a reduction in GS Lectin^{+} macrophages in the cortex and MGE of *Reck*$^{\Delta ex2/\Delta ex2}$*;Wnt7a*$^{\Delta/\Delta}$*;Wnt7b*$^{+/\Delta}$ embryos compared to *Reck* $^{+/\Delta ex2}$*;Wnt7a*$^{\Delta/\Delta}$*;Wnt7b*$^{+/\Delta}$ embryos, consistent with the suggestion above that an intact vascular network is required for efficient infiltration of macrophages into the brain parenchyma (Figures 10C, 10D, and 10F). In sum, these data provide genetic evidence that Reck functionally cooperates with Gpr124 and Wnt7a/Wnt7b in CNS angiogenesis.

3.5 The N-terminal domains of Reck and Gpr124 are required for synergistic Wnt7a/Wnt7b activation *in vitro*

Given the evidence that Reck and Gpr124 function as specific co-activators of Wnt7a/Wnt7b signaling (Zhou and Nathans, 2014; Posokhova et al., 2015; Vanhollebeke et al., 2015), we sought to define the regions that are required for this activity. The ectodomain of Gpr124 consists of an N-terminal leucine-rich repeat domain (LRR), an immunoglobulin-like domain (Ig), a hormone receptor domain (HormR), and a putative GPCR-Autoproteolysis Inducing domain (GAIN) (Figure 11A). We generated deletion mutants for each of these domains and used cell-surface biotinylation of C-terminally epitope tagged proteins to show that the plasma membrane localization of each mutant in transfected cells was comparable to WT Gpr124 (Figure 11B). Using a Super TOP Flash (STF) luciferase reporter cell line for canonical Wnt signaling (Xu et al., 2004), we co-transfected Reck, Wnt7a, and each of the Gpr124 mutants and observed that deletion of the LRR and/or Ig domains largely eliminated Gpr124 activity, consistent with a previous report (Posokhova et al., 2015), whereas deletion of the HormR or GAIN domain had only a modest effect on activity (Figure 11C).

The function of Reck as an MMP inhibitor has been attributed to its Kazal-like domains (Chang et al., 2008). The functions of other domains, which include five tandem copies of a domain with a di-cysteine motif (CC1-5), a Frizzled-like cysteine-rich domain

(Fz-like CRD), and two EGF-like domains, remain largely uncharacterized. To identify the domains of Reck required for canonical Wnt signaling, we inserted a Myc-epitope immediately after the signal peptide and then generated various domain deletions (Figure 12A). Plasma membrane localization for each mutant was confirmed by both cell-surface biotinylation and live-cell immunostaining for Myc (Figure 12D and 12E). We note a pattern of cell-surface puncta in our live-cell immunostaining images, which implies that Reck localizes in membrane zones, perhaps in lipid rafts or caveolae (Figure 12E). Using STF reporter cells co-transfected with Gpr124, Wnt7a, and each of the Reck mutants, we observed that deletion of the five tandem CC domains (ΔCC1-5) completely abolished Reck activity (Figure 12B). Other truncation mutants (ΔFz-like CRD, ΔC-term1, ΔC-term2) substantially reduced but did not eliminate activity; it is unclear whether these reductions represent an indirect effect due to the shortened distance from the plasma membrane to more N-terminal domains. These data imply that the most N-terminal domains of both Gpr124 (LRR-Ig) and Reck (CC1-5) play a critical role in activating Wnt7a/Wnt7b signaling.

Based on these results, we focused on CC1-5 and constructed a series of deletion mutants to more precisely define the role of individual CC domains (Figure 12C-E). ΔCC2 and ΔCC5 were able to stimulate Wnt activity at levels comparable to WT Reck, while ΔCC3 had ~50% WT activity. The most dramatic defects in activity were observed

for ΔCC1 and ΔCC4, with the latter showing a complete loss of function. We performed an initial analysis of Reck CC4 function by converting the presumptive surface residues to alanines in blocks of several amino acids per mutant; however, none of the 14 alanine-scanning mutants in CC4 showed a significant reduction in Wnt signaling when co-transfected with Wnt7a and Gpr124 (data not shown). One possible explanation for this result is that there are multiple non-adjacent surface regions that are functionally redundant for CC4 function. Alternatively, CC4 may be important only in relation to the overall architecture and/or spacing of other Reck domains.

3.6 Direct binding between domains of Reck and Gpr124 that activate canonical Wnt signaling

The biochemical mechanism by which Reck and Gpr124 synergistically enhance Wnt signaling has not been determined. Since both co-activators are membrane proteins, the simplest possibility is that they form part of the signaling complex with the receptor, co-receptor, and ligand. Thus far, the only reported experiment that directly addresses their physical association is a proximity ligation assay indicating that a measurable fraction of Reck and Gpr124 reside near one another when they are over-expressed in transiently co-transfected cells (Vanhollebeke et al., 2015). To test for a direct interaction between the domains of Reck and Gpr124 that are critical for canonical Wnt signaling, we generated

alkaline phosphatase (AP) fusion proteins with the critical Wnt-activating domains of Reck (CC1-5) and Gpr124 (LRR-Ig). In these initial constructs, we included a cartilage oligomeric matrix protein (COMP) domain for pentamerization to increase the avidity of the probes (Figures 13A and 14A). These COMP-AP fusion proteins were tested for their ability to bind Gpr124, Reck, or various of their deletion derivatives on the surface of transfected COS-7 cells.

The Reck(CC1-5)-COMP-AP probe bound robustly to COS-7 cells transfected with Gpr124 but not its close homologue Gpr125, which does not activate Wnt7a/Wnt7b signaling or synergize with Reck (Figure 13B; Zhou and Nathans, 2014; Vanhollebeke et al., 2015). Deletion of the Wnt-activating domains of Gpr124 (ΔLRR, ΔIg, and ΔLRR+Ig) abolished Reck(CC1-5)-COMP-AP binding, while deletion of the GAIN domain had little or no effect (Figure 13B). Deletion of the Gpr124 HormR domain, which reduces canonical signaling by ~50% in STF cells (Figure 11C), reduced Reck(CC1-5)-COMP-AP binding below the limit of detection (Figure 13B). It is possible that in Gpr124(ΔHormR), the LRR and Ig domains are positioned in a way that hinders their interaction with Reck(CC1-5)-COMP-AP. [In reciprocal experiments involving incubation of Gpr124(LRR-Ig)-COMP-AP to COS-7 cells transfected with Reck and its deletion derivatives, the greatest decrements in binding were with Reck ΔCC1-5, ΔCC2-5, ΔCC1, and ΔCC2 (Figures 14A and 14C), but we note that these binding experiments

have a relatively low signal-to-noise ratio.] These data point to the Reck(CC1-5) domain as important for both Gpr124(LRR-Ig) binding and Wnt7a/Wnt7b signaling.

To investigate protein-protein binding in a cell-free system, Gpr124(LRR-Ig)-Fc and Reck(CC1-5)-Fc fusion proteins ("baits") were captured on Protein-G-coated wells and incubated with various COMP-AP probes. Consistent with the COS-7 binding data, Reck(CC1-5)-COMP-AP bound robustly to Gpr124(LRR-Ig)-Fc but not to a negative control bait (Figure 13C). Reciprocally, Gpr124(LRR-Ig)-COMP-AP bound to Reck(CC1-5)-Fc, albeit weakly, but not to a negative control bait (Figure 14B). Importantly, Reck(CC1-2)-COMP-AP and Reck(CC1)-COMP-AP bound robustly to Gpr124(LRR-Ig)-Fc, showing that Reck(CC1) is not only necessary but also sufficient for direct binding (Figure 13C).

To identify the region of Reck(CC1) that contacts Gpr124, we constructed 16 alanine scanning block substitutions in Reck(CC1)-COMP-AP, together covering nearly all CC1 residues other than glycine and cysteine (Figure 13D). By immunoblotting and AP enzyme activity, seven of the 16 CC1 mutants were expressed at readily detectable levels (Ala Scan-2, -7, -9, -10, -14, -15, and -16; Figure 14D and 14E), and these were used for binding experiments after equalizing their concentrations. Only two of the seven CC1 mutants failed to bind to Gpr124(LRR-Ig)-Fc: Ala Scan-9 and -10 (Figure 13E). Single alanine substitution of the five residues encompassed by these two adjacent block

substitutions showed that three of the five – R69A, P71A, and Y73A – greatly decreased binding (Figure 13F). These three residues are highly conserved across vertebrates, whereas adjacent residues that are dispensable for binding are not (Figure 13G). Taken together, these experiments pinpoint a highly conserved region – most likely a binding surface – on Reck CC1 that is required for Gpr124(LRR-Ig) binding.

3.7 The Reck CC1 binding site for Gpr124 is important for Wnt signaling and CNS angiogenesis

To assess the importance of the Reck CC1 binding site for canonical Wnt signaling, we generated full-length Reck derivatives that contained the Ala Scan-9, -10, and -9+10 substitutions. The three mutants exhibited a level of plasma membrane accumulation similar to WT, as determined by surface biotinylation (Figure 14F). When cotransfected with Gpr124 and Wnt7a in STF cells, all three mutants showed ~50% of the activity level of WT Reck (Figure 15A), and this reduction was consistent over a wide range of Gpr124 and Reck DNA concentrations (Figure 15B and 15C).

If the Reck-Gpr124 interaction is important for Wnt7a/Wnt7b signaling, then its disruption *in vivo* should impair CNS angiogenesis. We therefore used CRISPR/Cas9 to generate mice carrying a *Reck* allele with the five Ala Scan-9+10 substitutions, hereafter referred to as $Reck^{Cr}$ (Figure 15D). At E13.5, immunoblotting shows that the abundance

and electrophoretic mobility of the Reck protein was the same in WT and *Reck*$^{Cr/Cr}$ embryos (Figure 15E), implying that any phenotypic consequences of the *Reck*^{Cr} mutation likely reflect a functional defect rather than a folding or stability defect.

Both *Reck*$^{Cr/+}$ and *Reck*$^{Cr/Cr}$ mice are viable, with the former showing no CNS vascular abnormalities and the latter showing very mild angiogenesis defects in the lateral ganglionic eminence (LGE) that are incompletely penetrant (data not shown). Different brain regions differ in their sensitivity to the loss of Wnt7a/Wnt7b components most likely due to redundancy in signaling by other Wnts and/or Norrin (Figure 8A-D; Daneman et al., 2009). Listed in order from most to least sensitive, the regions are LGE, MGE, cortex, and hindbrain. Based on the genetic interactions between *Reck* and *Gpr124* shown in Figure 9, we asked whether the *Reck*^{Cr} allele could be distinguished phenotypically from a WT *Reck* allele on a genetic background sensitized by heterozygous loss of *Gpr124*. Figure 15F-H shows that at E13.5 *Reck* $^{+/\Delta ex2}$*;Gpr124*$^{+/\Delta}$ embryos exhibit a normal vascular network, whereas *Reck* $^{Cr/\Delta ex2}$*;Gpr124*$^{+/\Delta}$ embryos show vascular defects in the LGE, with glomeruloid-like tufts and increased infiltration of GS Lectin^{+} macrophages. The *Reck* $^{Cr/\Delta ex2}$*;Gpr124*$^{+/\Delta}$ spinal cord shows a modest reduction in vascular density; the very small reduction in vascular density in the cortex is not statistically significant. These data are consistent with our STF data showing that the Ala Scan-9+10 substitutions that correspond to the *Reck*^{Cr} allele partially disrupt Reck

function, and they support a model in which Reck-Gpr124 binding is important for Wnt7a/Wnt7b signaling during CNS angiogenesis.

3.8 Frizzled- and Wnt7a/Wnt7b-dependent assembly of Reck and Gpr124 into a cell-surface complex

We next asked: does the Reck-Gpr124 complex interact directly with the Wnt/Frizzled complex to distinguish Wnt7a/Wnt7b from other Wnts and from Norrin? To address this question, we developed an experimental platform in which cell-surface binding by the essential N-terminal domains of Reck or Gpr124 could be used to assess protein-protein interactions with various co-expressed and co-assembled ligand/receptor components.

In an initial set of experiments, we explored the binding properties of Reck(CC1-5)-AP and AP-Gpr124(LRR-Ig) – i.e. AP fusion proteins that lack the COMP pentamerization motif (Figure 16A). In contrast to their higher avidity COMP-AP counterparts (Figures 13 and 14), Reck(CC1-5)-AP did not detectably bind to COS-7 or HEK293T cells expressing Gpr124, and AP-Gpr124(LRR-Ig) did not detectably bind to COS-7 or HEK293T cells expressing Reck. Additionally, Reck(CC1-5)-AP and AP-Gpr124(LRR-Ig) did not detectably bind to cells expressing Wnt7a, Fz4, or Wnt7a+Fz4; Reck(CC1-5)-AP did not detectably bind to cells expressing Gpr124+Fz4; and AP-Gpr124(LRR-Ig) did not detectably bind to cells expressing Reck+Fz4. However,

expression of Gpr124+Wnt7a+Fz4 or Gpr124+Wnt7a+Fz4+Lrp5 dramatically enhanced the binding of Reck(CC1-5)-AP, and expression of Reck+Wnt7a+Fz4 or Reck+Wnt7a+Fz4+Lrp5 dramatically enhanced the binding of AP-Gpr124(LRR-Ig) (Figure 16A). [Interestingly, Reck(CC1-5)-AP bound at a low level to cells expressing Gpr124+Wnt7a, and AP-Gpr124(LRR-Ig) bound at a moderate level to cells expressing Reck+Wnt7a. We attribute the binding signals observed in the absence of a co-transfected Frizzled or co-transfected Lrp5/Lrp6 to the low level expression of many Frizzed family members and Lrp5/Lrp6 by HEK293 cells, as determined by RNAseq (unpublished data).] Importantly, in all cases in which there was a positive binding signal, the co-expression of Wnt7a was required, suggesting that high affinity complex formation is ligand-dependent (Figure 16A, 17A, and 17B).

Having earlier identified the critical residues on Reck CC1 that facilitate binding to Gpr124 (Figure 13D-13F), we next tested whether the AP-Gpr124(LRR-Ig) probe could assemble into a complex in the presence of Wnt7a and Fz4 along with either WT Reck or the Reck-Ala9+10 mutant (Figure 17C). Consistent with the *in vitro* Reck CC1-COMP-AP binding experiments in Figure 13D-13F, mutating the critical CC1 amino acids to alanine abolishes AP-Gpr124(LRR-Ig) binding to the cell surface (Figure 17C). These data further support the importance of Reck CC1 in binding to Gpr124(LRR-Ig).

The simplest explanation for the binding data in Figure 16A, 17A, and 17B is that the AP probes co-assemble into a multi-protein signaling complex at the cell surface. However, it is conceivable that binding of Reck(CC1-5)-AP reflects high-level accumulation of Gpr124 at the cell surface and that binding of AP-Gpr124(LRR-Ig) reflects high-level accumulation of Reck at the cell surface – in both cases as a consequence of the combined production of multiple signaling proteins. To test this idea, we assessed total and cell-surface levels of Fz4-1D4 (1D4 is a C-terminal epitope tag), Wnt7a-1D4, Gpr124-3xHA, and Reck with various combinations of co-expressed proteins, by cell surface biotinylation, NeutrAvidin pull-down, and Western blotting [Figure 17D; the bioactivity for Fz4-1D4 and Wnt7a-1D4 was comparable to that of their WT counterparts by STF reporter activity (data not shown)]. For most combinations of co-transfected proteins, Fz4, Gpr124, and Reck exhibited little or no change in cell surface levels (Figure 17D). The only exception to this pattern is seen for Gpr124 co-transfected with Fz4, which leads to a ~2-4-fold increase in cell surface Gpr124 (Figure 17D). However, we note that co-transfection of Gpr124 and Fz4 does not lead to detectable Reck(CC1-5)-AP binding. Wnt7a-1D4 accumulation at the plasma membrane could not be defined as it was below the limit of detection of this assay (Figure 17D). These data show that cell-surface accumulation of individual binding proteins (Gpr124

and Reck) cannot account for the dramatically enhanced binding signals observed in Figures 16A, 17A, and 17B.

To determine whether the Reck(CC1-5)-AP and AP-Gpr124(LRR-Ig) binding reactions exhibit Wnt specificity, we co-transfected HEK293T cells with Gpr124+Fz4 or Reck+Fz4 together with each of the 19 Wnt ligands or Norrin. Strikingly, Reck(CC1-5)-AP only bound when cells expressed Gpr124+Fz4 together with Wnt7a or Wnt7b, and AP-Gpr124(LRR-Ig) only bound when cells expressed Reck+Fz4 together with Wnt7a or Wnt7b (Figure 16B). These binding specificities precisely mirror the signaling specificity of Reck and Gpr124 previously defined in STF cells (Zhou and Nathans, 2014; Vanhollebeke et al., 2015), and they further support the conclusion that binding reflects the assembly of a multi-protein ligand/receptor/co-activator complex.

To assess Frizzled specificity, we expressed Wnt7a+Gpr124 or Wnt7b+Gpr124 together with each of the 10 Frizzled receptors and probed the cells with Reck(CC1-5)-AP (Figure 16C). Seven of ten Frizzleds showed clear binding signals, with only Fz3, Fz6, and Fz10 showing no detectable binding. The strongest signals were observed with Fz5 and Fz8. [We did not perform the analogous experiment using AP-Gpr124(LRR-Ig) because, as shown in Figure 16A and noted above, this probe produces a moderate binding signal even in the absence of Frizzled transfection.] Consistent with these data, previous work using the STF reporter assay showed that (1) Wnt7a and Wnt7b elicited

the strongest responses when co-transfected with Fz5 or Fz8, and (2) Fz3 and Fz6 gave little or no response with any Wnt ligand and do not synergize with Reck and Gpr124 in the presence of Wnt7a (Yu et al., 2012; Vanhollebeke et al., 2015). RNAseq of FACS-purified P7 mouse brain ECs shows expression of Fz6 (~110 FPKM), Fz4 (35 FPKM), Fz1 (6 FPKM), and Fz8 (~4 FPKM) (Zhang et al., 2014). Integrating these gene expression data with our Reck/Gpr124 signaling and binding data suggests that Wnt7a/Wnt7b signaling in brain ECs is likely mediated by the combined actions of Fz4, Fz1, and Fz8.

Figure 4. Reck Activates Canonical Wnt Signaling to Promote CNS Angiogenesis.

(A-D) E13.5 embryos are shown (column 1) alongside coronal sections of brain (columns 2-4) and cross-sections of spinal cord (column 5). The white line in (A) depicts the plane for each brain section. Boxed regions in cortex (a) and MGE (b) in column 2 are shown at higher magnification in columns 3 and 4, respectively. (B) *Reck* $^{flex2/\Delta ex1}$*;Tie2-Cre* vascular knockout embryos show hemorrhaging in the forebrain (arrow) and distal spinal cord (white arrowhead). Vascular density is reduced in the cortex, MGE, and spinal cord, accompanied by infiltration of GS Lectin^{+} macrophages. (C) *Reck* $^{\Delta ex2/\Delta ex2}$ embryos display vascular defects similar to their *Tie2-Cre* conditional knockout counterparts in (B). (D) Beta-catenin was artificially stabilized in ECs of *Reck* $^{\Delta ex2/\Delta ex2}$*;Ctnnb1* $^{flex3/+}$*;Pdgfb-CreER* embryos following IP injection of 1.5 mg of tamoxifen in gestational day (G)10.5 females. At E13.5, the resulting embryos exhibit little or no hemorrhaging in the forebrain and spinal cord, and show a near-complete rescue of vascularization in these regions.

(E) Quantification of the relative vascular density in cortex, MGE, and spinal cord for each genotype shown in (A-D).

(F) Quantification of GS Lectin^{+} macrophages in cortex, MGE, and spinal cord for each genotype in (A-D). In this and subsequent figures, bars represent mean ± SD. Statistical

significance, determined by the unpaired t-test, is represented by * ($P<0.05$), **($P<0.01$), *** ($P<0.001$), and **** ($P<0.0001$).

Scale bars, 200 μm.

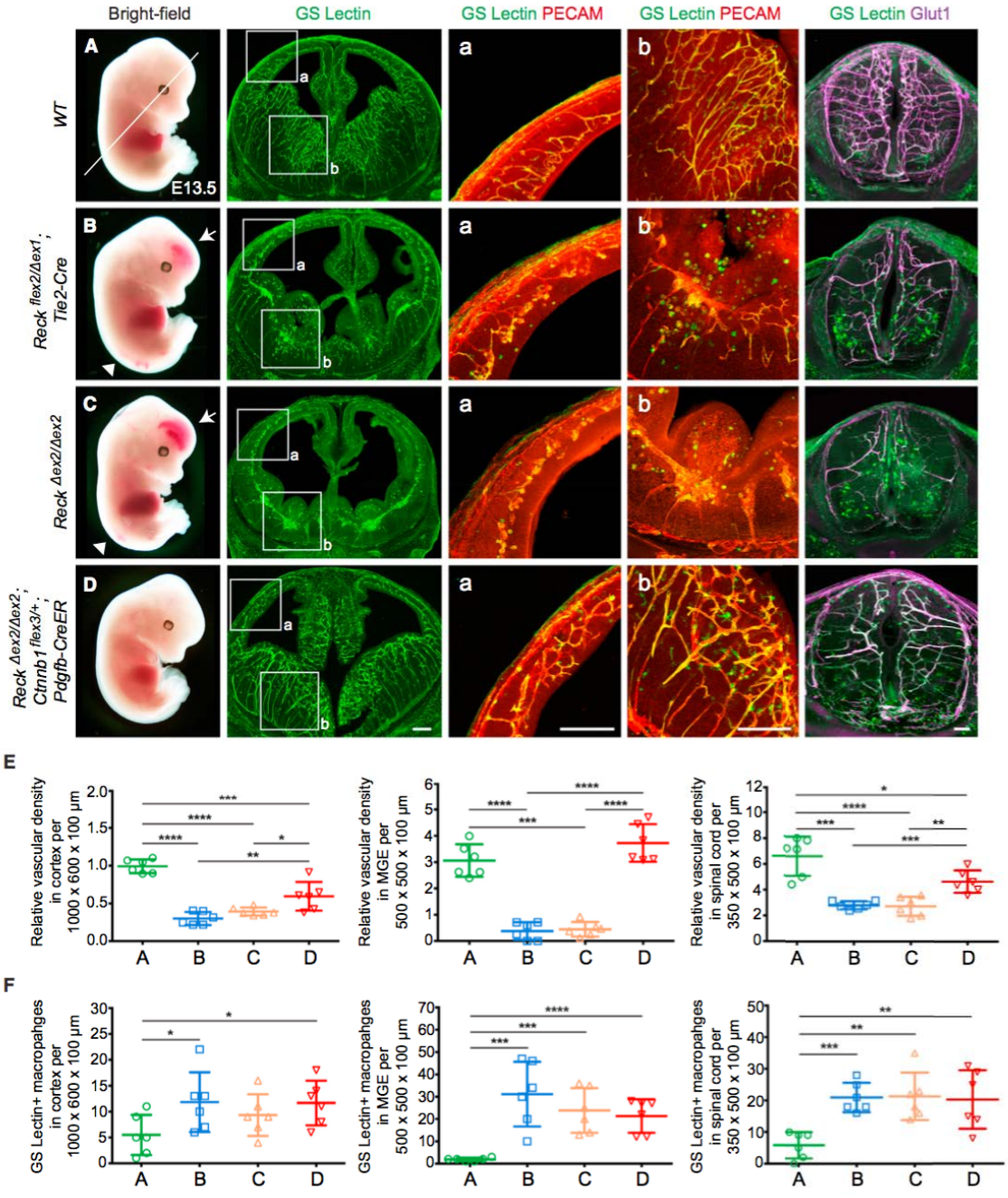
Bright-field
GS Lectin
GS Lectin PECAM
GS Lectin PECAM
GS Lectin Glut1
A
WT
E13.5
B
Reck flex2/Δex1 ; Tie2-Cre
C
Reck Δex2/Δex2
D
Reck Δex2/Δex2 ; Ctnnb1 flex3/+ ; Pdgfb-CreER
a
b
E
Relative vascular density in cortex per 1000 x 600 x 100 µm
Relative vascular density in MGE per 500 x 500 x 100 µm
Relative vascular density in spinal cord per 350 x 500 x 100 µm
F
GS Lectin+ macropahges in cortex per 1000 x 600 x 100 µm
GS Lectin+ macropahges in MGE per 500 x 500 x 100 µm
GS Lectin+ macropahges in spinal cord per 350 x 500 x 100 µm
A
B
C
D

Figure 5. Non-endothelial GS Lectin$^+$ Cells Immunostain Positive for Macrophage Markers F4/80 and Cd11b.

(A-B) Coronal sections of the MGE from E13.5 *Reck$^{flex2/\Delta ex2}$;Tie2-Cre* embryos. Sections were immunostained for GS Lectin and Glut1 along with either F4/80 (A) or Cd11b (B) macrophage markers. Boxed regions are shown at higher magnification in the last row. Many non-endothelial GS Lectin$^+$ cells immunostain for F4/80 and Cd11b (arrowheads). A minority of non-endothelial GS Lectin$^+$ cells fails to immunostain for F4/80 and Cd11b (arrows).

(C-D) Quantification of non-ECs in the *Reck$^{flex2/\Delta ex2}$;Tie2-Cre* MGE that stain for F4/80, Cd11b, GS Lectin (GSL), both Cd11b and GSL, or both F4/80 and GSL.

Scale bars, 100 μm (first and middle row) and 50 μm (last row).

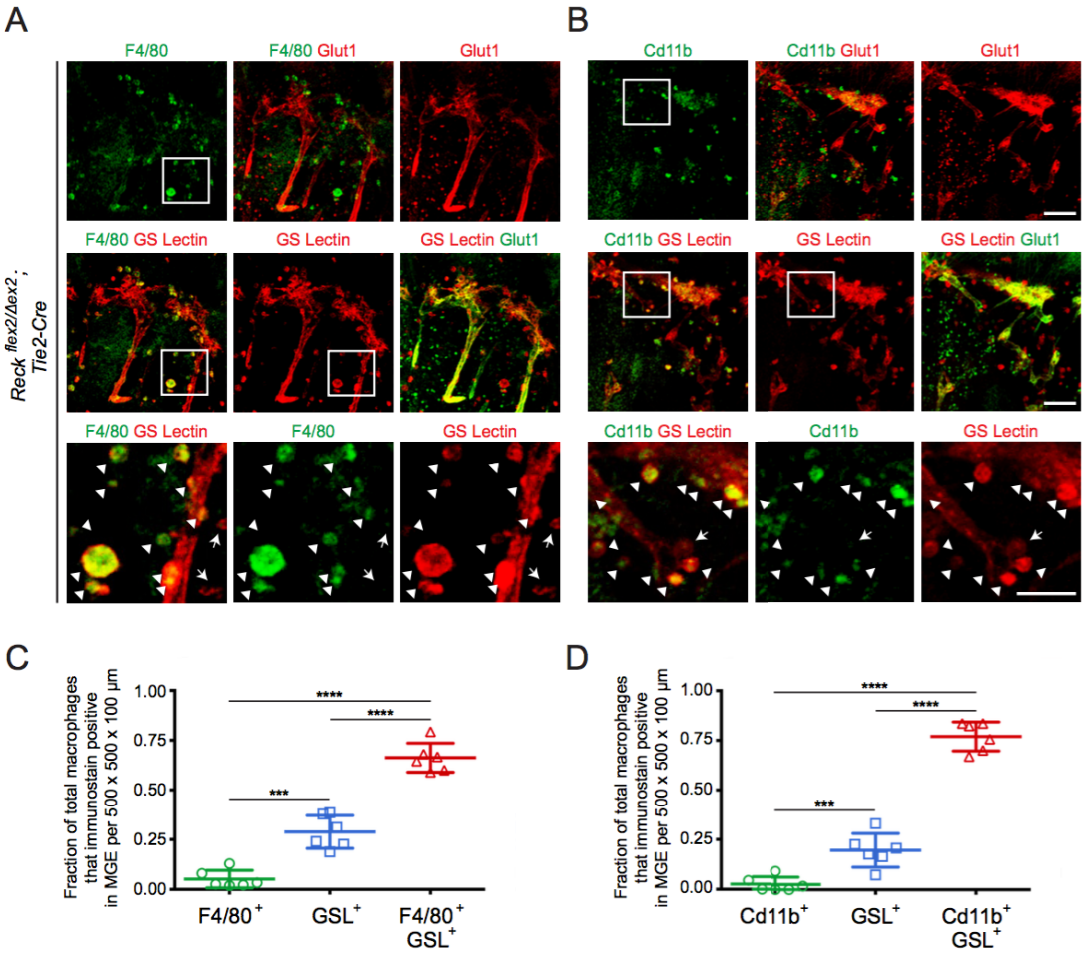
A
B
F4/80
F4/80 Glut1
Glut1
Cd11b
Cd11b Glut1
Glut1
F4/80 GS Lectin
GS Lectin
GS Lectin Glut1
Cd11b GS Lectin
GS Lectin
GS Lectin Glut1
F4/80 GS Lectin
F4/80
GS Lectin
Cd11b GS Lectin
Cd11b
GS Lectin
Reck flex2/Δex2 ; Tie2-Cre
C
D
Fraction of total macrophages that immunostain positive in MGE per 500 x 500 x 100 µm
1.00
0.75
0.50
0.25
0.00
****
****
***
F4/80+
GSL+
F4/80+ GSL+
Cd11b+
GSL+
Cd11b+ GSL+

Figure 6. Canonical Wnt Signaling in ECs is Reduced in Reck EC Knockout Embryos.

(A) Diagram of the *Rosa26-Tcf/Lef-LSL-H2B-GFP* reporter, before (top) and after (bottom) Cre-mediated excision of the LSL cassette.

(B-G) E13.5 coronal sections of cortex (column 1) and cross-sections of spinal cord (columns 2 and 3) stained for PECAM and GFP. For cortex images, regions within dashed boxes are enlarged in the lower right. For spinal cord, boxed regions in column 2 are shown at higher magnification in column 3. *Reck* $^{flex2/+}$*;Rosa26-Tcf/Lef-LSL-H2B-GFP;Tie2-Cre* control embryos (B-D) show strong nuclear GFP staining in ECs in cortex (arrowheads) and spinal cord. *Reck* $^{flex2/\Delta ex1}$*;Rosa26-Tcf/Lef-LSL-H2B-GFP;Tie2-Cre* embryos (E-G) show weak and sparse nuclear GFP staining in ECs in cortex and spinal cord.

(H) Quantification of absolute and normalized GFP^+ EC nuclei in cortex and spinal cord. Scale bars, 100 μm (panels B, C, E, and F) and 50 μm (insets in panels B and E, and panels D and G).

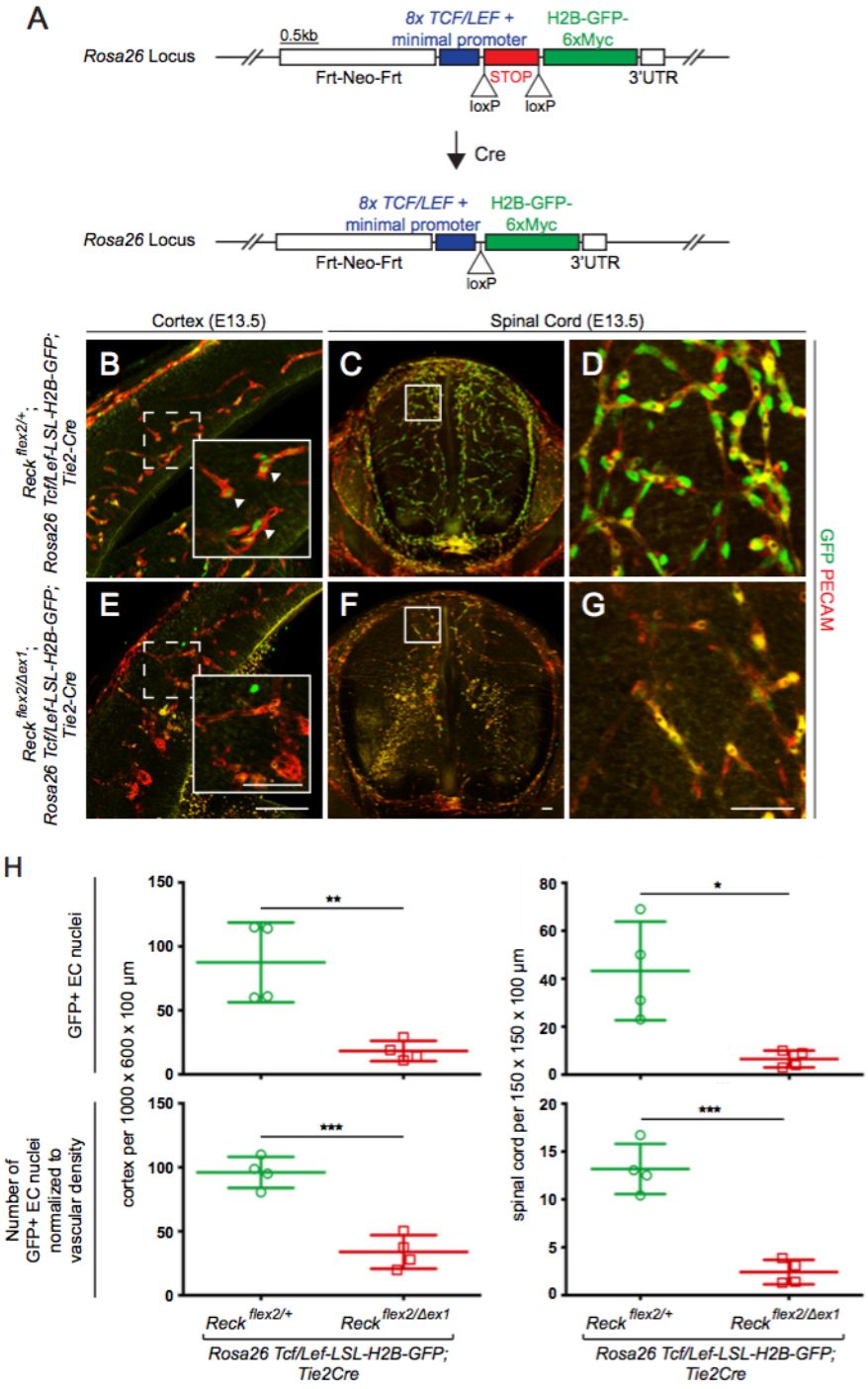
A
Rosa26 Locus
0.5kb
8x TCF/LEF + minimal promoter
H2B-GFP-6xMyc
Frt-Neo-Frt
STOP
3'UTR
loxP
loxP
Cre
Cortex (E13.5)
Spinal Cord (E13.5)
B
C
D
E
F
G
Reck flex2/+; Rosa26 Tcf/Lef-LSL-H2B-GFP; Tie2-Cre
Reck flex2/Δex1; Rosa26 Tcf/Lef-LSL-H2B-GFP; Tie2-Cre
GFP PECAM
H
GFP+ EC nuclei
Number of GFP+ EC nuclei normalized to vascular density
cortex per 1000 x 600 x 100 µm
spinal cord per 150 x 150 x 100 µm
**
*
***
***
Reck flex2/+
Reck flex2/Δex1
Rosa26 Tcf/Lef-LSL-H2B-GFP; Tie2Cre

Figure 7. Reck is Essential for the Development of the Blood-Brain Barrier.

(A,B) *Reck*$^{flex2/+}$*;Tie2-Cre* and *Reck*$^{flex2/\Delta ex1}$*;Tie2-Cre* P0 mice were injected IP with 2-3 mg of sulfo-NHS-biotin 30-45 minutes before sacrifice. Dorsal view (a) and sagittal section (d) of P0 brains, with the boxed region in (d) shown at higher magnification in (b) and (c). Left, anterior; right, posterior. *Reck*$^{flex2/+}$*;Tie2-Cre* control mice (A) have an intact BBB with no biotin leakage, except in the choroid plexus (arrows in (b) and (c)). *Reck*$^{flex2/\Delta ex1}$*;Tie2-Cre* mice (B) show severe hemorrhaging in the cortex along with biotin leakage in cortical, subcortical, and hindbrain regions. PLVAP is widely up-regulated in the CNS vasculature in *Reck*$^{flex2/\Delta ex1}$*;Tie2-Cre* mice. Scale bars, 50 μm.

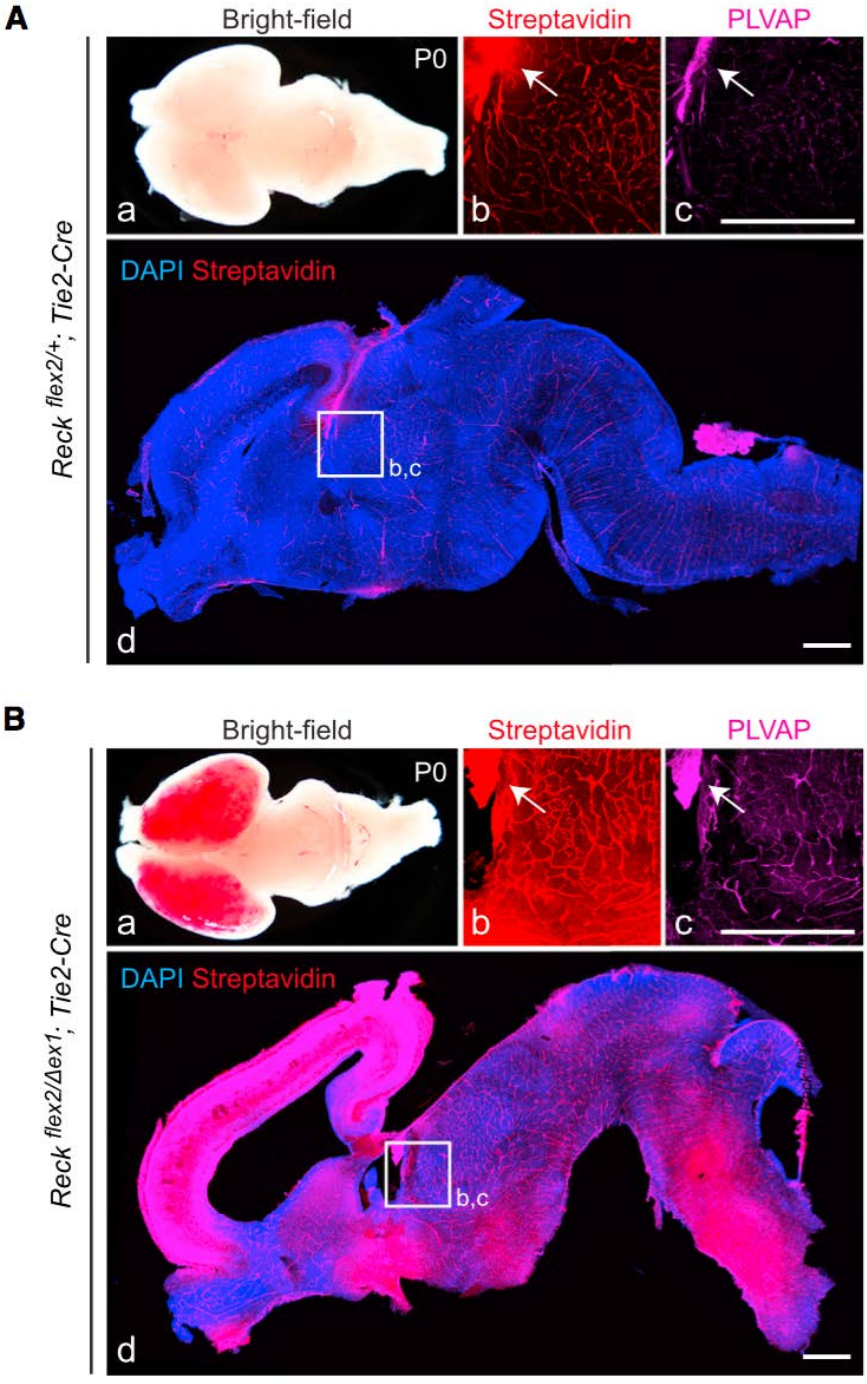
A
Bright-field
Streptavidin
PLVAP
P0
a
b
c
DAPI Streptavidin
b,c
d
Reck flex2/+; Tie2-Cre
B
Bright-field
Streptavidin
PLVAP
P0
a
b
c
DAPI Streptavidin
b,c
d
Reck flex2/Δex1; Tie2-Cre

Figure 8. Reck- and Norrin-Mediated Wnt Signaling Pathways Function Redundantly to Regulate CNS Angiogenesis and BBB Integrity.

(A-E) Coronal sections of E11.5 hindbrains (column 1). Boxed regions (a) and (b) are displayed at higher magnification in columns 2 and 3. In the hindbrain, *Reck*$^{flex2/+}$*;Tie2-Cre* (A), *Reck*$^{flex2/\Delta ex2}$*;Tie2-Cre* (B), and *Reck*$^{flex2/+}$*;Ndp*$^{\Delta/Y}$*;Tie2-Cre* (C) animals show little or no vascular defects. *Reck*$^{flex2/\Delta ex2}$*;Ndp*$^{\Delta/Y}$*;Tie2-Cre* (D) and *Reck*$^{flex2/\Delta ex2}$*;Gpr124*$^{fl/\Delta}$*;Tie2-Cre* (E) embryos show reduced vascular density with increased infiltration of GS Lectin^{+} macrophages.

(F) Quantification of relative vascular density (top) and GS Lectin^{+} macrophages (bottom) in the hindbrain for each genotype in (A-E).

(G-I) Coronal sections of P7 brains (column 1). Boxed regions are displayed at higher magnification (columns 2-4). Animals were injected IP with 50 μg of 4-HT at P3 and P4. *Reck*$^{flex2/\Delta ex1}$*;Pdgfb-CreER* (G) and *Reck*$^{flex2/+}$*;Ndp*$^{\Delta/Y}$*;Pdgfb-CreER* (H) animals show little or no biotin leakage into the brain parenchyma. Vessels are Claudin-5^{+};PLVAP^{-}, except in the choroid plexus where they are Claudin-5^{-};PLVAP^{+} (upper left of each boxed region). *Reck*$^{flex2/\Delta ex1}$*;Ndp*$^{\Delta/Y}$*;Pdgfb-CreER* (I) mice show extensive biotin leakage, most prominently in the cortex, with vessels in the brain parenchyma converted to Claudin-5^{-};PLVAP^{+}.

(J) Quantification of the fraction of vessels that immunostain positive for Claudin-5 (top)

and PLVAP (bottom) for each genotype in (G-I).

Scale bars, 200 μm.

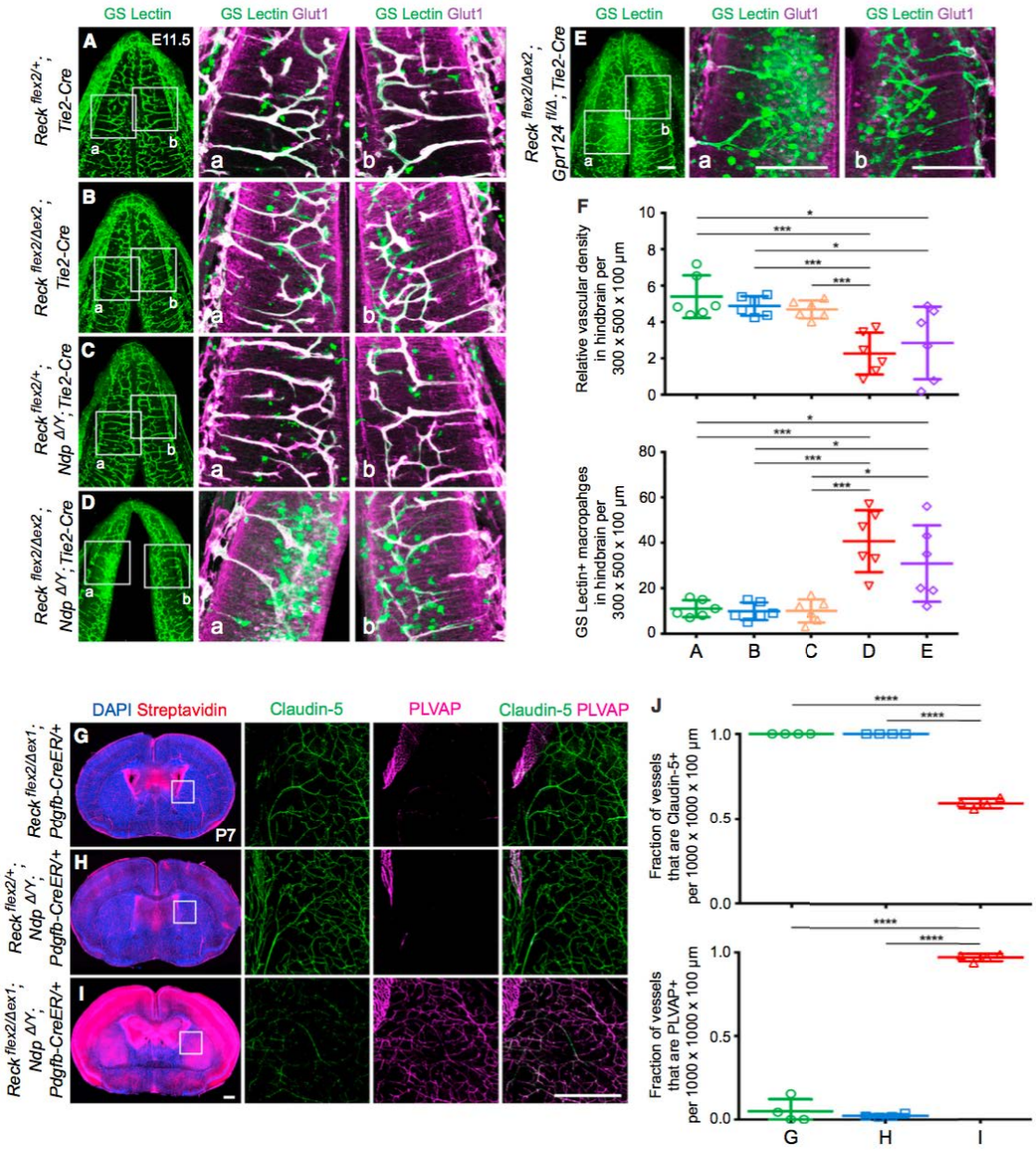

Figure 9. Genetic Evidence for Reck-Gpr124 Interaction in CNS Angiogenesis

(A-E) E13.5 embryos (columns 1 and 2), coronal sections of brain (columns 3-5), and cross-sections of spinal cord (column 6). Boxed regions of cortex (a) and MGE (b) in column 3 are shown at higher magnification in columns 4 and 5, respectively. *Reck* $^{flex2/+}$*;Gpr124* $^{fl/+}$*;Tie2-Cre* (A) embryos show normal vascular development, but ~2-3-fold greater numbers of GS Lectin^{+} macrophages compared to WT embryos (compare panel G to Fig. 4F). *Reck* $^{flex2/\Delta ex2}$*;Gpr124* $^{fl/+}$*;Tie2-Cre* (B) and *Gpr124* $^{fl/\Delta}$*;Tie2-Cre* (C) embryos show hemorrhaging in the forebrain (arrow) and distal spinal cord (white arrowhead). Vascular density is reduced in the cortex, MGE, and spinal cord, and hypovascular regions show increased infiltration of GS Lectin^{+} macrophages. *Reck* $^{flex2/+}$*;Gpr124* $^{fl/\Delta}$*;Tie2-Cre* (D) and *Reck* $^{flex2/\Delta ex2}$*;Gpr124* $^{fl/\Delta}$*;Tie2-Cre* (E) embryos show severe hemorrhaging in the forebrain (arrow) and along the length of the spinal cord (white arrowhead), as well as reduced vascular density in the cortex, MGE, and spinal cord.

(F) Quantification of relative vascular density in cortex, MGE, and spinal cord for each genotype in (A-E).

(G) Quantification of GS Lectin^{+} macrophages in cortex, MGE, and spinal cord for each genotype in (A-E).

Scale bars, 200 μm.

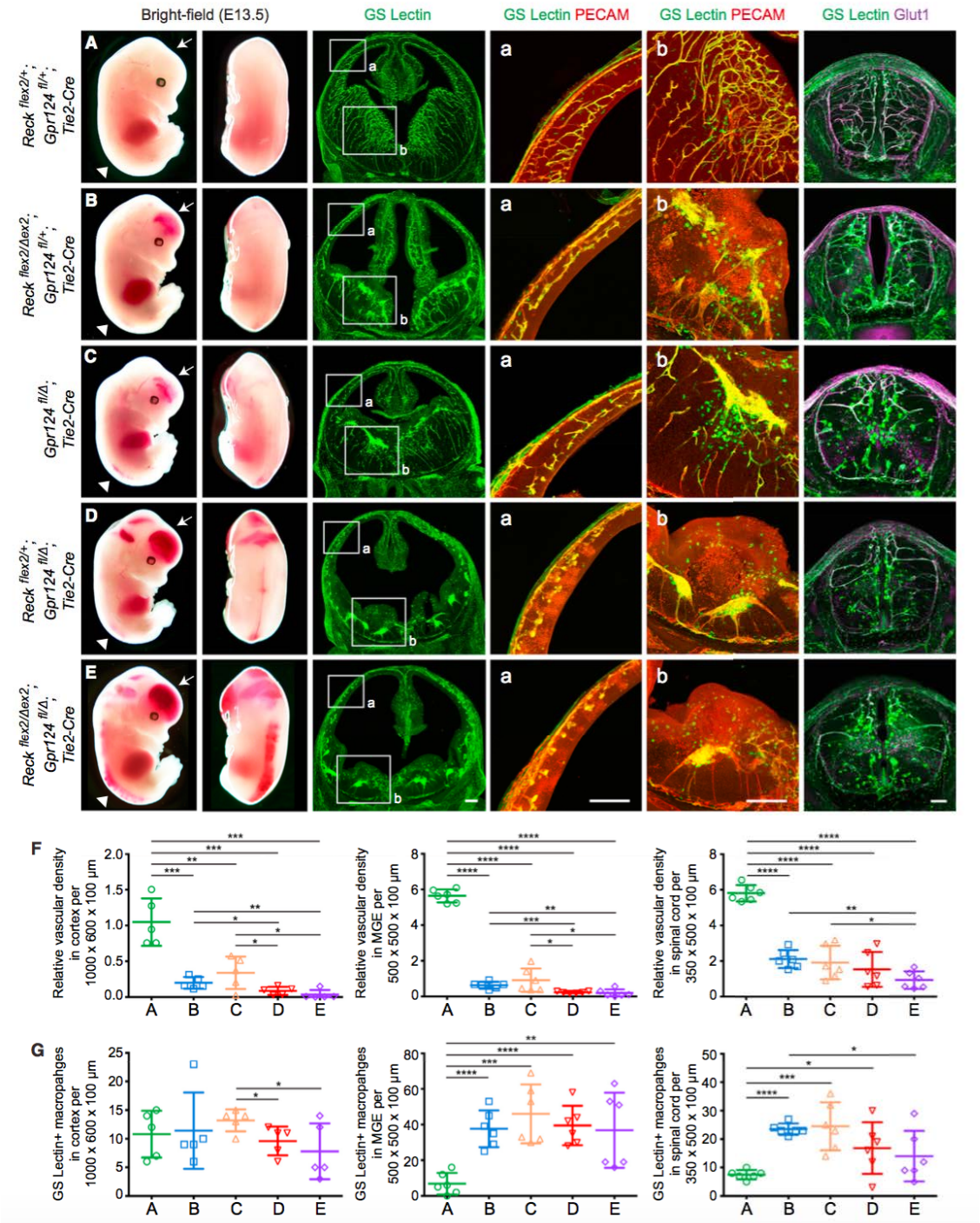
Bright-field (E13.5)
GS Lectin
GS Lectin PECAM
GS Lectin PECAM
GS Lectin Glut1
A
B
C
D
E
a
b
Reck flex2/+, Gpr124 fl/+, Tie2-Cre
Reck flex2/Δex2, Gpr124 fl/+, Tie2-Cre
Gpr124 fl/Δ, Tie2-Cre
Reck flex2/+, Gpr124 fl/Δ, Tie2-Cre
Reck flex2/Δex2, Gpr124 fl/Δ, Tie2-Cre
F
Relative vascular density in cortex per 1000 x 600 x 100 µm
Relative vascular density in MGE per 500 x 500 x 100 µm
Relative vascular density in spinal cord per 350 x 500 x 100 µm
G
GS Lectin+ macropahges in cortex per 1000 x 600 x 100 µm
GS Lectin+ macropahges in MGE per 500 x 500 x 100 µm
GS Lectin+ macropahges in spinal cord per 350 x 500 x 100 µm

Figure 10. Genetic Evidence for Reck-Wnt7a/Wnt7b Interaction

(A-D) Coronal sections of E13.5 brains (columns 1-3) and cross-sections of spinal cord (column 4). Boxed regions in cortex (a) and MGE (b) in column 1 are shown at higher magnification in columns 2 and 3, respectively. $Reck^{+/\Delta ex2}$;$Wnt7a^{+/\Delta}$;$Wnt7b^{+/\Delta}$ (A) and $Wnt7a^{\Delta/\Delta}$;$Wnt7b^{+/\Delta}$ (B) embryos exhibit normal vascular development, but have increased levels of GS Lectin$^+$ macrophages compared to WT embryos (Figure 4F). $Reck^{+/\Delta ex2}$;$Wnt7a^{\Delta/\Delta}$;$Wnt7b^{+/\Delta}$ embryos (C) show reduced vascular density and increased abundance of GS Lectin$^+$ macrophages in the MGE and spinal cord (C vs. A and B). $Reck^{\Delta ex2/\Delta ex2}$;$Wnt7a^{\Delta/\Delta}$;$Wnt7b^{+/\Delta}$ embryos (D) display a more severe vascular phenotype compared to $Reck^{\Delta ex2/\Delta ex2}$ embryos (Figure 4C). Specifically, in $Reck^{\Delta ex2/\Delta ex2}$;$Wnt7a^{\Delta/\Delta}$;$Wnt7b^{+/\Delta}$ embryos (D) the cortex, MGE, and spinal cord are nearly avascular, but relative to embryos with milder vascular defects, the number of GS Lectin$^+$ macrophages is decreased in the cortex (D vs. A, B, and C) and MGE (D vs. C).

(E) Quantification of vascular density in cortex, MGE, and spinal cord for each genotype shown in (A-D). (F) Quantification of GS Lectin$^+$ macrophages in cortex, MGE, and spinal cord for each genotype shown in (A-D).

Scale bars, 200 μm.

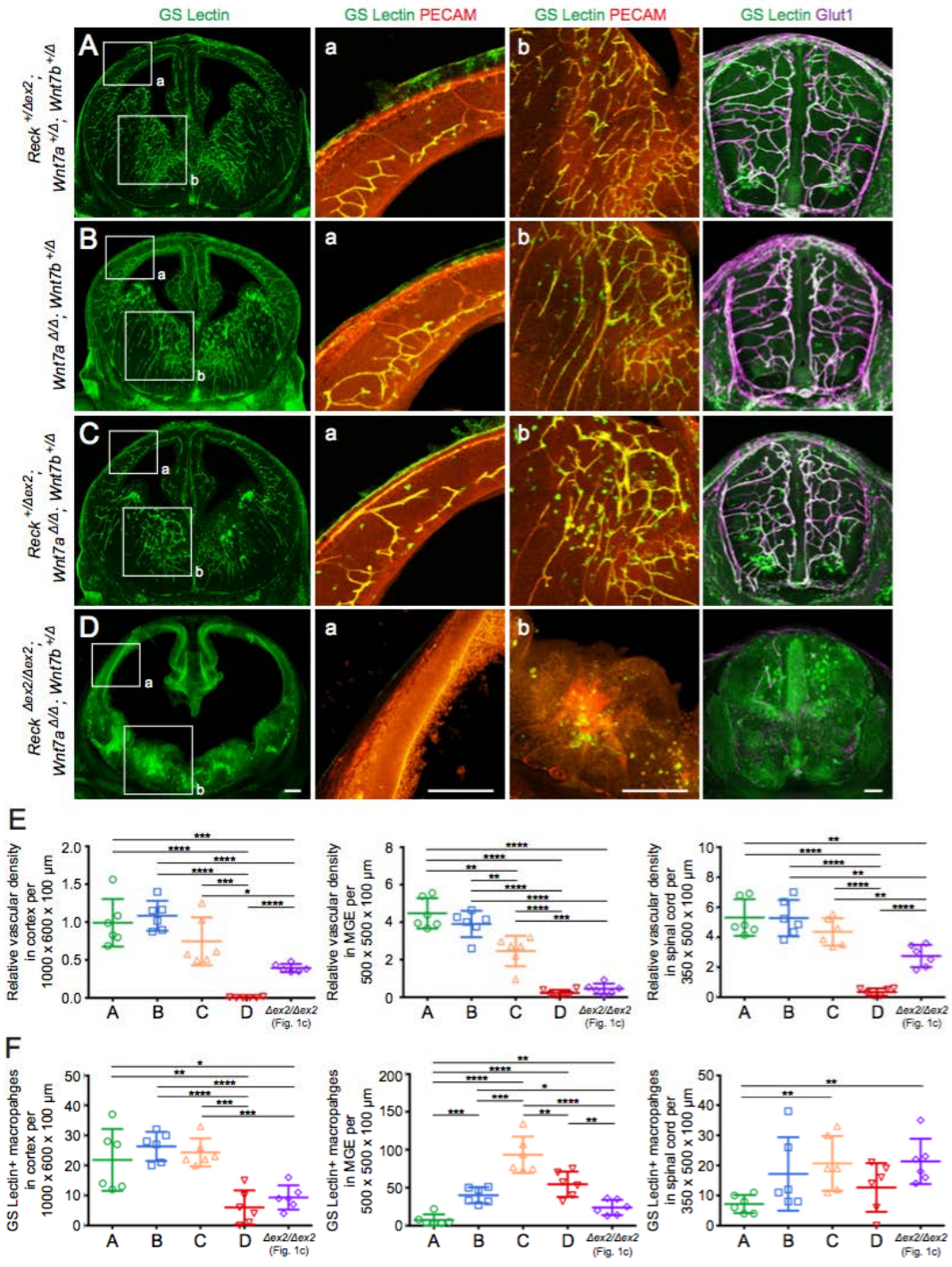
GS Lectin
GS Lectin PECAM
GS Lectin PECAM
GS Lectin Glut1
A
B
C
D
a
b
Reck +/Δex2 ; Wnt7a +/Δ ; Wnt7b +/Δ
Wnt7a Δ/Δ ; Wnt7b +/Δ
Reck +/Δex2 ; Wnt7a Δ/Δ ; Wnt7b +/Δ
Reck Δex2/Δex2 ; Wnt7a Δ/Δ ; Wnt7b +/Δ
E
Relative vascular density in cortex per 1000 x 600 x 100 µm
Relative vascular density in MGE per 500 x 500 x 100 µm
Relative vascular density in spinal cord per 350 x 500 x 100 µm
A
B
C
D
Δex2/Δex2 (Fig. 1c)
F
GS Lectin+ macropahges in cortex per 1000 x 600 x 100 µm
GS Lectin+ macropahges in MGE per 500 x 500 x 100 µm
GS Lectin+ macropahges in spinal cord per 350 x 500 x 100 µm

Figure 11. The N-terminal Domain of Gpr124 is Required for Co-activation of Canonical Wnt Signaling.

(A) Diagram of the domain structure of Gpr124. The sequence coding for a 3xHA epitope was inserted upstream of the C-terminal PDZ binding domain. The ectodomain of Gpr124 consists of an LRR domain, an Ig-like domain, a HormR domain, and a GAIN domain. TM, transmembrane domain. PDB, PDZ-binding domain.

(B) Plasma membrane expression of Gpr124-3xHA and its derivatives was assessed by cell surface biotinylation as described in 'Materials and Methods'.

(C) STF cells were transfected with: Wnt7a, Reck (blue) or Myc-Reck (red – see Figure 12), and Gpr124-3xHA or its derivatives. Luciferase assays were performed as described in 'Materials and Methods'. Co-transfection with Lrp5 or Lrp6 is not required as endogenous levels of these co-receptors are sufficient for signaling. Values represent means ± SD.

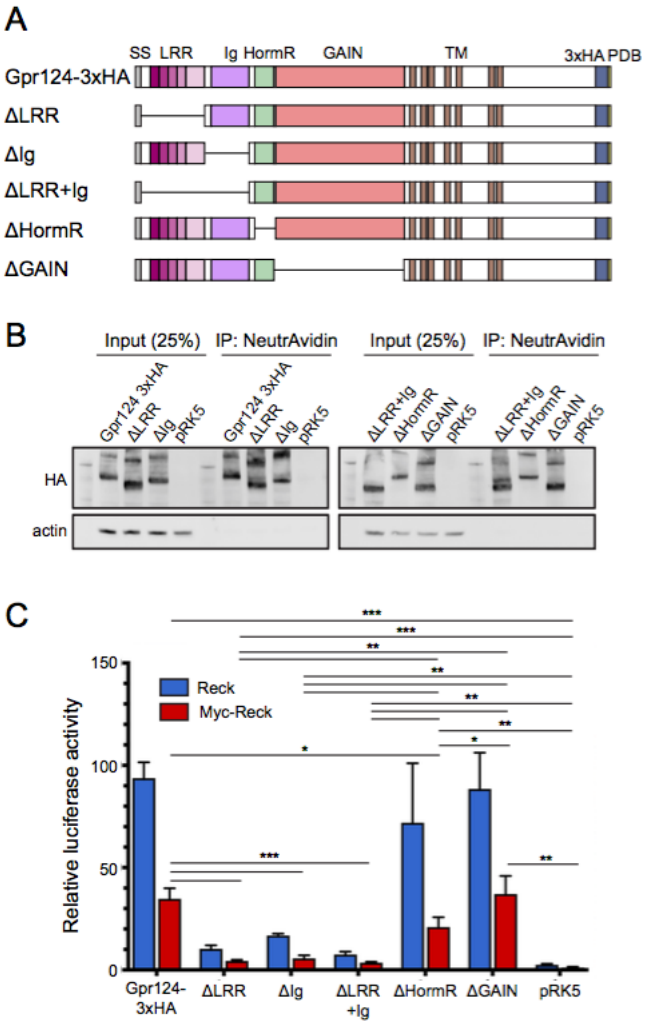
A
SS LRR Ig HormR GAIN TM 3xHA PDB
Gpr124-3xHA
ΔLRR
ΔIg
ΔLRR+Ig
ΔHormR
ΔGAIN
B
Input (25%)
IP: NeutrAvidin
Input (25%)
IP: NeutrAvidin
Gpr124 3xHA
ΔLRR
ΔIg
pRK5
ΔLRR+Ig
ΔHormR
ΔGAIN
HA
actin
C
Reck
Myc-Reck
Relative luciferase activity
150
100
50
0
Gpr124-3xHA
ΔLRR
ΔIg
ΔLRR +Ig
ΔHormR
ΔGAIN
pRK5

Figure 12. The N-terminal Domain of Reck is Required for Co-activation of Canonical Wnt Signaling.

(A) Diagram of the domain structure of Reck, with a Myc epitope inserted immediately after the signal sequence (SS). The sequence for GPI-anchor addition is at the C-terminus.

(B-C) STF cells were co-transfected with Wnt7a, WT Gpr124 (green) or Gpr124-3xHA (orange; see Figure 11), and WT Myc-Reck, its deletion derivatives, or the empty expression vector (pRK5). Luciferase assays were performed as described in 'Materials and Methods'. Values represent means ± SD.

(D) Plasma membrane expression of Myc-Reck and its derivatives was assessed by cell surface biotinylation as described in 'Materials and Methods'.

(E) Plasma membrane localization of Myc-Reck and its deletion derivatives was assessed by live-cell immunostaining as described in 'Materials and Methods'.

Scale bar, 10 um.

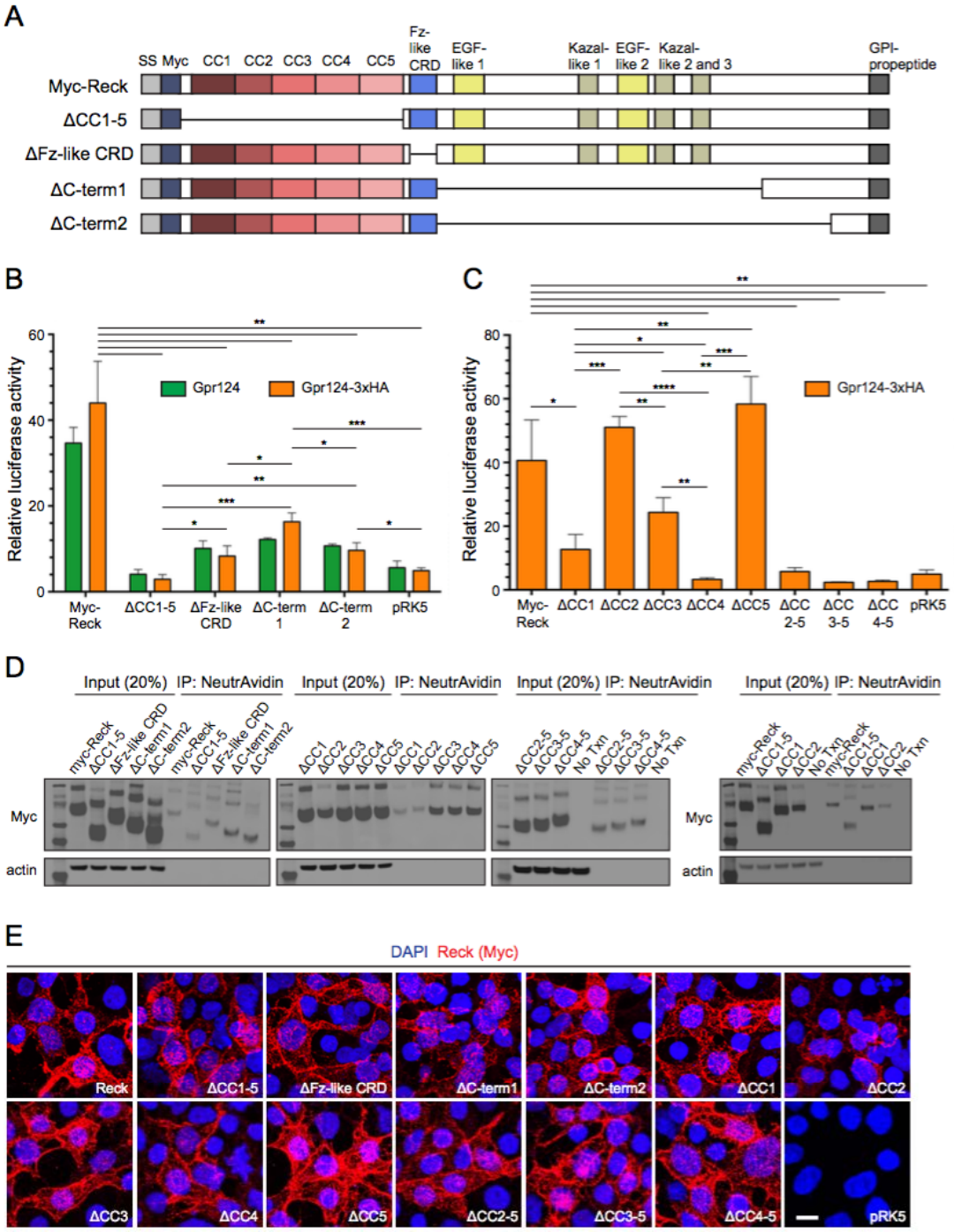
A
SS Myc
CC1
CC2
CC3
CC4
CC5
Fz-like CRD
EGF-like 1
Kazal-like 1
EGF-like 2
Kazal-like 2 and 3
GPI-propeptide
Myc-Reck
ΔCC1-5
ΔFz-like CRD
ΔC-term1
ΔC-term2
B
Relative luciferase activity
Gpr124
Gpr124-3xHA
Myc-Reck
ΔCC1-5
ΔFz-like CRD
ΔC-term 1
ΔC-term 2
pRK5
C
Relative luciferase activity
Gpr124-3xHA
Myc-Reck
ΔCC1
ΔCC2
ΔCC3
ΔCC4
ΔCC5
ΔCC 2-5
ΔCC 3-5
ΔCC 4-5
pRK5
D
Input (20%)
IP: NeutrAvidin
Myc
actin
E
DAPI Reck (Myc)
Reck
ΔCC1-5
ΔFz-like CRD
ΔC-term1
ΔC-term2
ΔCC1
ΔCC2
ΔCC3
ΔCC4
ΔCC5
ΔCC2-5
ΔCC3-5
ΔCC4-5
pRK5

Figure 13. Direct Binding of the Domains of Reck and Gpr124 Responsible for Canonical Wnt Signaling

(A) Diagram of COMP-AP probes (left) and Fc baits (right).

(B) AP binding assay using COS-7 cells transfected with Gpr124, Gpr124 deletion mutants, or Gpr125, a close homologue of Gpr124. Live cells were incubated with the Reck(CC1-5)-COMP-AP probe shown in (A). No Txn, no transfection.

(C) Cell-free binding assay using Gpr124(LRR-Ig) or Reck(CC1-5) (a negative control) Fc baits captured in Protein-G coated wells. Each bait was incubated with three COMP-AP probes: Reck(CC1), Reck(CC1-2), and Reck(CC1-5). After removing unbound probe, the bound probe was visualized with a colorimetric AP reaction.

(D) Amino acid sequence of mouse Reck CC1, with alanine scanning mutants indicated. Alanine substitution blocks 2, 7, 10, 14, and 16 were produced at near-WT levels and 9 and 15 at reduced levels (Figure 14A and 14B).

(E) Cell-free binding assay with the indicated alanine scanning mutants (top) and images of the AP reactions at the final time point (bottom). N.C., negative control.

(F) Cell-free binding assay with the indicated single alanine substitutions (top) and images of the AP reactions at the final time point (bottom). See Figure 14A and 14B for protein yield.

(G) Alignment and conservation of Reck CC1 across vertebrates, generated by Clustal Omega. Alignment symbols denote: (*) fully conserved residues; (:) residues with strongly similar properties; and (.) residues with weakly similar properties.
Scale bars, 200 μm.

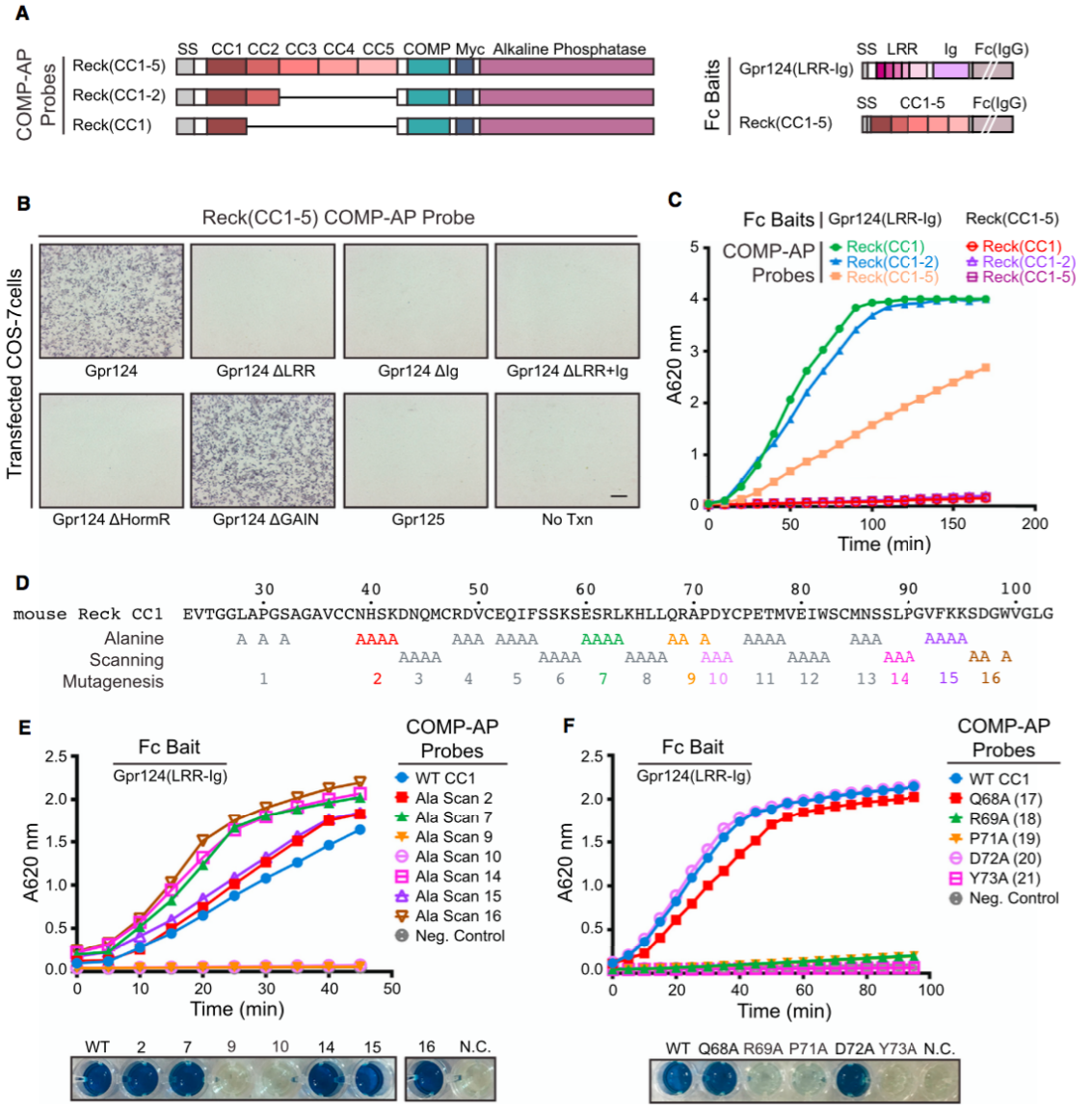
A
COMP-AP Probes
Reck(CC1-5)
Reck(CC1-2)
Reck(CC1)
SS CC1 CC2 CC3 CC4 CC5 COMP Myc Alkaline Phosphatase
Fc Baits
Gpr124(LRR-Ig)
Reck(CC1-5)
SS LRR Ig Fc(IgG)
SS CC1-5 Fc(IgG)
B
Reck(CC1-5) COMP-AP Probe
Transfected COS-7cells
Gpr124
Gpr124 ΔLRR
Gpr124 ΔIg
Gpr124 ΔLRR+Ig
Gpr124 ΔHormR
Gpr124 ΔGAIN
Gpr125
No Txn
C
Fc Baits | Gpr124(LRR-Ig) Reck(CC1-5)
COMP-AP Probes
Reck(CC1)
Reck(CC1-2)
Reck(CC1-5)
A620 nm
Time (min)
D
mouse Reck CC1 EVTGGLAPGSAGAVCCNHSKDNQMCRDVCEQIFSSKSESRLKHLLQRAPDYCPETMVEIWSCMNSSLPGVFKKSDGWVGLG
Alanine Scanning Mutagenesis
E
Fc Bait
Gpr124(LRR-Ig)
COMP-AP Probes
WT CC1
Ala Scan 2
Ala Scan 7
Ala Scan 9
Ala Scan 10
Ala Scan 14
Ala Scan 15
Ala Scan 16
Neg. Control
A620 nm
Time (min)
WT 2 7 9 10 14 15 16 N.C.
F
Fc Bait
Gpr124(LRR-Ig)
COMP-AP Probes
WT CC1
Q68A (17)
R69A (18)
P71A (19)
D72A (20)
Y73A (21)
Neg. Control
A620 nm
Time (min)
WT Q68A R69A P71A D72A Y73A N.C.
G
Homo sapiens CCNHSKDNQMCRDVCEQIFSSKSESRLKHLLQRAPDYCPETMVEIWNCMNSSLPGVFKKSDGWVGLG
Mus musculus CCNHSKDNQMCRDVCEQIFSSKSESRLKHLLQRAPDYCPETMVEIWSCMNSSLPGVFKKSDGWVGLG
Rattus norvegicus CCNHSKDNQMCRDVCEQIFSSKSESRLKHLLQRAPDYCPETMVEIWSCMNSSLPGVFKKSDGWVGLG
Gallus gallus CCYHAKDNLMCRDVCEQILSSKSDSRLKHLLQRAPEYCPESMGEVWGCINSSLPGVLKKSDGWVGLG
Taeniopygia guttata CCYHAKDNLMCRDVCEQILSSKSDSRLKHLLQRAPEYCPESMREVWGCINSSLPGVLKKSDGWVGLG
Xenopus tropicalis CCNQAKDNLMCRDVCEQILSSKSESRIKHLFLRAPDYCPTSMIDVWTCINSSLPGVSKKSDGWVGLG
Callorhinchus milii CCYQAREYPICRDACEQLTSTKSESRLKHLLQRLPGYCPESMVEFWVCINSSLPGASKKPEGWVGLG
Danio rerio CVHHAADIPRCRDACEQLASIRSESRLRHLLHRLPSYCPETLSELWICINNSLPGASRKSDGWVGLG

Figure 14. Wnt-activating domains of Gpr124 and Reck are sufficient for direct binding.

(A) Diagram of Gpr124(LRR-Ig)-COMP-AP (top) used for cell-based AP binding (bottom). COS-7 cells expressing Reck, Reck derivatives, or bovine rhodopsin (a negative control) were incubated with Gpr124(LRR-Ig)-COMP-AP. Gpr124(LRR-Ig)-COMP-AP gives ~10-fold lower signal than Reck(CC1-5)-COMP-AP, which reduces the signal-to-noise ratio.

(B) Cell-free AP binding assay using Reck(CC1-5)-Fc and Fz4(CRD)-Fc (a negative control) baits captured on Protein-G wells. Gpr124(LRR-Ig)-COMP-AP was used as probe. After removing unbound probe, the bound probe was visualized with a colorimetric AP reaction. Values represent means ± SD.

(C) AP binding assay using COS-7 cells transfected with Reck and each of the indicated CC subdomain deletions. Live cells were incubated with Gpr124 (LRR-Ig)-COMP-AP. pRK5-ScrPep is a negative control.

(D,E) Conditioned medium for each Reck(CC1)-COMP-AP Ala Scan probe was collected to assess its level of expression by immunoblotting (D) and solution AP activity (E).

(F) Surface biotinylation, as described in 'Materials and Methods', for WT Reck and Ala Scan mutants 9, 10, and 9+10.

Scale bars, 200 μm.

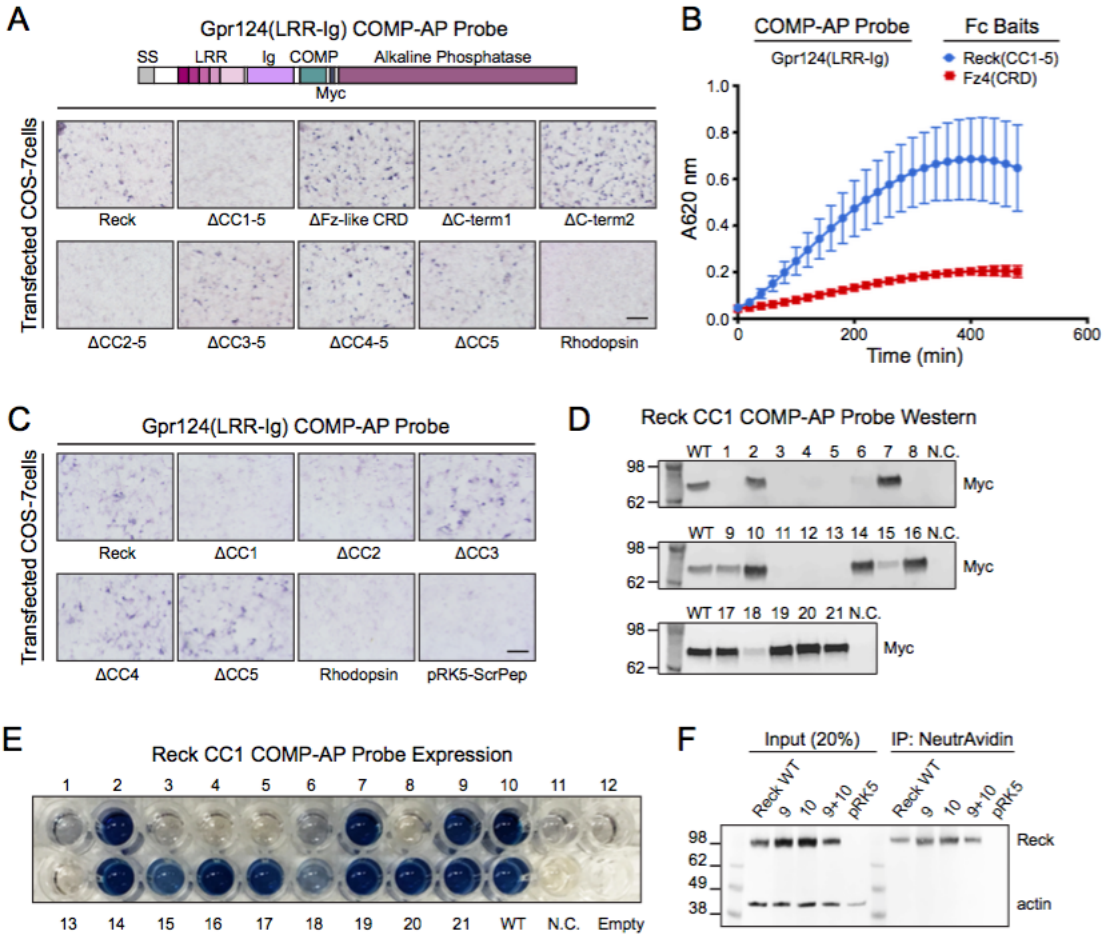

Figure 15. Reck-Gpr124 Complex Formation is Important for Wnt Activation and CNS Angiogenesis.

(A) STF cells were transfected with: Wnt7a, Gpr124, and Reck WT or Ala Scan mutant plasmids. Luciferase assays were performed as described in 'Materials and Methods'.

(B) As in (A), but showing the dose response curve for varying concentrations of Gpr124 DNA in the presence of constant WT Reck (blue) or Ala Scan 9+10 (red).

(C) As in (A), but showing the dose response curve for varying concentrations of WT Reck (blue) or Ala Scan 9+10 (red) in the presence of constant WT Gpr124.

(D) Diagram of the mouse *Reck* WT and *CRISPR-edited* alleles. The region corresponding to Ala Scan mutants 9 and 10 in Reck(CC1) is encoded by exon 3.

(E) Reck protein abundance at E13.5 is unaltered in *Reck* $^{Cr/Cr}$ embryos compared to a WT control, as determined by immunoblotting. The disappearance of the full-size Reck band in the *Reck* $^{\Delta ex2/\Delta ex2}$ embryos confirms the specificity of the anti-Reck antibody. (*) denotes a non-specific band in the actin immunoblot. MW standards are shown at left.

(F-G) E13.5 coronal sections of brain (columns 1-3) and cross-sections of spinal cord (column 4). Boxed regions in LGE (a) and cortex (b) are shown at higher magnification in columns 2 and 3, respectively. *Reck* $^{Cr/\Delta ex2}$*;Gpr124*$^{+/\Delta}$ mutant embryos (G) show reduced vascular density and glomeruloid tufts in the LGE, accompanied by infiltration of GS Lectin^{+} macrophages. Vascular density in the spinal cord is also reduced.

(H) Quantification of relative vascular density (top) and the number of GS Lectin^{+} macrophages (bottom) in LGE, cortex, and spinal cord for the genotypes shown in (F-G). Values represent means ± SD. Scale bars, 200 μm.

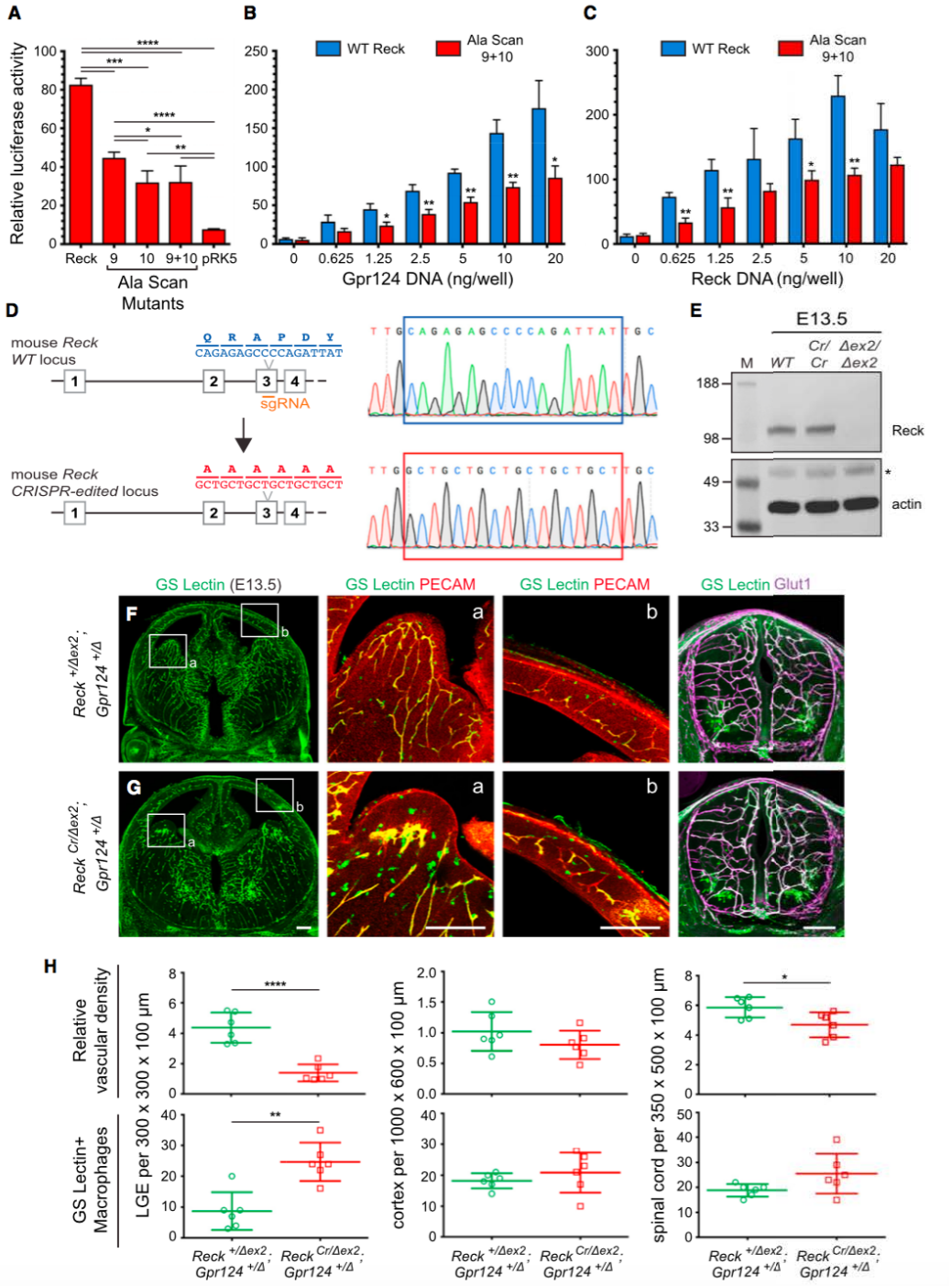
A
Relative luciferase activity
Reck
9
10
9+10
pRK5
Ala Scan Mutants
B
WT Reck
Ala Scan 9+10
Gpr124 DNA (ng/well)
C
WT Reck
Ala Scan 9+10
Reck DNA (ng/well)
D
mouse Reck WT locus
Q R A P D Y
CAGAGAGCCCCAGATTAT
sgRNA
mouse Reck CRISPR-edited locus
A A A A A A
GCTGCTGCTGCTGCTGCT
E
E13.5
M
WT
Cr/Cr
Δex2/Δex2
188
98
49
33
Reck
actin
GS Lectin (E13.5)
GS Lectin PECAM
GS Lectin PECAM
GS Lectin Glut1
F
G
Reck +/Δex2; Gpr124 +/Δ
Reck Cr/Δex2; Gpr124 +/Δ
H
Relative vascular density
GS Lectin+ Macrophages
LGE per 300 x 300 x 100 µm
cortex per 1000 x 600 x 100 µm
spinal cord per 350 x 500 x 100 µm
Reck +/Δex2; Gpr124 +/Δ
Reck Cr/Δex2; Gpr124 +/Δ

Figure 16. Reck-Gpr124 Assembles into a Multi-Protein Complex with Wnt7a/Wnt7b and Frizzled.

(A) AP binding assay using HEK293T cells transfected with Gpr124, Wnt7a, Fz4, and/or Lrp5 (left) or Reck, Wnt7a, Fz4, and/or Lrp5 (right). Live cells were incubated with Reck(CC1-5)-AP (left) or AP-Gpr124(LRR-Ig) (right).

(B) AP binding assay using HEK293T cells transfected with Gpr124 and Fz4, along with each of the 19 Wnts and Norrin. Live cells were incubated with Reck(CC1-5)-AP (left) or AP-Gpr124(LRR-Ig) (right).

(C) AP binding assay using HEK293T cells transfected with Gpr124 and Wnt7a (top) or Wnt7b (bottom), toegther with each of the 10 Fz receptors or a no transfection control. Live cells were incubated with Reck(CC1-5)-AP.

(D) Model of the multi-protein signaling complex, consisting of Reck, Gpr124, Wnt7a or Wnt7b, Frizzled, and Lrp5 or Lrp6. The straight double-headed arrow indicates a direct interaction between Reck(CC1) and Gpr124(LRR-Ig). The curved double-headed arrow indicates a direct interaction between Reck/Gpr124 and Fz/(Wnt7a or Wnt7b) sub-complexes. Modified from Zhou and Nathans (2014).

Scale bars, 200 μm.

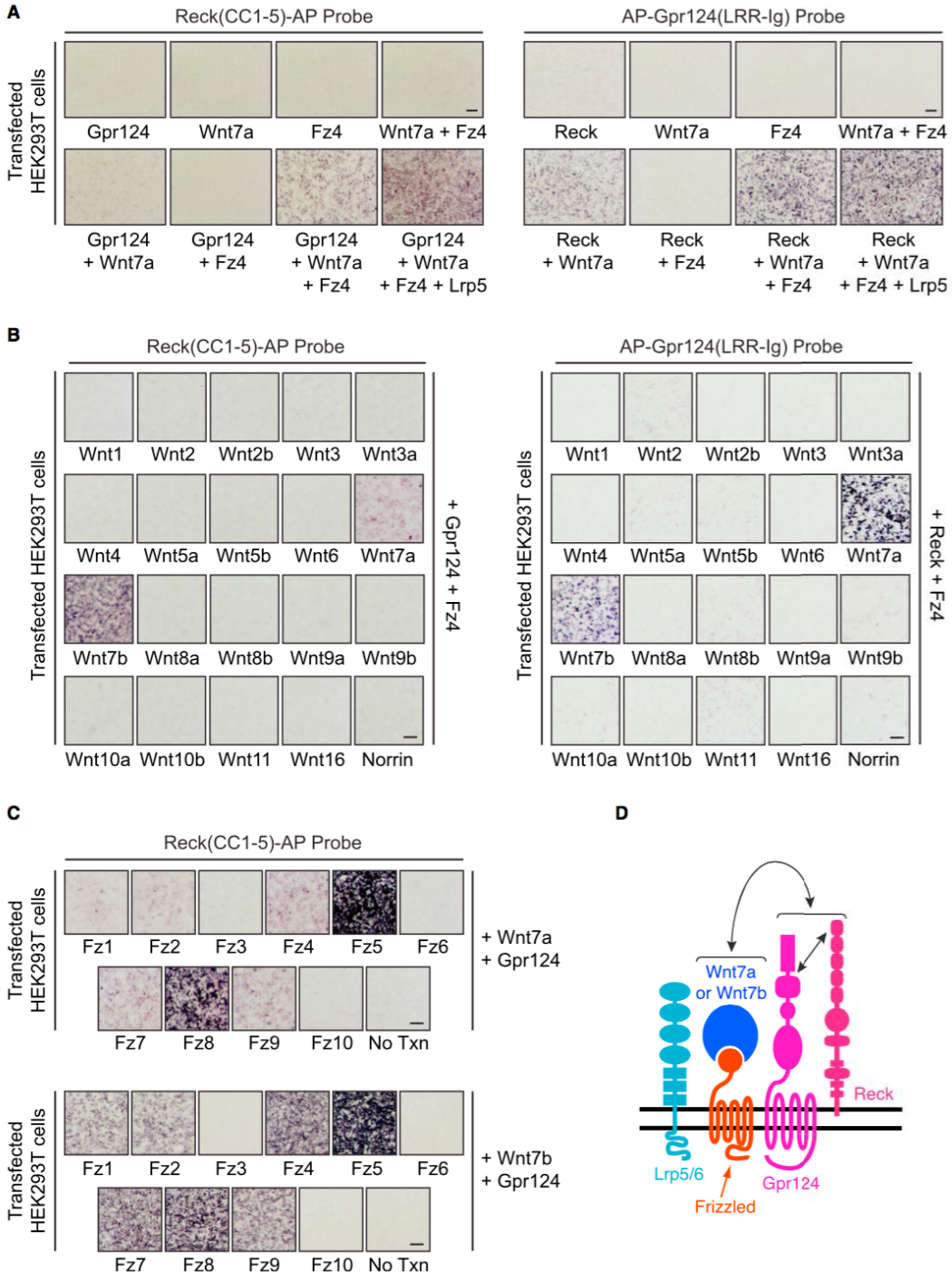
A
Reck(CC1-5)-AP Probe
AP-Gpr124(LRR-Ig) Probe
Transfected HEK293T cells
Gpr124
Wnt7a
Fz4
Wnt7a + Fz4
Reck
Gpr124 + Wnt7a
Gpr124 + Fz4
Gpr124 + Wnt7a + Fz4
Gpr124 + Wnt7a + Fz4 + Lrp5
Reck + Wnt7a
Reck + Fz4
Reck + Wnt7a + Fz4
Reck + Wnt7a + Fz4 + Lrp5
B
Reck(CC1-5)-AP Probe
AP-Gpr124(LRR-Ig) Probe
Transfected HEK293T cells
Wnt1
Wnt2
Wnt2b
Wnt3
Wnt3a
Wnt4
Wnt5a
Wnt5b
Wnt6
Wnt7a
Wnt7b
Wnt8a
Wnt8b
Wnt9a
Wnt9b
Wnt10a
Wnt10b
Wnt11
Wnt16
Norrin
+ Gpr124 + Fz4
+ Reck + Fz4
C
Reck(CC1-5)-AP Probe
Transfected HEK293T cells
Fz1
Fz2
Fz3
Fz4
Fz5
Fz6
Fz7
Fz8
Fz9
Fz10
No Txn
+ Wnt7a + Gpr124
+ Wnt7b + Gpr124
D
Wnt7a or Wnt7b
Reck
Lrp5/6
Gpr124
Frizzled

Figure 17. Ligand-dependent assembly and cell surface expression of complex components

(A,B) AP binding assay using HEK293T cells transfected with Gpr124, Wnt7a, Fz4, and/or Lrp5 (A) or Reck, Wnt7a, Fz4, and/or Lrp5 (B). Live cells were incubated with Reck(CC1-5)-AP (A) or AP-Gpr124(LRR-Ig) (B).

(C) AP binding assay using HEK293T cells transfected with Wnt7a, Fz4, and either WT Reck, Ala9+10 Reck, or no Reck. Live cells were incubated with AP-Gpr124(LRR-Ig).

(D) Plasma membrane expression of Wnt7a-1D4, Fz4-1D4, Gpr124, and/or Reck was assessed by cell surface biotinylation as described in 'Materials and Methods'.

Scale bars, 200 μm.

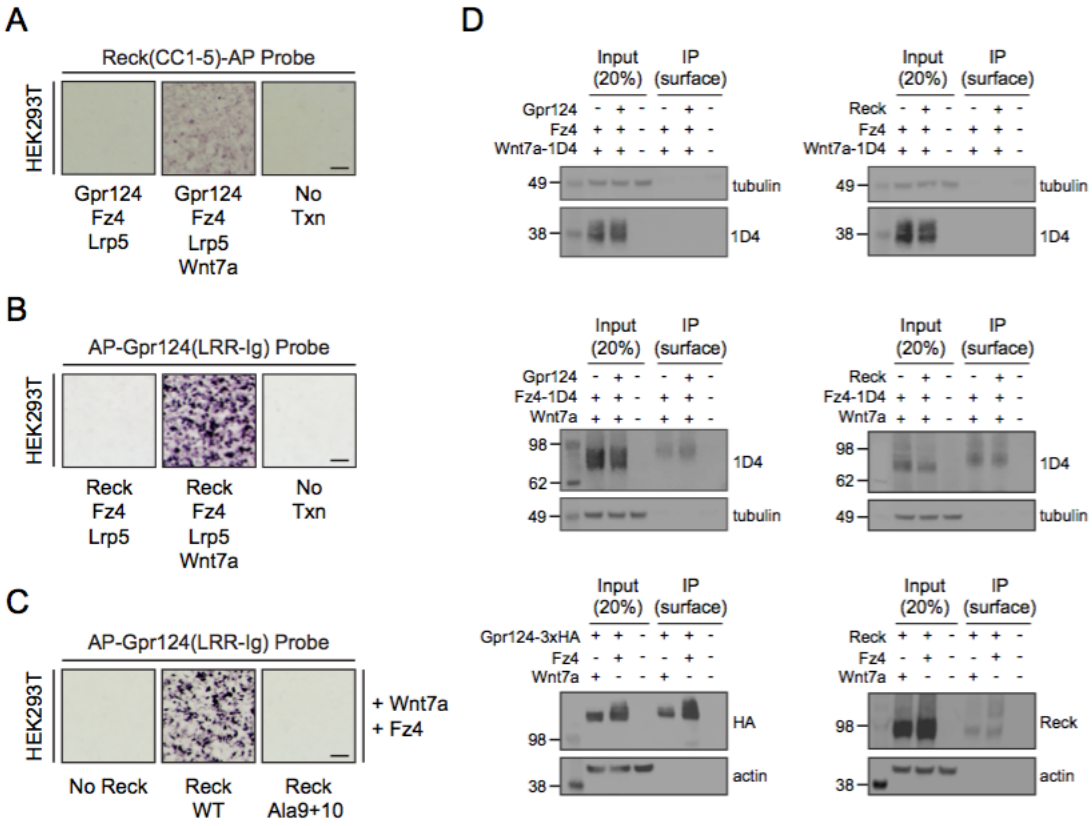
A
Reck(CC1-5)-AP Probe
HEK293T
Gpr124 Fz4 Lrp5
Gpr124 Fz4 Lrp5 Wnt7a
No Txn
B
AP-Gpr124(LRR-Ig) Probe
HEK293T
Reck Fz4 Lrp5
Reck Fz4 Lrp5 Wnt7a
No Txn
C
AP-Gpr124(LRR-Ig) Probe
HEK293T
+ Wnt7a
+ Fz4
No Reck
Reck WT
Reck Ala9+10
D
Input (20%)
IP (surface)
Gpr124
Fz4
Wnt7a-1D4
49
tubulin
38
1D4
Reck
Fz4-1D4
Wnt7a
98
62
Gpr124-3xHA
HA
actin
Reck

Table 1. Scoring of the relative vascular defects for each genotype examined

Embryonic Age	Genotype	Relative Severity of Vascular Defects					Corresponding Figure
		Cortex	MGE	LGE	Hindbrain	Spinal Cord	
E13.5	*WT*	0	0	0	0*	0	Figure 4A
E13.5	*Reck$^{flex2/\Delta ex1}$; Tie2-Cre*	1-2	2	2	0*	1-2	Figure 4B
E13.5	*Reck$^{flex2/\Delta ex2}$; Tie2-Cre*	1-2*	2	2*	0*	1-2*	Figure 5
E13.5	*Reck$^{\Delta ex2/\Delta ex2}$*	1-2	2	2	0*	1-2	Figure 4C
E13.5	*Reck$^{\Delta ex2/\Delta ex2}$; Ctnnb1$^{flex3/+}$; Pdgfb-CreER*	0-1	0-1	0-1	0*	0-1	Figure 4D
E11.5	*Reck$^{flex2/+}$; Tie2-Cre*	0*	0*	0*	0	0*	Figure 8A
E11.5	*Reck$^{flex2/\Delta ex2}$; Tie2-Cre*	1-2*	2*	2*	0	1-2*	Figure 8B
E11.5	*Reck$^{flex2/+}$; Ndp$^{\Delta/Y}$; Tie2-Cre*	0*	0*	0*	0	0*	Figure 8C
E11.5	*Reck$^{flex2/\Delta ex2}$; Ndp$^{\Delta/Y}$; Tie2-Cre*	2-3*	2-3*	2-3*	1-2	2*	Figure 8D
E11.5	*Reck$^{flex2/\Delta ex2}$; Gpr124$^{fl/\Delta}$; Tie2-Cre*	3*	3*	3*	2	2-3*	Figure 8E
E13.5	*Reck$^{flex2/+}$; Gpr124$^{fl/+}$; Tie2-Cre*	0	0	0	0*	0	Figure 9A
E13.5	*Reck$^{flex2/\Delta ex2}$; Gpr124$^{fl/+}$; Tie2-Cre*	1-2	2	2	0*	1-2	Figure 9B
E13.5	*Gpr124$^{fl/\Delta}$; Tie2-Cre*	1-2	2	2	0*	1-2	Figure 9C
E13.5	*Reck$^{flex2/+}$; Gpr124$^{fl/\Delta}$; Tie2-Cre*	2-3	3	3	1*	1-2	Figure 9D
E13.5	*Reck$^{flex2/\Delta ex2}$; Gpr124$^{fl/\Delta}$; Tie2-Cre*	2-3	3	3	2*	2-3	Figure 9E
E13.5	*Reck$^{+/\Delta ex2}$; Wnt7a$^{+/\Delta}$; Wnt7b$^{+/\Delta}$*	0	0	0	0*	0	Figure 10A
E13.5	*Wnt7a$^{\Delta/\Delta}$; Wnt7b$^{+/\Delta}$*	0	0	1	0*	0	Figure 10B
E13.5	*Reck$^{+/\Delta ex2}$; Wnt7a$^{\Delta/\Delta}$; Wnt7b$^{+/\Delta}$*	0	1-2	2	0*	0	Figure 10C
E13.5	*Reck$^{\Delta ex2/\Delta ex2}$; Wnt7a$^{\Delta/\Delta}$; Wnt7b$^{+/\Delta}$*	3	3	3	N/A[a]	3	Figure 10D
E13.5	*Reck$^{Cr/+}$*	0*	0*	0*	0*	0*	Data not shown
E13.5	*Reck$^{Cr/Cr}$*	0*	0*	0-1*	0*	0*	Data not shown
E13.5	*Reck$^{+/\Delta ex2}$; Gpr124$^{+/\Delta}$*	0	0	0	0*	0	Figure 15F
E13.5	*Reck$^{Cr/\Delta ex2}$; Gpr124$^{+/\Delta}$*	0	0-1	2	0*	1	Figure 15G

* Data not shown in main or supplemental figures.
[a] Not analyzed

For each genotype examined, a score of 0 to 3 was assigned as an approximate measure of the severity of the vascular defects observed in the different CNS regions, where 0 = no defects, and 3 = most severe defects.

Chapter 4

Discussion

4.1 Overview

In this thesis, we have identified: (1) Reck as a novel co-activator of Wnt7a/Wnt7b-specific signaling; (2) endothelial-cell knockout of Reck in mice results in impaired CNS angiogenesis and the failure of a proper BBB to form; (3) Reck and Norrin signaling function redundantly to promote angiogenesis in the hindbrain and to maintain BBB integrity in the post-natal brain; (4) Reck and Gpr124 synergize to activate Wnt7a/Wnt7b-specific signals *in vitro* and to control CNS angiogenesis *in vivo*; (5) N-terminal regions of both Reck and Gpr124 directly interact, and disrupting this binding interface on Reck results in reduced Wnt activation and defective CNS angiogenesis; (6) a soluble Gpr124 probe binds specifically to cells expressing Frizzled (Fz), Wnt7a or Wnt7b, and Reck; and (7) a soluble Reck probe binds specifically to cells expressing Fz,

Wnt7a or Wnt7b, and Gpr124. These data support a model in which Reck, Gpr124, Wnt7a/Wnt7b, and Frizzled assemble into a multi-protein complex to activate Wnt7a/Wnt7b-specific signals in CNS ECs for the proper development of the neurovasculature (Figure 16D).

4.2 Reck is a multi-functional protein involved in canonical Wnt signaling

First identified in 1989 by a Ras-transformation suppressor screen, Reck has been extensively characterized as an inhibitor of a disintegrin and metalloproteinase domain 10 (ADAM10) and a suite of matrix metalloproteinases (MMPs) (Noda et al., 1989; Takahashi et al., 1998; Oh et al., 2001; Miki et al., 2007; Muraguchi et al., 2007; Omura et al., 2009). Reck is expressed in a wide range of cell types, such as mural cells, endothelial cells, and neural progenitor cells (NPCs), and knockout mice die at E10.5 with severe defects, such as smaller body sizes, disrupted integrity of mesenchymal tissue, hemorrhaging in the abdomen, and under-developed vascular plexuses (Oh et al., 2001). Interestingly, the Reck knockout phenotype could be partially rescued on the genetic background of an MMP2 null animal, supporting the importance of Reck function in regulating MMP activity, albeit these double knockout mice only survive to E11.5 with modest improvements in tissue integrity (Oh et al., 2001). One group has shown that

mural-specific knockout of Reck in mice closely matches the mid-gestational lethality of the straight knockout animals, and that Reck's MMP inhibition in mural cells is important for: (1) their proper association with endothelial tip cells; and (2) the integrity of the extracellular matrix that surrounds the vessels (de Almeida et al., 2015).

In NPCs, Reck plays an important role in inhibiting ADAM10 activity to regulate Notch signaling for proper cortical development in the mouse (Muraguchi et al., 2007). For example, NPC-specific deletion of Reck results in precocious differentiation of these progenitor cells due to increased ADAM10-mediated shedding of Notch ligands, such as Delta, which ultimately results in impaired Notch signaling (Muraguchi et al., 2007). Another layer of regulation for this developmental process was appreciated when glycerophosphodiester phosphodiesterase 2 (Gde2) was identified as a critical enzyme responsible for cleaving GPI-anchored proteins, such as Reck, to also control Notch signaling in cortical neurogenesis (Park et al., 2013).

Our work identifies a novel function of Reck in a different tissue-specific context. In CNS endothelial cells, we demonstrate that Reck activates canonical Wnt signaling to promote CNS angiogenesis and regulate the BBB. While we cannot exclude the possibility that Reck is inhibiting MMPs and/or ADMAM10 to indirectly stabilize β-catenin in CNS endothelial cells, it appears unlikely that this form of inhibition would be generalized to protect all Wnts, Frizzleds, and/or Lrp5/Lrp6, especially given the

Wnt7a/Wnt7b ligand and Frizzled receptor specificity that is required for both signaling and complex formation. Certainly, it is possible that within this multi-protein complex state, Reck's primary function is to inhibit the cleavage of one or more of the other components, including Gpr124.

Unique to this novel function of Reck is the identification of the N-terminal domain (CC1-5) as the key region responsible for activating Wnt7a/Wnt7b-mediated signaling. Unlike the Kazal-like domains, which are responsible for its MMP and ADAM10 inhibitory function, CC1-5 has until now been uncharacterized with no known homology to other proteins (Takahashi et al., 1998; Oh et al., 2001; Chang et al., 2008). We have identified a key interface on CC1 that is required for direct interaction with Gpr124. Furthermore, based on our *in vitro* reporter assay for Wnt signaling, CC3 and CC4 appear to be critical for Reck function. The mechanism by which these latter CC sub-domains operate remains unclear and warrants further studies. One possible explanation for their importance could be that CC3 and CC4 are responsible for directly associating with Wnt7a/Wnt7b and/or the Fz receptor.

Given the established role of Gde2 to regulate cell-surface abundance of Reck, it is interesting to speculate whether Gde2 plays a role in CNS angiogenesis by controlling canonical Wnt signaling (Park et al., 2013). Notably, in FACS-purified P7 mouse brains, ECs exhibit expression of Gde2 (~23 FPKM) (Zhang et al., 2014). It is conceivable that

genetic depletion of Gde2 in ECs could lead to hyperactive CNS angiogenesis, while overexpression of Gde2 in ECs could lead to impaired CNS angiogenesis and a disrupted BBB.

4.3 Wnt-Frizzled specificity in signaling

Since the appreciation that the mammalian genome encodes 19 Wnt ligands and 10 Fz receptors, alongside the achievement of the first co-crystal structure of the Wnt-Fz CRD complex, it has remained unclear how ligand-receptor specificity is achieved and whether such specificity plays a significant biological role. For example, the co-crystal structure of *Xenopus* Wnt8 (XWnt8) with the mouse Fz8 CRD reveals that the binding interface between ligand and receptor is minimally limited to: (1) ~600 $Å^2$ where a covalent lipid modification on the Wnt ligand is buried within a hydrophobic groove of the Fz8 CRD, and (2) an additional ~1400 $Å^2$ of buried surface area between ligand and receptor (Janda et al., 2012). Both of these interfaces are highly conserved across all family members of Wnts and Fz CRDs, thereby presenting a puzzling degeneracy at the molecular level.

Additionally, by *in vitro* reporter assays for canonical Wnt signaling, it is clear that many Wnt ligands can activate multiple Fz receptors, consistent with the notion that binding and signaling are perhaps promiscuous (Yu et al., 2012). Genetic evidence *in vivo* supports this idea of functional redundancy, as the combined loss of multiple Wnts

or Frizzleds can lead to an enhanced phenotype compared to a single knockout alone (i.e., Wnt1 and Wnt4, Mulroy et al., 2002; Wnt3a and Wnt8a, Cunningham et al., 2015; Fz4 and Fz8, Ye et al., 2011; Fz1, Fz2, and Fz7, Yu et al., 2012).

In the developing CNS, many Wnts are expressed by neural progenitors, such as Wnt1, Wnt3, Wnt3a, Wnt4, Wnt7a, and Wnt7b, the latter two being the primary Wnts responsible for CNS angiogenesis (Stenman et al., 2008; Daneman et al., 2009). Additionally, many Frizzleds are expressed in CNS endothelial cells, such as Fz1, Fz4, Fz6, and Fz8 (Zhang et al., 2014). If specificity between ligand and receptor is negligible, then several questions immediately come to mind: (1) Do Wnt7a and Wnt7b activate canonical Wnt signaling in other non-endothelial CNS cell types that also express Fz receptors? and (2) Do Wnt1, Wnt3, Wnt3a, and Wnt4 activate the canonical pathway in CNS ECs to promote angiogenesis?

These questions essentially point at one obvious problem that results from the promiscuity of Wnts and Frizzleds – that is, how do CNS tissues, which are comprised of a complex, heterogeneous collection of different cells, achieve tightly regulated Wnt signaling. One possible solution to this problem would be if there were, in addition to Fz receptors and Lrp5/Lrp6 co-receptors, other cell-surface proteins that: (1) are expressed in specific CNS cell-types; and (2) function as Wnt-specific co-factors. Our work supports this model. We have identified Reck and Gpr124 as essential receptor co-factors

for Wnt7a- and Wnt7b-mediated signaling in CNS ECs for angiogenesis. While Gpr124 is predominantly expressed in CNS ECs, Reck is more broadly expressed in other cell types (i.e. ECs, mural cells, neurons, oligodendrocyte progenitor cells, and astrocytes) (Zhang et al., 2014). Despite the differences in cell-type expression for Reck and Gpr124, our work suggests that maximal signaling by Wnt7a and Wnt7b is transduced when both receptor co-factors are present in the same cell-type, as demonstrated by the fact that the individual elimination of one or the other leads to defects in CNS angiogenesis. In the 20 years since the discovery that Frizzleds constitute the principal receptors for Wnt ligands, Reck and Gpr124 represent the first examples of Wnt-specific receptor co-factors. Whether other receptor co-factors exist for the remaining 17 Wnt ligands has yet to be explored.

The identification of Reck and Gpr124 as specificity factors warrants further studies on how exactly these cell-surface proteins are ligand-specific. One explanation, and possibly the simplest, is that Reck and/or Gpr124 directly interact(s) with Wnt7a/Wnt7b and not with the other Wnt ligands. Another important consideration is the degree of Fz specificity that is observed. Whether Reck and/or Gpr124 also directly interact(s) with Fz has yet to be explored. In our experiments, we have shown that the extracellular domains of Reck and Gpr124 are critical for signaling and complex assembly; however, deletion of the intracellular PDZ binding domain of Gpr124 also

results in a reduction of Wnt7a-specific activity (Posokhova et al., 2015). It will be important to determine if and how other regions of Gpr124, such as the transmembrane and intracellular domains, play a role in interacting with Fz, Lrp5/6, and/or cytoplasmic components that are involved in canonical Wnt signaling. Finally, while we propose a simple model of multi-protein complex formation, we acknowledge that there may be a specific temporal order in which each of the different components is assembled.

4.4 Region-specific Wnt signaling in CNS angiogenesis

While Wnt7a/Wnt7b-Fz-Reck-Gpr124 largely controls angiogenesis in the forebrain, a separate signaling cassette consisting of Norrin-Fz4-Tspan12 is responsible for promoting angiogenesis in the retina. In other regions of the brain, such as the hindbrain, both signaling axes appear to be important, as demonstrated by the exacerbated severity of the vascular phenotype upon the combined loss of Reck/Gpr124 and Norrin. It remains unclear why separate signaling cassettes, which ultimately transduce the same signal, have emerged to control the same developmental process in different regions of the CNS. One important consideration is that perhaps functional redundancy, such as in the hindbrain, provides a layer of protection in the event that one of the signaling axes is compromised. For example, patients with Norrie disease, an X-linked disorder due to mutations in Norrin, have impaired retinal angiogenesis and are almost always blind.

Despite their vascular defects in the retina, the vasculature in other CNS regions may have been largely preserved due to redundancy by Wnt7a/Wnt7b-Fz-Reck-Gpr124. It is interesting to note that if retinal angiogenesis mirrored vascular development in the hindbrain, with redundant Norrin- and Wnt7a/7b-signaling, then Norrie disease would likely not exist.

4.5 Beyond CNS angiogenesis: potential role of Reck and Gpr124 in other developmental processes

In addition to CNS angiogenesis, Wnt7a and Wnt7b are involved in other developmental processes. For example, Wnt7a has been shown to be important for the proper development and patterning of the limbs (Parr and McMahon, 1995). Specifically, knockout mice for Wnt7a exhibit forelimb defects, which include dorsal-to-ventral transformation as well as the absence of the 4^{th} and 5^{th} digits (Parr and McMahon, 1995). Curiously, hypomorphic knockout mice for Reck exhibit a similar patterning defect, in which the same 4^{th} and 5^{th} digits are missing in the forelimbs (Yamamoto et al., 2012). It remains unclear whether Reck is activating Wnt7a-specific signals in the limb mesenchyme, in a fashion similar to that in the CNS endothelium. It will be of interest to determine whether this signaling cassette consisting of Wnt7a/Wnt7b-Fz-Reck-Gpr124 is active in other tissue types beyond CNS ECs. Additional tissues of interest include the

lung, pancreas, and kidney where Wnt7b is required for organogenesis (Shu et al., 2002; Yu et al., 2009; Afelik et al., 2015).

4.6 Canonical Wnt signaling in BBB integrity and CNS disease: implications for Reck and Gpr124

The breakdown of the BBB has been observed in patients with a wide range of CNS disease, such as stroke, multiple sclerosis (MS), Alzheimer's disease, Parkinson's disease, and epilepsy (Daneman, 2012; Zhao et al., 2015). Given the importance of canonical Wnt signaling in BBB development and maintenance, there has been a growing interest in whether this signaling pathway is involved in the context of different CNS pathological conditions. Recent work has shown that using the experimental autoimmune encephalomyelitis (EAE) mouse model for MS, genetic inhibition of β-catenin signaling in post-natal ECs results in an exacerbated EAE disease phenotype (Lengfeld et al., 2017). In a different disease context, mouse models for ischemic stroke and glioblastoma also demonstrated a more severe disease phenotype upon sensitization of the BBB by EC-depletion of Gpr124 in the adult brain (Chang et al., 2017). Remarkably, this disease phenotype could be rescued upon β-catenin stabilization in ECs, supporting the importance of canonical Wnt signaling in establishing a functional BBB that may serve to protect against CNS disease progression (Chang et al., 2017). These findings imply that

reduced canonical Wnt signaling in CNS ECs can predispose individuals to worse clinical outcomes, and that enhancing the Wnt7a/Wnt7b-Fz-Reck-Gpr124 signaling pathway could be of therapeutic value.

Materials and Methods

Zebrafish Husbandry and Transgenic Line Used

Zebrafish were maintained and embryos were obtained and raised under standard conditions. Establishment and characterization of the *Tg(kdrl:GFP)*^{s843} transgenic line has been described elsewhere (Jin et al., 2005).

Zebrafish Imaging

All images were acquired using a Leica (Wetzlar, Germany) M165 stereomicroscope or a Zeiss (Oberkochen, Germany) LSM710 confocal microscope after embryo anesthesia with a low dose of tricaine and immobilization in 1% low-melting agarose in glass-bottom Petri dishes (MatTek Corporation, Ashland, MA). The microscope stage was enclosed in a temperature-controlled chamber, and samples were kept at 28.5℃. In all confocal images, brightness and contrast were adjusted linearly and equally. Three-

dimensional reconstructions were done with the Imaris FilamentTracer software (Bitplane, Zurich, Switzerland) in automatic detection mode before manual false-coloring and editing to highlight extra- and intra-cerebral vessels.

Morpholino Injections

Splice-blocking morpholinos against *erbb3b* (TGGGCTCGCAACTGGGTGGAAACAA) (Lyons et al., 2005; Budi et al., 2008), sorbs3 (TTTCCGACAGGGAAAGCACATACCC) (Malmquist et al., 2013), *reck* (CAGGTAGCAGCCGTCACTCACTCTC) (Prendergast et al., 2012) and *gpr124* (ACTGATATTGATTTAACTCACCACA) were obtained from Gene Tools (Eugene, OR) and injected at the one-cell stage at 0.5, 4, 1, and 2 ng, respectively, unless otherwise stated. Injection of a standard control morpholino (up to 8 ng) did not affect brain vasculature or DRG formation.

Mouse Gene Targeting

To construct the Cre-dependent reporter for canonical Wnt signaling, the following elements were inserted (in the order listed) into a standard Rosa26 targeting vector: an *frt-phosphoglycerate kinase (PGK)-neomycin (Neo)-frt* (FNF) cassette, which includes a strong poly-adenylation signal; six tandem repeats of a consensus LEF/TCF binding site CCTTTGATC and a minimal Heat shock protein 68 promoter (Ferrer-Vaquer et al., 2010); a LSL cassette; an open reading frame coding for a histone H2B-GFP-6xMyc fusion protein; and a bovine growth hormone 3'UTR. The *R26-Tcf/Lef-LSL-H2B-GFP* targeting construct with a flanking Diphteria toxin-A coding sequence was electroporated into R1 ES cells, which were then subjected to G418 selection. Clones harboring the targeted allele were identified by Southern blot hybridization, karyotyped, and injected into blastocysts. Germline transmission to progeny of founder males was determined by PCR.

The $Reck^{Cr}$ mouse was generated using CRISPR/Cas9 gene editing. A sgRNA (gattattgccctgaaacaat) targeting exon 3 of *Reck* was selected and synthesized, as described by Pelletier et al. (2015). Briefly, a dsDNA template containing the sequences for a T7 promoter, the sgRNA, and a tracrRNA scaffold was generated by tandem PCR amplification and purification on a Qiagen column (Qiagen 28106). *In vitro* transcription of this dsDNA template was performed using the MEGAshortscript T7 Kit (Invitrogen

AM1354), and products were purified using the MEGAclear Transcription Clean-Up Kit (Invitrogen AM1908). The Cas9 mRNA was transcribed from a modified pX330 plasmid (Addgene 42230), which contains a T7 promoter (pX330+T7), using the mMESSAGE mMACHINE T7 Ultra Transcription Kit (Invitrogen AM1345). The transcript was purified by LiCl precipitation. The quality of all purified transcripts was confirmed using the Agilent 2100 Bioanalyzer. The ssODN HDR template (tttctcctcaaaaagtgaatcccgactgaaacatctgttggctgctgctgctgcttgccctgaaacaatggtgagtcttacggagctgtggaag) was synthesized by IDT. The sgRNA, Cas9 mRNA, and HDR template were injected into C57BL/6 x SJL F2 embryos and correctly targeted founders were backcrossed to C57BL/6 mice for a total of four generations.

Mouse lines

The following mouse alleles were used: *Reck*^{flex2} (Acc. No. CDB0488K: http://www.cdb.riken.jp/arg/mutant%20mice%20list.html; Chandana et al., 2010), *Reck*$^{\Delta ex1}$ (Oh et al., 2001), *Ctnnb1*^{flex3} (Harada et al., 1999), *Ndp*$^{\Delta}$ (JAX 012287; Ye et al., 2009), *Gpr124*^{fl} (JAX 016881; Cullen et al., 2011), *Wnt7a*^{fl} (Dunlap et al., 2011), *Wnt7b*^{fl} (JAX 008467; Rajagopal et al., 2008), *Tie2-Cre* (JAX 008863), and *Pdgfb-CreER*

(Claxton et al., 2008). The following null alleles were generated by breeding mice carrying the germline *Sox2-Cre* transgene with floxed (*fl*) mice: $Reck^{\Delta ex2}$, $Gpr124^{\Delta}$, $Wnt7a^{\Delta}$, and $Wnt7b^{\Delta}$. All mice were housed and handled according to the approved Institutional Animal Care and Use Committee (IACUC) protocol MO16M369 of the Johns Hopkins Medical Institutions.

Antibodies and Other Reagents

The following antibodies were used for tissue immunohistochemistry: rat anti-mouse PECAM/CD31 (BD Biosciences 553370); rabbit anti-Glut1 (Thermo Fisher Scientific RB-9052-P1); rat anti-mouse PLVAP/MECA-32 (BD Biosciences 553849); mouse anti-Claudin5, Alexa Fluor 488 conjugate (Thermo Fisher Scientific 352588); Texas Red streptavidin (Vector Laboratories SA-5006); rabbit anti-GFP, Alexa Fluor 488 conjugate (Thermo Fisher Scientific A21311); rabbit anti-6xMyc (JH6204); Brilliant Violet 421 rat anti-mouse/human Cd11b (BioLegend 101235); and rat anti-F4/80, Alexa Fluor 488 conjugate (Bio-Rad MCA497A488T). Alexa Fluor-labeled secondary antibodies and GS Lectin (Isolectin GS-IB4) were from Thermo Fisher Scientific.

The following antibodies were used for immunoblot analysis: rabbit anti-6xMyc (JH6204); rabbit anti-HA (Cell Signaling 3724); mouse anti-actin (EMD Millipore MAB1501); rabbit anti-Reck (Cell Signaling 3433); mouse anti-1D4 (MacKenzie et al., 1984); and rat anti-alpha tubulin (Invitrogen MA1-80017). Fluorescent secondary antibodies for immunoblotting were from Li-Cor.

Tissue Processing and Immunohistochemistry

Tissue were prepared and processed for immunohistochemical analysis as described by Wang et al. (2012) and Zhou et al. (2014). Briefly, embryos and early postnatal brains were harvested and immersion fixed overnight at 4ºC in 1% PFA, followed by 100% MeOH dehydration overnight at 4ºC. Embryos that were specifically prepared for F4/80 or Cd11b staining were harvested and dehydrated without fixation in 100% acetone overnight at 4ºC. All tissues were re-hydrated the following day in 1x PBS at 4ºC for at least 3 hours before embedding in 3% agarose. Tissue sections of 150-180 μm thickness were cut using a vibratome (Leica).

Sections were incubated overnight with primary antibodies (1:400) or Texas Red streptavidin (1:100) diluted in 1x PBSTC (1x PBS + 0.5% Triton X-100 + 0.1mM $CaCl_2$) + 10% normal goat serum (NGS). Sections were washed at least 3 times with 1x PBSTC over the course of 6 hours, and subsequently incubated overnight with secondary antibodies (1:400) diluted in 1x PBSTC + 10% NGS. If a primary antibody raised in rat was used, secondary antibodies were additionally incubated with 1% normal mouse serum (NMS) as a blocking agent. The next day, sections were washed at least 3 times with 1x PBSTC over the course of 6 hours, and flat-mounted using Fluoromount G (EM Sciences 17984-25). Sections were imaged using a Zeiss LSM700 confocal microscope, and processed with ImageJ, Adobe Photoshop, and Adobe Illustrator software. Incubation and washing steps were performed at 4ºC.

4-HT and Tamoxifen Preparation and Administration

4-HT and Tamoxifen were prepared as described by Zhou and Nathans (2014). In short, solid 4-HT (Sigma-Aldrich H7904) or Tamoxifen (Sigma-Aldrich T5648) was dissolved in an ethanol:sunflower seed oil (Sigma-Aldrich S5007) mixture (1:5 volume) to a final concentration of 4 mg/ml or 50 mg/ml, respectively, and stored in aliquots at -80ºC.

Thawed aliquots of 4-HT and Tamoxifen were diluted to a final concentration of 1 mg/ml and 10 mg/ml, respectively. All injections were performed intraperitoneally. Pups were injected with 50 µl of 4-HT at P3 and again at P4. Gestational day (G)10.5 females were injected with 150 µl of Tamoxifen.

Sulfo-NHS-Biotin Preparation and Administration

Sulfo-NHS-Biotin (Thermo Scientific 21335) was dissolved in 1x PBS to a final concentration of 20 mg/ml. Pups were injected with 100-150 µl Sulfo-NHS-Biotin IP 30-45 minutes before sacrifice.

Plasmids

The mouse Reck cDNA sequence (GE Dharmacon; clone BC138065) was cloned into the pRK5 mammalian expression vector. The Myc epitope (EQKLISEEDL) was inserted at an endogenous XmaI site downstream of the Reck signal sequence to generate Myc-Reck. Myc-tagged Reck was used as a backbone to generate ΔCC1-5 (Δ amino acids

(Δaa)30-339), ΔFz-like CRD (Δaa348-468), ΔC-term1 (Δaa477-830), and ΔC-term2 (Δaa477-906). An 11 amino acid spacer (GGTRGSGAPGG) replaced each of these deleted segments. Additional deletions in Myc-Reck were constructed without the spacer: ΔCC1 (Δaa30-103), ΔCC2 (Δaa104-150), ΔCC3 (Δaa151-215), ΔCC4 (Δaa216-291), ΔCC5 (Δaa292-342), ΔCC2-5 (Δaa104-342), ΔCC3-5 (Δaa151-342), and ΔCC4-5 (Δaa216-342). The COMP domain in the COMP-AP vector encompassed the pentameric domain of COMP (Malashkevich et al., 1996).

The Gpr124 plasmid was a kind gift from Dr. Calvin Kuo (Stanford) and was cloned into a pRK5 expression vector. A 3xHA epitope tag (SGSSGYPYDVPDYAGGYPYDVPDYAGGYPYDVPDYATRG) was inserted between amino acids 1322 and 1323 to generate Gpr124-3xHA. The epitope tagged Gpr124 was used as a backbone to generate the following deletions: ΔLRR (Δaa37-245), ΔIg (Δaa253-348), ΔLRR+Ig (Δaa37-348), ΔHormR (Δaa352-427), and ΔGAIN (Δaa428-751).

Inserts for AP and Fc constructs were PCR amplified from Reck and Gpr124 pRK5 expression vectors. Alanine scanning mutagenesis was performed by tandem PCR. All constructs were confirmed by sequencing.

Expression plasmids for the mouse Wnts and Frizzleds are described in Yu et al. (2012).

Luciferase Assays

Dual luciferase assays were performed as described by Xu et al. (2004). Briefly, STF cells were plated on 96-well plates at a confluency of 30-40%. The following day, fresh DMEM/F-12 (Thermo Fisher Scientific 12500) supplemented with 10% fetal bovine serum (FBS) was replaced in each of the wells. Three hours later, cells were transfected in triplicate with expression plasmids (180-240 ng of DNA per 3 wells) using FuGENE HD Transfection Reagent (Promega E2311). The DNA master mix (unless otherwise specified) included: 1.5 ng of the internal control Renilla luciferase plasmid (pRL-TK), and 60 ng each of the pRK5 expression plasmids for Gpr124, Reck, Wnt7a, mutants, and control vector. 48 hours post-transfection, cells were harvested in 1x Passive Lysis Buffer (Promega E194A) for 20 minutes at room temperature. Lysates were used to measure Firefly and Renilla luciferase activity using the Dual-Luciferase Reporter Assay System (Promega E1910) and a Turner BioSystems Luminometer (TD-20/20). Relative luciferase activity was calculated by normalizing Firefly/Renilla values. GraphPad Prism 7 software

was used to generate plots and perform statistical analysis. The mean ± standard deviations are shown.

Alkaline Phosphatase Binding Assays

Conditioned DMEM/F-12 media containing AP and Fc fusion proteins were collected from HEK293T cells that were transfected with pRK5 expression plasmids using FuGENE HD Transfection Reagent. For Fc fusion proteins, the conditioned media was removed 24 hours after transfection, and cells were washed at least 3 times with 1x PBS prior to incubating them in serum-free DMEM/F-12. All conditioned media were collected 72 hours post-transfection and spun-down to remove detached cells. To quantify yield of AP fusion proteins, an aliquot of the conditioned medium was incubated with BluePhos phosphatase substrate solution (5-bromo-4-chloro-3-indolyl phosphate/tetrazolium; Kirkegaard and Perry Laboratories 50-88-00).

For cell-based COMP-AP binding assays (Figures 12 and 14), COS-7 cells were transfected for 48 hours and subsequently incubated with the COMP-AP probe in serum-containing conditioned medium at 4ºC for 2 hours. Cells were washed 6 times with cold

PBS prior to fixing with cold 4% paraformaldehyde (PFA) in PBS. Fixed cells were placed in a 70ºC water bath for 1 hour to heat denature endogenous AP. Bound AP was visualized by incubation with nitro blue tetrazolium/5-bromo-4-chloro-3-indolyl phosphate (NBT/BCIP) substrate (Roche 11383213001) at room temperature.

For cell-based AP binding assays to assess multi-protein complexes (Figure 15), HEK293T cells were used because their high transfection efficiency facilitates co-transfection of multiple plasmids. Cells were plated on 0.2% gelatin coated coverslips, and 48 hours post-transfection the coverslips were incubated with serum-containing conditioned medium at 4ºC for 2 hours. Cells were washed 3 times with cold serum-free DMEM/F-12 media prior to fixation, heat denaturation, and AP visualization as described above.

The following probes were tested for cell-based binding assays: Reck(CC1-5)-AP, Gpr124(LRR-Ig)-AP (data not shown), AP-Gpr124(LRR-Ig), Reck(CC1-5)-COMP-AP, and Gpr124(LRR-Ig)-COMP-AP. Gpr124(LRR-Ig)-AP bound minimally to COS-7 cells expressing Reck (data not shown); a stronger signal was obtained with Gpr124(LRR-Ig)-COMP-AP. AP-Gpr124(LRR-Ig), which contains a 3xMyc linker between AP and

Gpr124(LRR-Ig), did not bind to COS-7 cells expressing Reck, but bound specifically to HEK293T cells expressing Frizzled/Wnt/Reck multi-protein complexes.

For cell-free AP binding assays, Fc fusion proteins in serum-free conditioned medium were captured on 96-well Protein-G plates (Thermo Fisher Scientific 15131) at 4ºC overnight. Wells were washed 3x with PBS, and incubated with conditioned medium containing COMP-AP fusion proteins at 25ºC for 1-2 hours. Wells were subsequently washed 6x with PBS, and incubated with BluePhos phosphatase substrate solution. AP activity was detected by measuring absorbance at 620 nm using a SpectraMax M3 Microplate Reader (Molecular Devices). For experiments involving a comparison among different COMP-AP probes, probe concentrations were equalized based on AP activity.

Non-permeabilized Live-Cell Immunostaining, Cell Surface Biotinylation Assay, and Immunoblot Analysis

For non-permeabilized live-cell immunostaining, COS-7 cells were transfected with pRK5 expression plasmids using FuGENE HD Transfection Reagent. The media was removed 48 hours post-transfection, and cells were washed 3 times with PBS. Cells were

incubated with diluted primary antibodies (1:500) in serum-containing media at 4ºC for 1 hour, and then washed 5-6 times with cold PBS, prior to fixation with 4% PFA/PBS. Coverslips were mounted using Fluoromount G and imaged using a Zeiss LSM700 confocal microscope. Images were processed with ImageJ, Adobe Photoshop, and Adobe Illustrator software.

Cell surface biotinylation was performed as described by Pavel et al. (2014). In short, COS-7 cells were transfected with pRK5 expression plasmids with FuGENE HD Transfection Reagent. The media was removed 48 hours post-transfection, and cells were washed 3 times with PBS. Cells were incubated in PBS containing Sulfo-NHS-Biotin (250 μg/ml) at 4ºC for 30 minutes. Excess biotin was quenched by adding Tris-HCl pH 7.4 to a final concentration of 50 mM at 4ºC for 5 minutes. After removing the Tris buffer, cells were detached, washed 3 times in 1x Tris buffered saline (TBS), and lysed in RIPA buffer (50 mM Tris-HCl pH 7.4, 150 mM NaCl, 1% Triton X-100, and 0.5% deoxycholate) containing protease inhibitor (Roche 11836170001). Cell lysates were incubated at 4ºC for 30 minutes and subsequently centrifuged at 10,000xg at 4ºC for 20 minutes to remove cellular debris. Cell-surface proteins were captured by incubating cleared lysates with NeutrAvidin Agarose Resin (Thermo Fisher Scientific 29200) overnight at 4ºC. Resin was washed 5 to 6 times with RIPA buffer, and captured proteins,

along with input controls, were resolved by SDS-PAGE and transferred to PVDF membranes (EMD Millipore IPFL00010) for immunoblotting. Immunoblots were incubated with primary antibodies (1:10,000 mouse anti-HA and rabbit anti-6xMyc; 1:2000 rabbit anti-Reck) diluted in Odyssey Blocking Buffer (LiCor 927-40000) overnight at 4ºC. Membranes were washed with 1x PBS-T (1x PBS + 0.1% Tween 20), and incubated with LiCor secondary antibodies (1:10,000) diluted in Odyssey Blocking Buffer for 1 hour at room temperature. Membranes were washed at least 3 times with 1x PBS-T and developed using the Odyssey Fc Imaging System (LiCor).

For whole tissue lysates, E13.5 embryos were harvested and homogenized using a plastic pestle in RIPA buffer supplemented with protease inhibitors. Tissue lysates were incubated at 4ºC for 1 hour, cleared by centrifugation, and prepared for immunoblot analysis, as described above.

Quantification and Statistical Analysis

For quantifying relative vascular density, 150-180 μm thick coronal sections of embryonic brain or cross sections of embryonic spinal cord were stained with GS Lectin,

anti-PECAM, and anti-Glut1. Confocal images were scanned at 10-12 μm intervals along the Z-axis, of which 8-10 images were Z-stacked. The following areas of the Z-stacked images were analyzed: cortex (1000 x 600 μm), MGE (500 x 500 μm), LGE (300 x 300 μm), hindbrain (300 x 500 μm), and spinal cord (350 x 500 μm). All of the blood vessels within the designated volume were manually traced using a Wacom tablet and Adobe Illustrator software. The lengths of the traced vessels were quantified by calculating pixel coverage as a fraction of the total area using ImageJ. For quantifying GS Lectin$^+$ macrophages, individual GS Lectin$^+$ cells that did not co-localize with a vascular marker (i.e. anti-PECAM and anti-Glut1) were manually counted in each of the designated volumes. Quantification of the fraction of macrophages that immunostained positive for F4/80, Cd11b, and/or GS Lectin, was conducted as follows: non-ECs (cells that did not co-localize with anti-Glut1) were manually counted for each of the different markers and divided by the total number of non-ECs that immunostained positive for F4/80 and/or GS Lectin or Cd11b and/or GS Lectin.

For quantifying GFP$^+$ nuclei in the *Rosa26 Tcf/Lef-lsl-H2B-GFP* Wnt reporter mouse, 150-180 μm thick coronal sections of embryonic brain or cross sections of embryonic spinal cord were stained with anti-GFP and anti-PECAM. Quantification followed the procedure outlined above, with the following areas cropped: cortex (1000 x 600 μm) and

spinal cord (150 x 150 μm). GFP^+ nuclei that co-localized with $PECAM^+$ cells were manually counted in each of the designated volumes. Relative vascular density within that volume was also measured (as described above). To calculate the number of GFP^+ EC nuclei normalized to vascular density, the absolute number of GFP^+ EC nuclei was divided by the length of the vasculature within the designated volume.

For quantifying the fraction of vessels that immunostained positive for Claudin-5 or PLVAP, vessels in the designated volume of 1000 x 1000 x 100 μm were manually traced and pixel coverage of the traced image was determined as a fraction of the total designated volume (as described above) for each marker. The vascular density for Claudin-5^+ and $PLVAP^+$ vessels was then divided by the total vascular density in the designated volume.

GraphPad Prism 7 software was used to generate plots and to perform statistical analysis. The mean ± standard deviations are shown. Statistical significance was determined by the unpaired t-test, and is represented by * ($P<0.05$), **($P<0.01$), *** ($P<0.001$), and **** ($P<0.0001$).

The analysis of alignment and conservation of Reck CC1 across vertebrates was generated using Clustal Omega (McWilliam et al., 2013).

References

Afelik, S., Pool, B., Schmerr, M., Penton, C., and Jensen, J. (2015). Wnt7b is required for epithelial progenitor growth and operates during epithelial-to-mesenchymal signaling in pancreatic development. Development 399, 204-217.

Anderson, K.D., Pan, L., Yang, X.M., Hughes, V.C., Walls, J.R., Dominguez, M.G., Simmons, M.V., Burfeind, P., Xue, Y.Z., Wei, Y., *et al*. (2011). Angiogenic sprouting into neural tissue requires Gpr124, an orphan G protein-coupled receptor. Proc. Natl. Acad. Sci. USA 108, 2807-2812.

Ben-Zvi, A., Lacoste, B., Kur, E., Andreone, B.J., Mayshar, Y., Yan, H., and Gu, C. (2014). Mfsd2a is critical for the formation and function of the blood-brain barrier. Nature 509, 507-511.

Bhanot, P., Brink, M., Samos, C.H., Hsieh, J.C., Wang, Y., Macke, J.P., Andrew, D., Nathans, J., and Nusse, R. (1996). A new member of the frizzled family from Drosophila functions as a Wingless receptor. Nature 382, 225-230.

Blanchette, M. and Daneman, R. (2015). Formation and maintenance of the BBB. Mech. Dev. 138, 8-16.

Budi, E.H., Patterson, L.B., and Parichy, D.M. (2008). Embryonic requirements for ErbB signaling in neural crest development and adult pigment pattern formation. Development 135, 2603–2614.

Chandana, E.P., Maeda, Y., Ueda, A., Kiyonari, H., Oshima, N., Yamamoto, M., Kondo, S., Oh, J., Takahashi, R., Yoshida, Y., *et al*. (2010). Involvement of the Reck tumor suppressor protein in maternal and embryonic vascular remodeling in mice. BMC Dev. Biol. 10, 84.

Chang, C.K., Hung, W.C., and Chang, H.C. (2008). The Kazal motifs of RECK protein inhibit MMP-9 secretion and activity and reduce metastasis of lung cancer cells in vitro and in vivo. J. Cell Mol. Med. 12, 2781-2789.

Chang, J., Mancuso, M., Maier, C., Liang, X., Yuki, K., Yang, L., Kwong, J.W., Wang, J., Rao, V., Vallon, M., *et al*. (2017) Gpr124 is essential for blood-brain barrier integrity in central nervous system disease. Nat. Med. 23, 450-460.

Claxton, S., Kostourou, V., Jadeja, S., Chambon, P., Hodivala-Dilke, K., and Fruttiger, M. (2008). Efficient, inducible Cre-recombinase activation in vascular endothelium. Genesis 46, 74-80.

Cullen, M., Elzarrad, M.K., Seaman, S., Zudaire, E., Stevens, J., Yang, M.Y., Li, X.J., Chaudhary, A., Xu, L.H., Hilton, M.B., *et al*. (2011). GPR124, an orphan G protein-coupled receptor, is required for CNS-specific vascularization and establishment of the blood-brain barrier. Proc. Natl. Acad. Sci. USA 108, 5759-5764.

Cunningham, T.J., Kumar, S., Yamaguchi, T.P., and Duester, G. (2015). Wnt8a and Wnt3a cooperate in the axial stem cell niche to promote mammalian body axis extension. Dev. Dyn. 244, 797-807.

Daneman, R. (2012). The blood-brain barrier in health and disease. Ann. Neurol. 72, 648-672.

Daneman, R., Agalliu, D., Zhou, L., Kuhnert, F., Kuo, C.J., and Barres, B.A. (2009). Wnt/beta-catenin signaling is required for CNS, but not non-CNS, angiogenesis. Proc. Natl. Acad. Sci. USA 106, 6422-6422.

Daneman, R., and Prat, A. (2015). The blood-brain barrier. Cold Spring Harb. Perspect. Biol. 7, a020412.

de Almeida, G.M., Yamamoto, M., Morioka, Y., Ogawa, S., Matsuzaki, T., and Noda, M. (2015). Critical roles for murine Reck in the regulation of vascular patterning and stabilization. Sci. Rep. *5*, 17860.

Dunlap, K.A., Filant, J., Hayashi, K., Rucker, E.B. 3rd, Song, G., Deng, J.M., Behringer, R.R., DeMayo, F.J., Lydon, J., Jeong, J.W., *et al*. (2011). Postnatal deletion of Wnt7a inhibits uterine gland morphogenesis and compromises adult fertility in mice. Biol. Reprod. 85, 386-396.

Ferrer-Vaquer, A., Piliszek, A., Tian, G., Aho, R.J., Dufort, D., and Hadjantonakis, A.K. (2010). A sensitive and bright single-cell resolution live imaging reporter of Wnt/ß-catenin signaling in the mouse. BMC Dev. Biol. 10, 121.

Harada, N., Tamai, Y., Ishikawa, T., Sauer, B., Takaku, K., Oshima, M., and Taketo, M.M. (1999). Intestinal polyposis in mice with a dominant stable mutation of the beta-catenin gene. EMBO J. 18, 5931-5942.

Honjo, Y., Kniss, J., and Eisen, J.S. (2008). Neuregulin-mediated ErbB3 signaling is required for formation of zebrafish dorsal root ganglion neurons. Development 135, 2615–2625.

Janda, C.Y., Waghray, D., Levin, A.M., Thomas, C., and Garcia, K.C. (2012). Structural Basis of Wnt Recognition by Frizzled. Science 337, 59-64.

Jho, E.H., Zhang, T., Domon, C., Joo, C.K., Freund, J.N., and Costantini, F. (2002). Wnt/beta-catenin/Tcf signaling induces the transcription of Axin2, a negative regulator of the signaling pathway. Mol. Cell. Biol. 22, 1172-1183.

Jin, S.W., Beis, D., Mitchell, T., Chen J.N., and Stainier, D.Y.R. (2005). Cellular and molecular analyses of vascular tube and lumen formation in zebrafish. Development 132, 5199–5209.

Junge, H.J., Yang, S., Burton, J.B., Paes, K., Shu, X., French, D.M., Costa, M., Rice, D.S., and Ye, W.L. (2009). TSPAN12 Regulates Retinal Vascular Development by Promoting Norrin- but Not Wnt-Induced FZD4/beta-Catenin Signaling. Cell 139, 299-311.

Kuhnert, F., Mancuso, M.R., Shamloo, A., Wang, H.T., Choksi, V., Florek, M., Su, H., Fruttiger, M., Young, W.L., Heilshorn, S.C., *et al*. (2010). Essential Regulation of CNS Angiogenesis by the Orphan G Protein-Coupled Receptor GPR124. Science 330, 985-989.

Lai, M.B., Zhang, C., Shi, J., Johnson, V., Khandan, L., McVey, J., Klymkowsky, M.W., Chen, Z., and Junge, H.J. (2017). TSPAN12 is a Norrin co-receptor that amplifies Frizzled4 ligand selectivity and signaling. Cell Rep. 19, 2809-2822.

Lengfeld, J.E., Lutz, S.E., Smith, J.R., Diaconu, C., Scott, C., Kofman, S.B., Choi, C., Walsh, C.M., Raine, C.S., Agalliu, I., *et al*. (2017). Endothelial Wnt/β-catenin signaling reduces immune

cell infiltration in multiple sclerosis. Proc. Natl. Acad. Sci. USA 114, E1168-E1177.

Liebner, S., Corada, M., Bangsow, T., Babbage, J., Taddei, A., Czupalla, C.J., Reis, M., Felici, A., Wolburg, H., Fruttiger, M., *et al*. (2008). Wnt/beta-catenin signaling controls development of the blood-brain barrier. J. Cell Biol. 183, 409-417.

Lyons, D.A., Pogoda, H.M., Voas, M.G., Woods, I.G., Diamond, B., Nix, R., Arana, N., Jacobs, J., and Talbot, W.S. (2005). Erbb3 and erbb2 are essential for schwann cell migration and myelination in zebrafish. Curr. Biol. 15, 513–524.

MacDonald, B.T., Tamai, K., and He, X. (2009). Wnt/β-catenin signaling: components, mechanisms, and diseases. Dev. Cell 17, 9-26.

MacKenzie, D., Arendt, A., Hargrave, P., McDowell, J.H., and Molday, R.S. (1984). Localization of binding sites for carboxyl terminal specific anti-rhodopsin monoclonal antibodies using synthetic peptides. Biochemistry 23, 6544-6549.

Malashkevich, V.N., Kammerer, R.A., Efimov, V.P., Schulthess, T., and Engel, J. (1996). The crystal structure of a five-stranded coiled coil in COMP: a prototype ion channel? Science 274, 761–765.

Malmquist, S.J., Abramsson, A., McGraw, H.F., Linbo, T.H., and Raible, D.W. (2013). Modulation of dorsal root ganglion development by ErbB signaling and the scaffold protein Sorbs3. Development 140, 3986–3996.

Maretto, S., Cordenonsi, M., Dupont, S., Braghetta, P., Broccoli, V., Hassan, A.B., Volpin, D., Bressan, G.M., and Piccolo, S. (2003). Mapping Wnt/beta-catenin signaling during mouse development and in colorectal tumors. Proc. Natl. Acad. Sci. USA 100, 3299-3304.

McWilliam, H., Li, W., Uludag, M., Squizzato, S., Park, Y.M., Buso, N., Cowley, A.P., and Lopez, R. (2013). Analysis Tool Web Services from the EMBL-EBI. Nucleic Acids Res. 41, W597-600.

Miki, T., Takegami, Y., Okawa, K., Muraguchi, T., Noda, M., and Takahashi, C. (2007). The reversion-inducing cysteine-rich protein with Kazal motifs (RECK) interacts with membrane type 1 matrix metalloproteinase and CD13/aminopeptidase N and modulates their endocytic pathways. J. Biol. Chem. 282, 12341-12352.

Mulroy, T., McMahon, J.A., Burakoff, S.J., McMahon, A.P., and Sen, J. (2002). Wnt-1 and Wnt-

4 regulate thymic cellularity. Eur. J. Immunol. 32, 967-971.

Muraguchi, T., Takegami, Y., Ohtsuka, T., Kitajima, S., Chandana, E.P., Omura, A., Miki, T., Takahashi, R., Matsumoto, N., Ludwig, A., *et al*. (2007). RECK modulates Notch signaling during cortical neurogenesis by regulating ADAM10 activity. Nat. Neurosci. 10, 838-845.

Noda, M., Kitayama, H., Matsuzaki, T., Sugimoto, Y., Okayama, H., Bassin, R.H., and Ikawa, Y. (1989). Detection of genes with a potential for suppressing the transformed phenotype associated with activated ras genes. Proc. Natl. Acad. Sci. USA 86, 162-126.

Oh, J., Takahashi, R., Kondo, S., Mizoguchi, A., Adachi, E., Sasahara, R.M., Nishimura, S., Imamura, Y., Kitayama, H., Alexander, D.B., *et al*. (2001). The membrane-anchored MMP inhibitor RECK is a key regulator of extracellular matrix integrity and angiogenesis. Cell 107, 789-800.

Omura, A., Matsuzaki, T., Mio, K., Ogura, T., Yamamoto, M., Fujita, A., Okawa, K., Kitayama, H., Takahashi, C., Sato, C., *et al*. (2009). RECK forms cowbell-shaped dimers and inhibits matrix metalloproteinase-catalyzed cleavage of fibronectin. J. Biol. Chem. 284, 3461-3469.

Park, S., Lee, C., Sabharwal, P., Zhang, M., Meyers, C.L., and Sockanathan, S. (2013). GDE2 promotes neurogenesis by glycosylphosphatidylinositol-anchor cleavage of RECK. Science 339, 324-328.

Parr, B.A. and McMahon, A.P. (1995). Dorsalizing signal Wnt-7a required for normal polarity of D-V and A-P axes of mouse limb. Nature 374, 350-353.

Pavel, M.A., Lam, C., Kashyap, P., Salehi-Najafabadi, Z., Singh, G., and Yu, Y. (2014). Analysis of the cell surface expression of cytokine receptors using the surface protein biotinylation method. Methods Mol. Biol. 1172, 185-192.

Pelletier, S., Gingras, S., and Green, D.R. (2015). Mouse genome engineering via CRISPR-Cas9 for study of immune function. Immunity 42, 18-27.

Posokhova, E., Shukla, A., Seaman, S., Volate, S., Hilton, M.B., Wu, B., Morris, H., Swing, D.A., Zhou, M., Zudaire, E., *et al*. (2015). GPR124 functions as a WNT7-specific coactivator of canonical β-catenin signaling. Cell Rep. 10, 123-130.

Prendergast, A., Linbo, T.H., Swarts, T., Ungos, J.M., McGraw, H.F., Krispin, S., Weinstein,

B.M., and Raible, D.W. (2012). The metalloproteinase inhibitor Reck is essential for zebrafish DRG development. Development 139, 1141-1152.

Rajagopal, J., Carroll, T.J., Guseh, J.S., Bores, S.A., Blank, L.J., Anderson, W.J., Yu, J., Zhou, Q., McMahon, A.P., and Melton, D.A. (2008). Wnt7b stimulates embryonic lung growth by coordinately increasing the replication of epithelium and mesenchyme. Development 135, 1625-1634.

Shu, W., Jiang, Y.Q., Lu, M.M., and Morrisey, E.E. (2002). Wnt7b regulates mesenchymal proliferation and vascular development in the lung. Development 129, 4831-4842.

Stan, R.V., Tkachenko, E., and Niesman, I.R. (2004). PV1 is a key structural component for the formation of the stomatal and fenestral diaphragms. Mol. Biol. Cell 15, 3615-3630.

St. Croix, B., Rago, C., Velculescu, V., Traverso, G., Romans, K.E., Montgomery, E., Lal, A., Riggins, G.J., Lengauer, C., Vogelstein, B., *et al*. (2000). Genes expressed in human tumor endothelium. Science 289, 1197-1202.

Stenman, J.M., Rajagopal, J., Carroll, T.J., Ishibashi, M., McMahon, J., and McMahon, A.P. (2008). Canonical Wnt Signaling Regulates Organ-Specific Assembly and Differentiation of CNS Vasculature. Science 322, 1247-1250.

Takahashi, C., Sheng, Z., Horan, T.P., Kitayama, H., Maki, M., Hitomi, K., Kitaura, Y., Takai, S., Sasahara, R.M., Horimoto, A., *et al*. (1998). Regulation of matrix metalloproteinase-9 and inhibition of tumor invasion by the membrane-anchored glycoprotein RECK. Proc. Natl. Acad. Sci. USA 95, 13221-13226.

Vanhollebeke, B., Stone, O.A., Bostaille, N., Cho, C., Zhou, Y., Maquet, E., Gauquier, A., Cabochette, P., Fukuhara, S., Mochizuki, N., *et al*. (2015). Tip cell-specific requirement for an atypical Gpr124- and Reck-dependent Wnt/β-catenin pathway during brain angiogenesis. Elife 4, e06489.

Wang, Y., Rattner, A., Zhou, Y.L., Williams, J., Smallwood, P.M., and Nathans, J. (2012). Norrin/Frizzled4 Signaling in Retinal Vascular Development and Blood Brain Barrier Plasticity. Cell 151, 1332-1344.

Xu, Q., Wang, Y., Dabdoub, A., Smallwood, P.M., Williams, J., Woods, C., Kelley, M.W., Jiang, L., Tasman, W., Zhang, K., *et al*. (2004). Vascular development in the retina and inner

ear: Control by Norrin and Frizzled-4, a high-affinity ligand-receptor pair. Cell 116, 883-895.

Yamamoto, M., Matsuzaki, T., Takahashi, R., Adachi, E., Maeda, Y., Yamaguchi, S., Kitayama, H., Echizenya, M., Morioka, Y., Alexander, D.B., *et al*. (2012). The transformation suppressor gene Reck is required for postaxial patterning in mouse forelimbs. Biol. Open 1, 458-466.

Ye, X., Wang, Y., Cahill, H., Yu, M.Z., Badea, T.C., Smallwood, P.M., Peachey, N.S., and Nathans, J. (2009). Norrin, Frizzled-4, and Lrp5 Signaling in Endothelial Cells Controls a Genetic Program for Retinal Vascularization. Cell 139, 285-298.

Ye, X., Wang, Y., Rattner, A., and Nathans, J. (2011). Genetic mosaic analysis reveals a major role for frizzled 4 and frizzled 8 in controlling ureteric growth in the developing kidney. Development 138, 1161-1172.

Yu, H., Ye, X., Guo, N., and Nathans, J. (2012). Frizzled 2 and frizzled 7 function redundantly in convergent extension and closure of the ventricular septum and palate: evidence for a network of interacting genes. Development 139, 4383-4394.

Yu, J., Carroll, T.J., Rajagopal, J., Kobayashi, A., Ren, Q., and McMahon, A.P. (2009). A Wnt7b-dependent pathway regulates the orientation of epithelial cell division and establishes the cortico-medullary axis of the mammalian kidney. Development 136, 161-171.

Zhang, Y., Chen, K., Sloan, S.A., Bennett, M.L., Scholze, A.R., O'Keeffe, S., Phatnani, H.P., Guarnieri, P., Caneda, C., Ruderisch, N., *et al*. (2014). An RNA-sequencing transcriptome and splicing database of glia, neurons, and vascular cells of the cerebral cortex. J. Neurosci. 34, 11929-11947.

Zhao, Z., Nelson, A.R., Betsholtz, C., and Zlokovic, B.V. (2015). Establishment and Dysfunction of the Blood-Brain Barrier. Cell 163, 1064-1078.

Zhou, Y., and Nathans, J. (2014). Gpr124 controls CNS angiogenesis and blood-brain barrier integrity by promoting ligand-specific canonical Wnt signaling. Dev. Cell 31, 248-256.

Zhou, Y., Wang, Y., Tischfield, M., Williams, J., Smallwood, P.M., Rattner, A., Taketo, M.M., and Nathans, J. (2014). Canonical WNT signaling components in vascular development and barrier formation. J. Clin. Invest. 124, 3825-3846.

Curriculum Vitae

CHRIS CHO

1200 Steuart Street, Unit #421, Baltimore, MD 21230 ccho21@jhmi.edu
10934 Boulder Canyon Road, Alta Loma, CA 91737 909-800-5367

BORN December 25, 1989
Corona, CA

EDUCATION

Johns Hopkins University School of Medicine, Baltimore, MD 21205
M.D./Ph.D. Candidate
Expected graduation: June 2021

Yale University, New Haven, CT 06520
B.S./M.S. in Molecular, Cellular, and Developmental Biology, May 2012
Cum laude, Distinction in the Major

Los Osos High School, Rancho Cucamonga, CA 91737
Valedictorian, Diploma, June 2008

RESEARCH

Jeremy Nathans Lab, July 2014 – Present
- Doctoral candidate
- Department of Molecular Biology and Genetics at The Johns Hopkins School of Medicine
- Novel co-activators of canonical Wnt signaling in CNS angiogenesis

Dieter Söll Lab, Fall 2010 – May 2013
- Combined B.S./M.S. student

- Department of Molecular Biophysics and Biochemistry at Yale University
- Investigated cellular defense against protein mistranslation in bacteria
- Characterized and engineered a yeast mitochondrial threonyl-tRNA synthetase (MST1)

Joanne Weidhaas Lab (in collaboration with Frank Slack Lab), Fall 2008 – Spring 2010

- Undergraduate student
- Department of Therapeutic Radiology at Yale School of Medicine (and Department of Molecular, Cellular, and Developmental Biology at Yale University)
- Researched microRNAs as a potential lung cancer therapeutic in a mouse model

John J. Rossi Lab, Summer 2007 and 2008

- High school student
- Department of Molecular Biology at the Beckman Research Institute of the City of Hope
- Researched anti-HIV therapeutics using the RNA interference cellular pathway

PUBLICATIONS

Liu, M.M., **Cho, C.**, Jefferys, J.L., Quigley, H.A., Scott, A.W. (2017). Use of optical coherence tomography by nonexpert personnel as a screening approach for glaucoma. *J Glaucoma*. 27, 64-70.

Cho, C., Smallwood, P.M., Nathans, J. (2017). Reck and Gpr124 are essential receptor cofactors for Wnt7a/Wnt7b-specific signaling in mammalian CNS angiogenesis and blood-brain barrier regulation. *Neuron*. 95, 1056-1073.

Vanhollebeke, B., Stone, O.A., Bostaille, N., **Cho, C.**, Zhou, Y., Maquet, E., Gauquier, A., Cabochette, P., Fukuhara, S., Mochizuki, N., Nathans, J., Stainier, D.Y. (2015). Tip cell-specific requirement for an atypical Gpr124- and Reck-dependent Wnt/β-catenin pathway during brain angiogenesis. *eLife*. 4:e06489.

Ling, J., **Cho, C.**, Guo, L., Aerni, H., Rinehart, J., and Söll, D. (2012). Protein aggregation caused by aminoglycoside action is prevented by a hydrogen peroxide scavenger. *Mol. Cell.* 48, 713-722.

Ling, J., Peterson, K.M., Simonović, I., **Cho, C.**, Söll, D., and Simonović, M. (2012). Yeast mitochondrial threonyl-tRNA synthetase recognizes tRNA isoacceptors by distinct mechanisms and promotes CUN codon reassignment. *Proc. Natl. Acad. Sci. USA* 109, 3281-3286.

Trang, P., Wiggins, J.F., Daige, C., **Cho, C.**, Omotola, M., Brown, D., Weidhaas, J.B., Bader, A.G., and Slack, F.J. (2011). Systemic delivery of tumor suppressor microRNA mimics using a neutral lipid emulsion inhibits lung tumors in mice. *Mol. Ther.* 19, 1116-1122.

CONFERENCE TALKS (selected from abstracts)

Cho. C., Smallwood, P.M., Nathans, J. (2017). Reck and Gpr124 are essential receptor cofactors for Wnt7a/Wnt7b-specific signaling in mammalian central nervous system angiogenesis and blood-brain barrier regulation. Gordon Research Conference (Wnt Signaling). Stowe, VT.

Cho. C., Smallwood, P.M., Nathans, J. (2016). The Reck-Gpr124 complex activates Wnt7a/7b signaling to promote CNS angiogenesis in mammals. Cold Spring Harbor Laboratory (Blood Brain Barrier Conference). Cold Spring Harbor, NY.

Cho. C., Ling, J., Guo, L., Aerni, H., Rinehart, J., and Söll, D. (2012). Cellular Defense Against Protein Mistranslation in Bacteria. Beckman Scholars and Beckman Young Investigators Symposium (Arnold and Mabel Beckman Foundation). Irvine, CA.

CONFERENCE POSTERS

Cho, C., Liu, M.M., Jefferys, J.L., Quigley, H.A., Scott, A.W. (2017). Detecting glaucoma using the portable Optovue iVue SD-OCT: implications for an improved method in community screenings. ARVO Annual Meeting. Baltimore, Maryland.

Cho, C., Ling, J., Guo, L., Aerni, H., Rinehart, J., and Söll, D. (2012). Protein aggregation caused by aminoglycoside action is prevented by a hydrogen peroxide scavenger. XXIV tRNA Conference. Olmué, Chile.

AWARDS

The Michael A. Shanoff Research Award, April 2018
- The Johns Hopkins University School of Medicine
- Awarded to a graduate student in recognition of outstanding research contributions

National Eye Institute Travel Grant, May 2017
- The Association for Research in Vision and Ophthalmology (ARVO)
- Awarded $750 to attend and present at the ARVO Annual Meeting

Outstanding Presentation Prize, June 2016
- The Johns Hopkins University School of Medicine
- Department of Molecular Biology and Genetics,
- Awarded annually to the top 3 graduate students for outstanding presentations in the departmental journal club seminar series

SOURCE Service Scholar, August 2014-June 2015
- Johns Hopkins Medical Institution
- Awarded to health professional students to lead and organize service-learning projects in collaboration with community based organizations in the greater Baltimore area.

Beckman Scholar, Spring 2011 – Summer 2012
- Awarded a scholarship of $19,300 (over the course of two summers and one academic year) that is sponsored by the Arnold and Mabel Beckman Foundation through the Beckman Scholars Program
- Granted to two Yale undergraduates every year in order to stimulate, encourage, and support research activities

Yale College Dean's Research Fellowship in the Sciences, Summer 2009

- Awarded a scholarship of $4,150 (for one summer) to conduct research under the supervision of a Yale faculty member

TEACHING

Yale University, Spring 2013
- Teaching Assistant for an undergraduate course: *An Issues Approach to Biology* (taught by Dieter Söll, Ronald Breaker, and Charles Sindelar)

SERVICE

Student Sight Savers Program, Fall 2013 – Present
- Medical Student Director (2017 – Present):
  - Responsible for leading vision screening events for community members in Baltimore, MD and coordinating ophthalmological evaluation and care at Wilmer Eye Institute for those in need, regardless of their ability to pay
- Follow-up coordinator (2015 – 2017):
  - Schedule appointments at Wilmer Eye Institute for screened individuals who require follow-up eye
- Co-community liaison (2014 – 2015):
  - Partner with different community-based organizations to provide free screenings for their group members
  - Recruit, assign, and manage 15 medical student volunteers per screening event

OTHER ACTIVITIES

Gertrude Stein Society, Fall 2013 – Present
- To maintain and develop a welcoming and affirming environment for Lesbian, Gay, Bisexual, and Transgender (LGBT) students and employees of the Johns Hopkins Medical Institute, including the Schools of Public Health, Nursing, and Medicine.
- Board member (Spring 2014 – Spring 2016):

- Serve as the leader and representative on behalf of the School of Medicine
- Promote the interest of GSS members and provide social and intellectual enrichment

Charm City Ballet Company, Fall 2015 – Present
- Involved in classical ballet technique and master classes
- Performances: *A Christmas Carol* (2015, 2016, 2017), *Beauty and the Beast* (2016), and *Aladdin* (2017)